

THESIS FOR THE DEGREE OF DOCTOR OF PHILOSOPHY (PH.D.)

Development of cytometric methods for the detection of genetic and
epigenetic changes

by László Imre

Supervisor: Dr. Gábor Szabó



UNIVERSITY OF DEBRECEN
DOCTORAL SCHOOL OF MOLECULAR CELL AND IMMUNE BIOLOGY

DEBRECEN, 2019

TABLE OF CONTENTS:

<i>ABBREVIATIONS</i>	4
<i>PREMISES</i>	7
<i>SPECIFIC AIMS</i>	7
¹ A. CYTOMETRIC MICROBEAD ASSAYS FOR GENETIC ANALYZIS	8
A. 1. INTRODUCTION	8
A. 2. RESULTS	9
A. 2. 1. Detection of CAG triplet expansion in Huntington’s disease	9
A. 2. 2. Detection of BRCA1 5382insC mutation.....	15
A. 2.3. Detection of single-stranded DNA regions	17
A. 3. DISCUSSION	19
B. QUANTITATIVE IMAGING CYTOMETRY FOR EPIGENETIC ANALYZIS	22
B. 1. INTRODUCTION	22
B. 2. RESULTS	26
B. 2. 1. PTM-dependence of nucleosome stability	26
B. 2. 2. Effect of histone variants on nucleosome stability	34
B. 2. 3. Superhelicity dependence of nucleosome stability.....	45
B. 2. 4 General characteristics of the elution assays	50
B. 3. DISCUSSION	53
C. CYTOMETRIC MICROBEAD ASSAYS FOR EPIGENETIC ANALYZIS	63
C. 1. INTRODUCTION	63
C. 2. RESULTS	64
C. 2. 1. Detection of PTM-specific histone associations.....	65
C. 2. 2. Detection of nick-proximal RNA Pol II and R-loops.....	67
C. 3. DISCUSSION	72
<i>GENERAL DISCUSSION AND CONCLUSIONS</i>	74
GENERAL DISCUSSION.....	74
CONCLUSIONS.....	75

¹A is based on and contains excerpts from: (Imre et al. 2011), and (Hegedus et al. 2008); B comprises description of a method as published in (Imre et al. 2017), as well as unpublished data (B.2.2.) on the stability features of nucleosomes containing the H2A.Z histone variant.. C contains data published in (Hegedüs et al. 2018) and data not yet submitted for publication. The Introduction and Discussion chapters contain new, thesis-specific text.

<i>MATERIALS AND METHODS</i>	77
Chemicals	77
Plasmids	77
DNA isolation	77
Cells and clinical samples	77
PCR reactions	78
Hybridization of PCR products and cleavage by Pvu II	80
Binding of PCR products to beads	80
Heat treatment in formamide.....	80
Coating of beads by biotinylated anti- γ H2A.X antibody.....	81
Detection of combinatorial histone PTMs	81
Detection of nicks and nick proximal R-loops.....	82
Flow cytometry	83
Global „ChIP-on-beads” assay.....	83
Embedding live cells into low melting point agarose	85
Preparation of nuclei/permeabilization and histone eviction by salt or intercalators.....	86
Immunofluorescence labeling	87
Etoposide treatment.....	88
Nickase and DNase I treatment.....	88
Immuno- cross-linking experiments.....	88
Gel electrophoretic analyzes	89
Automated microscopy	89
Confocal Laser Scanning Microscopy (CLSM).....	90
STED microscopy	90
Chromatin immunoprecipitation and sequencing	90
Bioinformatics analyzes	91
Sample preparation for MS measurement.....	91
SDS-PAGE and LC-MS/MS analyzes	92
<i>SUMMARY</i>	93
<i>ÖSSZEFOGLALÁS</i>	94
<i>REFERENCES</i>	95
<i>KEYWORDS</i>	105
<i>ACKNOWLEDGEMENTS</i>	106
<i>APPENDIX</i>	107

ABBREVIATIONS

6FAM - 6-carboxyfluorescein
ADD - ATRX–DNMT3–DNMT3L
ADP - adenosine diphosphate
ATM - ataxia telangiectasia mutated
ATRX - ATP-dependent helicase
BAH - bromodomain-associated homology
BRCA - breast cancer
CAG - cytosine adenine guanine
CHEF - contour-clamped homogeneous electric field
ChIP - chromatin immunoprecipitation
CLSM - Confocal Laser Scanning Microscopy
CFP - cyan fluorescent protein
C.V. - coefficient of variation
DDR - DNA damage response
DMSO - dimethyl sulfoxide
DNA - deoxyribonucleic acid
DNA Pol I - DNA Polymerase I
DNMT - DNA methyltransferase
ds - double stranded
DSB - double-strand break
EBr - ethidium bromide
mES – mouse embryonic stem cell
FACS - fluorescence activated cell sorter
FISH - fluorescence *in situ* hybridization
FRAP - fluorescence recovery after photobleaching
FRET - Förster resonance energy transfer
GFP - green fluorescent protein
HCT116 - human colorectal tumor cell line 116
HD - huntington disease
HeLa - Henrietta Lack's cell line
HMGA2 - high-mobility group AT-hook 2
HPLC - high pressure liquid chromatography

HRR - homologous recombinational repair
HTT - huntington
IT15 - interesting transcript 15
kDa – kilodalton
LAD - lamina-associated domains
LCR - ligase chain reaction
LMP - low melting point
LSC - laser scanning cytometer
MCA - melting curve analyzis
MLL - multilineage leukemia
MMA - multiplex microbead assay
MNase - micrococcal nuclease
MS - mass spectrometry
NAD - nucleolar-associated domains
NFR - nucleosome free region
NGS - next generation sequencing
NHEJ - non-homologous end joining
NPC - neural progenitor cell
PCR - polymerase chain reaction
PHD - plant homeodomain
PMT - photomultiplier tube
PTM - post-translational modification
PWWP - Proline-Triptophane-Triptophane-Proline
QINESIn - Quantitative Imaging of Nuclei after Elution with Salt/Intercalators
qPCR - quantitative polymerase chain reaction
RNA - ribonucleic acid
RNA Pol I - RNA Polymerase I
SD - standard deviation
SDS-PAGE - sodium dodecyl sulfate polyacrylamide gel electrophoresis
SEM - standard error of mean
Seq - sequencing
SNP - single nucleotide polymorphism
ss - single stranded
STED - stimulated emission depletion

TAF3 - TATA-Box Binding Protein Associated Factor 3
Taq polymerase - *Thermus aquaticus* DNA polymerase I
TC-NER - transcription-coupled nucleotide excision repair
TdT - terminal deoxynucleotidyl transferase
TIRF - total internal reflection fluorescence microscope
TOP1 - topoisomerase I
TOP2 - topoisomerase II
TSS - transcriptional start site
YFP - yellow fluorescent protein

PREMISES

Development of new methods may lead to novel observations or a deeper understanding of phenomena already observed. Novel approaches include hitherto untested combinations of known techniques and their application for new purposes. Our lab has got a longstanding interest in developing novel methodical platforms based on the creative combination of cytometric methods with molecular biological technology. This strategy has been successfully applied in the development of various lab-on-beads tools (Pataki et al. 2005; Szekvolgyi et al. 2006) and also to answer basic biological questions related to global aspects of nuclear structure and chromatin architecture (Szekvolgyi et al. 2009). My Ph.D. program fits this research strategy: I have explored and further exploited the potentials of cytometry in genetic and epigenetic research, for possible diagnostic applications and in support of ongoing basic research projects related to chromatin structure. I have developed new flow cytometric microbead assays what can be used for the diagnosis of certain genetic diseases, and flow and laser scanning cytometric techniques to address global epigenetic features.

SPECIFIC AIMS

Exploring the possibilities offered by flow cytometry for the detection of genetic and epigenetic alterations, our aim was:

A - to develop methods to detect insertions, deletions, triplet expansions and point mutations by microbead based flow cytometric analyzes.

Exploring the possibilities offered by laser scanning cytometry and flow cytometry for global epigenetic analyzes, our aim was:

B - to develop *in situ* methods to assess intrinsic or superhelicity dependent nucleosome stability, a chromatin feature of regulatory significance, in a post-translational modification and histone subtype dependent manner and with special emphasis of possible long-range effects of changes in the superhelical state of the chromatin.

C - to develop microbead-based assays to detect the presence of different epigenetic traits in a particular chromatin context.

A. CYTOMETRIC MICROBEAD ASSAYS FOR GENETIC ANALYZIS

A. 1. INTRODUCTION

Flow cytometric platforms offer possibilities for the investigation of populations of many types of particulate material (e.g.: live or fixed cells, beads), measuring different parameters (e.g.: side scatter, forward scatter, fluorescence intensity) in a multiplex and high-throughput manner (using FACSarray, compatible with the 96 well plate format).

Flow cytometry has a broad range of applications in the field of medicine as well as in research including determination of immune phenotype, the measurement of antigen expression (Ostendorf et al. 2016), cellular DNA content analyzis (Darzynkiewicz et al. 2010), cell proliferation (Pozarowski and Darzynkiewicz 2004) assays, cell death assays (Wlodkowic et al. 2011), RNA content analyzis (Shapiro 1981), Flow-FISH (Wand et al. 2016), measurement of molecular distances by Förster Resonance Energy Transfer (FRET) (Szollosi et al. 2016), to mention just a few, so as to emphasize their wide spectrum. Although most routine applications of flow cytometry address qualitative and quantitative features of fixed or live cells, the possibility to anchor macromolecules to microbeads that are amenable to flow cytometric analyzes has opened a new realm of possibilities. In conjunction with microbead analyzes, flow cytometry has proved to be a sensitive and versatile platform of biochemical, immunological, or molecular biological investigation of proteins and nucleic acids (Ornatsky et al. ; Brodsky et al. 2003; Morgan et al. 2004; Deshpande et al. 2005; Pataki et al. 2005; Nolan et al. 2006; Szekvolgyi et al. 2006; Hsu et al. 2009; Darzynkiewicz et al. 2010; Brind'Amour and Lansdorp 2011; Wu and Singh 2012; Forment and Jackson 2015). Our lab, based on its strong background in both cytometric and biochemical - molecular biological analytical techniques has got a longstanding interest in developing novel applications combining these approaches, having realized the advantages in sensitivity, simplicity, costs and through-put of the lab-on-beads concept (Pataki et al. 2005; Szekvolgyi et al. 2006).

I tested and demonstrated the utility of two novel microbead based strategies. On the one hand, I asked if *dependence of the melting temperature* of double-stranded (ds) DNA molecules (T_m ; the temperature where 50 % of the DNA molecules is present in denatured, single-stranded (ss) form) on their length (T_m (°C) = $(7.35 \times E) + [17.34 \times \ln(\text{Len})] + [4.96 \times \ln(\text{Conc})] + [0.89 \times \ln(\text{DNA})] - 25.42$; E = DNA strength parameter per base, Len = Length of nucleotide sequence (number of base pairs), Conc = $[\text{Na}^+]$ concentration of the solution (Molar), DNA = Total nucleotide strand concentration (Khandelwal and Bhyravabhotla 2010)) could be exploited to detect various genetic alterations. Above its T_m , a sample

containing a PCR product prepared using a pair of biotinylated and fluorescent primers and immobilized on microbeads via the biotin moiety, will dissociate into free ssDNA molecules labeled with the fluorescent tag and the bead-attached, non-fluorescent, biotinylated complementary strand. The degree of denaturation, i.e. ratio of the ds and ss species at equilibrium, will depend on the incubation temperature relative to the T_m . To aid the implementation of the method, melting temperature can be reduced to near ambient conditions in the presence of H-bond destabilizing reagents such as DMSO or formamide (Blake and Delcourt 1996; Sambrook and Russell 2001). In view of the fact that the degree of denaturation at a given temperature is expected to depend also on the length of the DNA molecule (Dimitrov and Zuker 2004; Panjkovich and Melo 2005), measurement of the above ratio by flow cytometry was used for the length comparison of PCR products prepared from DNA samples in diseases where this approach might be of diagnostic value.

In another experimental strategy, I tested if I can detect single-stranded regions in heteroduplices formed after denaturation and reannealing of different size PCR products, using restriction enzymes unable to cleave their recognition motives in the single-stranded overhang area. When a deletion or rearrangement due to chromosome translocation removes a particular restriction enzyme recognition site, the PCR products of the normal and pathological sample yield homo- and heteroduplices what can be distinguished based on the presence or absence of the recognition site. I used streptavidinated microbeads anchoring the fluorescently tagged hybrids through their biotinylated ends.

A. 2. RESULTS

The potentialities in genetic analysis of the cytometric platform developed has been demonstrated in three examples: in the characterization of triplet expansions predisposing for Huntington's disease, in the case of a point mutation of the BRCA1 gene and, for detection of single-stranded regions, in a general model system involving heteroduplices.

A. 2. 1. Detection of CAG triplet expansion in Huntington's disease

Expansions of certain nucleotide triplets in the genomic DNA are responsible for several neurodegenerative diseases. Among them Huntington's chorea is caused by the expanded repetition of the CAG triplet localized in exon 1 of the Huntingtin gene (also called IT15/HTT/HD) encoding the 350 kDa huntingtin protein. The disease was first described by George Huntington in 1872 (Wexler et al. 2016) and was shown to be a hereditary form of chorea. The disease phenotype is characterized by progressive chorea, dystonia, incoordination, cognitive decline, and behavioral difficulties. Currently there are no therapeutic

treatments that can inhibit the progression of the disease which invariably leads to the death of the patients.

The CAG repeats encode a polyglutamine region at the N-terminal domain of the huntingtin protein that is a key player in Huntington’s disease. It is known that the development of the disease correlates with the length of the CAG triplets. There are four categories based on the number of CAG-repetitions: healthy (<27 CAG), and intermediate (27-35 CAG) are not associated with the manifestation of symptoms, but occasionally fathers with repeats in the latter range will transmit the repeat to their children what is then expanded to the pathological range. From among those with reduced penetrance (36-39 CAG), some individuals will develop Huntington’s disease, while others will not. In the diseased phenotype (>40 CAG), symptoms appear at the age between 35 and 50 (Margolis and Ross 2003; Myers 2004; Semaka et al. 2006) and correlation can be observed between the CAG repeat length and the age of onset (**Table 1**).

Category	Number of CAG repeats
healthy	<27 CAG
intermediate (healthy but higher risk in the offsprings)	27-35 CAG
reduced penetrance (appearance of the symptoms is 40%≤)	36-39 CAG
diseased phenotype (appearance of the symptoms is 100%)	40 CAG≤

Table 1. Patient categories according to the number of CAG repeats in exon 1 of the Huntingtin gene.

People with repeats of 60 or larger commonly have very young onset, i.e. before the age of 20. For diagnosis, the length of genomic DNA fragments carrying the CAG-repeats are to be compared; typically this is performed after PCR amplification, sometimes following restriction enzyme digestion and ligation to adaptors (Vos et al. 1995) and the products are analyzed in a standard way by agarose or polyacrylamide gel electrophoresis (Muglia et al. 1996; Margolis and Ross 2003; Milunsky et al. 2003), with capillary gel electrophoresis (Toth

et al. 1997; Margolis and Ross 2003; Falk et al. 2006), or by sequencing (Loomis et al. 2013; Liu et al. 2017). Although we anticipated that by introducing a new technique we could not possibly compete with the already established and standardized, routine procedures, we could make use of the above model system to test the principle of our approach.

The principle of the microbead-based melting temperature analyzes is shown in **Figure 1**. A pair of short and long PCR products are prepared using a fluorescent dye-conjugated and a biotinylated primer to label the two ends. The two samples of the PCR products are immobilized on streptavidine coated microbeads and heat-treated at a temperature between the melting points of the long and the short PCR products. This temperature range was down-shifted using formamide (Blake and Delcourt 1996), to avoid damage of the beads and evaporation of the buffer. The mean fluorescence intensity of the beads carrying the shorter PCR products is expected to decrease relative to the beads with the longer ones. To demonstrate the feasibility of this strategy, we first tested if triplet expansions of different length can be distinguished in the case of Huntington's disease.

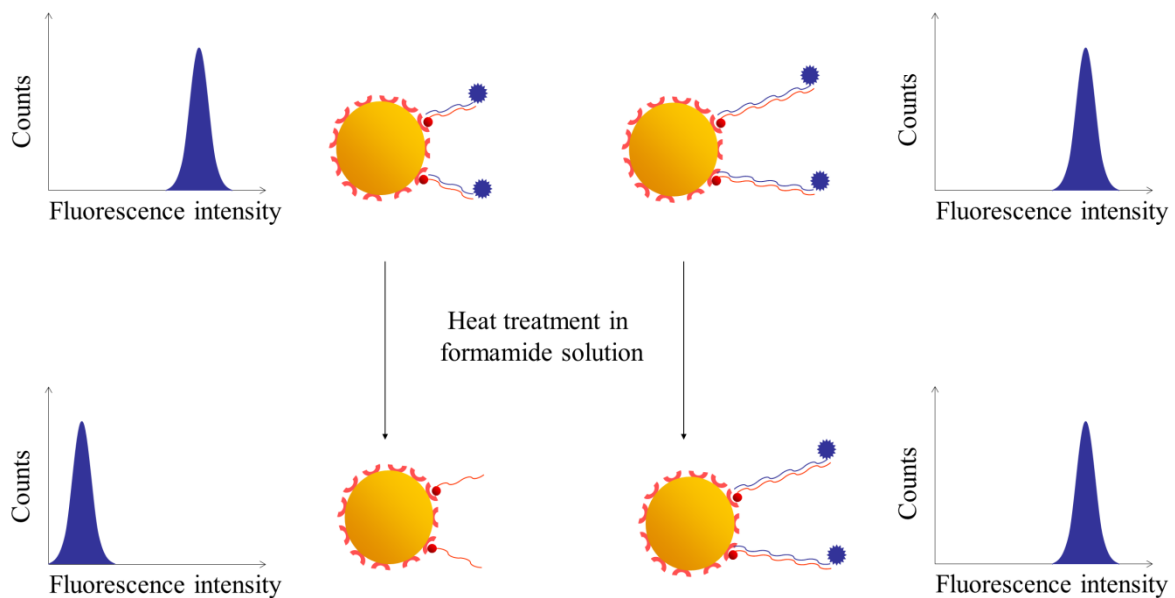


Figure 1. Principle of the microbead based melting temperature analyzes.

Short and long PCR products, labeled on the two ends with a fluorescent dye () and biotin (), respectively, are immobilized on streptavidine () coated microbeads through the biotin moiety and heat-treated in the presence of formamide. After heat treatment at temperatures between the melting point of the longer and that of the shorter PCR product the mean fluorescence intensity of the beads carrying the short ones are expected to decrease in contrast

with the beads carrying the long products. The melting temperatures are decreased to ~ 40 °C using formamide.

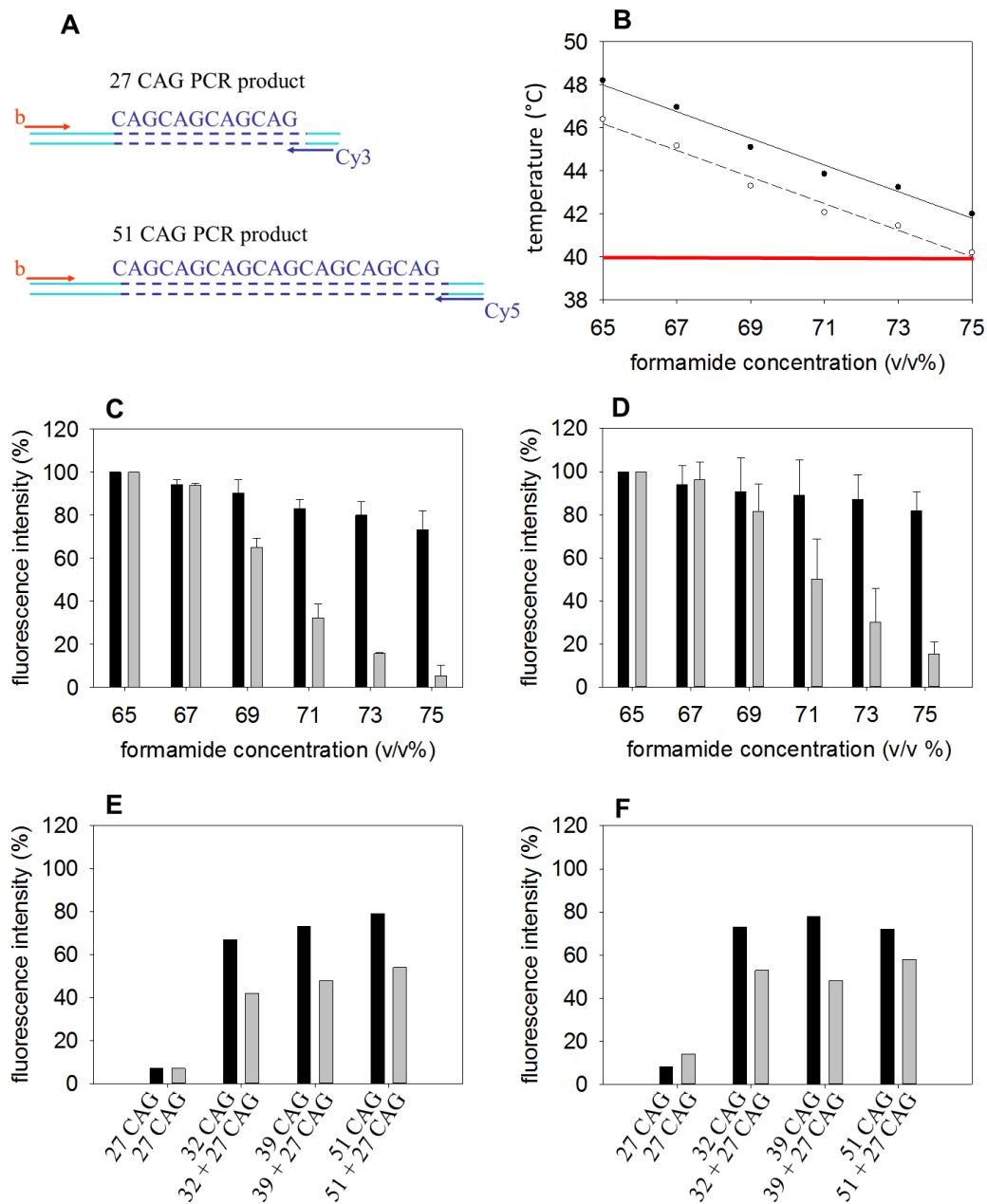


Figure 2. Optimization of formamide concentration for the detection of triplet expansion in Huntington's disease.

(A) PCR products applied. Two biotin and dye labeled PCR products, containing 27 and 51 CAG repeats, respectively, were examined after heat treatment at different formamide concentrations. The PCR products were immobilized on streptavidine coated microbeads at a ratio of 1:1.

(B) Dependence of T_m on formamide concentration. The T_m of the two PCR products at different formamide concentration, were predicted by an on-line oligonucleotide properties

calculator (<http://www.basic.northwestern.edu/biotools/oligocalc.html>). 27 CAG repeat containing PCR product: dashed line; 51 CAG-containing product: continuous line.

(C) Differential strand separation of bead-attached long and short PCR products after heat treatment at different formamide concentrations. Samples of Cy5 labeled long (51 CAG-containing; black columns) and Cy3 labeled short (27 CAG-containing; gray columns) PCR products mixed at a ratio of 1:1 and attached to microbeads were exposed to heat-treatment. The mean fluorescence intensities are expressed in percentages (%) of the values measured in 65 % (v/v) formamide.

(D) Experiments on panel C were repeated changing the fluorophores between the short and long PCR products. The long PCR products were labeled with Cy3 (black columns); the short PCR products were labeled with Cy5 (gray columns).

(E) Detection of triplet expansion in PCR products representing homozygous or heterozygous samples. Percentages of fluorescence intensity remaining after heat treatment in the presence of 75 % (v/v) formamide as compared to the intensities measured at 65 % (v/v) formamide. Black columns represent the homozygous state when either of the 27, 32, 39, or 51 CAG repeat-containing PCR products were analyzed; gray columns represent the heterozygous state when 27 CAG containing PCR products (normal allele) were mixed at a ratio of 1:1 with the longer products (expanded allele), each labeled with Cy5 and biotin as above.

(F) Experiment on panel E was repeated using Cy3 as fluorophore.

Error bars represent the SD of three independent measurements. (Panel E and F show the results of a single experiment.)

The model system used included a set of plasmids containing exon 1 of the Huntingtin (IT15/HTT/HD) gene harbouring different length CAG repeats (Scherzinger et al. 1999). In the experiments shown in **Figure 2** the DNA region of the CAG repeats was amplified using the plasmids carrying 27 and 51 CAG-repetitions. The Cy5 and Cy3 labeled reverse and biotin labeled forward primers were positioned as shown in **Figure 2A**. A 1:1 mixture of the PCR products was immobilized on streptavidinated microbeads, then heat treatment was performed at 40°C in the presence of formamide. The concentration of formamide was titrated in a range encompassing such low and high concentrations, where both PCR products are expected to stay annealed, and where they may be differentially denatured, respectively (see **Figure 2B**). At 75 % formamide, 96 % of the short PCR products were denatured, i.e. their fluorescent-labeled strands dissociated upon incubation at 40°C, while the intensity of the beads carrying

the longer products decreased only by 26 % at the same time, which did not depend on the fluorescent label carried by the PCR products (compare **Figure 2C and D**).

As shown in **Figure 2E and F**, PCR products amplified from the plasmids containing intermediate length CAG repetition could also be clearly distinguished from those amplified from the 27 CAG plasmids representing the upper limit of normal length. Since the patients suffering from Huntington's disease are mostly heterozygous for the pathological triplet-expansion (Squitieri et al. 2003), the measurement was also performed in such a way that the samples contained a 1:1 mixture of the PCR product of the >27 CAG plasmid and the PCR product derived from the 27 CAG plasmid. The assay could clearly distinguish between the templates representing normal and pathological triplet expansions in the case of this model experiment representing heterozygotes, irrespective of the fluorescent labels used. Next, genomic DNA isolated from lymphocytes of healthy volunteers, the Jurkat cell line expected to exhibit normal CAG repetition at the locus, and anonymous patients suffering from Huntington's disease with predetermined number of CAG repeats were amplified and treated as before (**Figure 3**). All the samples with CAG repeat numbers in the healthy range gave low average fluorescence values as compared to the samples derived from people afflicted with the disease.

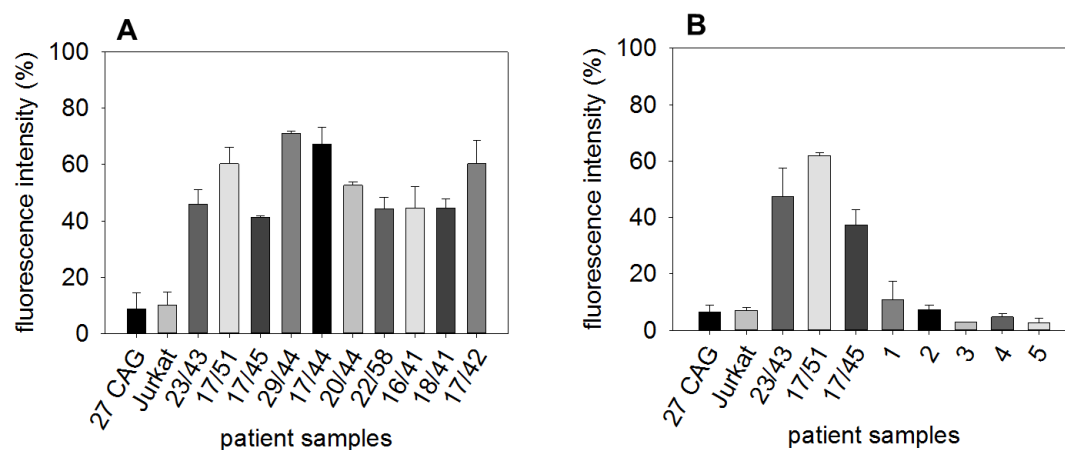


Figure 3. Detection of Huntington's disease in heterozygous patient blood samples.

(A) Determination of CAG repeat length of ten patients afflicted with Huntington's disease (full penetrance category), as compared to Jurkat cells and the 27 CAG repeat-containing plasmid (controls). The repeat length of the the two alleles are as indicated.

(B) Comparison of CAG repeat length in three patient samples and in blood samples derived from five volunteers (considered healthy), Jurkat cells and 27 CAG repeat-containing plasmids.

Error bars represent the SD of three independent measurements.

A. 2. 2. Detection of BRCA1 5382insC mutation

The BRCA1 gene, coding for an 1863 amino acid nuclear phosphoprotein, is known to be involved in the Homologous Recombinational Repair (HRR), Non-Homologous End Joining (NHEJ) and Transcription-Coupled Nucleotide Excision Repair (TC-NER) pathways as well as in the regulation of diverse though interrelated, and fundamental processes like transcription, cell cycle and apoptosis, in part through its interaction with histone deacetylase and chromatin-remodelling factors (Deng and Wang 2003; Reguart et al. 2008; Kass and Jasin 2010). Its point mutations predispose women to breast and ovarian cancer (Foulkes 2004; Antoniou et al. 2005; Ramus and Gayther 2009; Petrucelli et al. 2010; Zhu et al. 2016; Godet and Gilkes 2017). From among these BRCA1 mutations the 185delAG, 5382insC and the missense C61G are the most common (Ramus and Gayther 2009). Several methods are available for the detection of point mutations based on electrophoresis, primer extension, the use of mismatch binding proteins like MutS (a member of the mismatch repair system in *Escherichia coli*), ligation of adjacent primers at the site of the mutation (ligase chain reaction, LCR), enzymatic cleavage by cleavase (cleavase fragment length polymorphism) or chemical cleavage on chemically modified unpaired nucleotides by piperidine (Nollau and Wagener 1997; Kwok 2001), by microarray (chip) and qPCR (Taq-man assay) technologies (Deng and Wang 2003), and by next generation sequencing (NGS) (Wallace 2016; Dong et al. 2018). Sensitivity of qPCR and NGS can be further improved by up to 100-fold using co-amplification at lower denaturation temperature - PCR (COLD-PCR) instead of regular PCR (Li and Makrigiorgos 2009). Application of these methods for screening of wider populations is apparently limited due to cost considerations. Aside from a potential practical utility of the method, the principle of a flow cytometric measurement platform for the detection of point mutations was considered worth testing on its own right.

For the detection of BRCA1 5382insC, a modified allele specific PCR reaction was used, applying three primers in a multiplex reaction: wild type and mutation specific forward primers and a common reverse primer. The specificity of the forward primers was determined by the 3' terminal nucleotide, as shown in **Figure 4A**. Separate primers were designed to permit amplification if the nucleotide at the 3'-end of the primer is complementary to the sequence harboring a point mutation and to the wild-type sequence. Due to the presence of an extension sequence (CAG tag) at the 5' end of the mutation specific forward primer, two different length PCR products are generated if the analyzed sample is heterozygous for the mutation; thus the mutant and the wild type alleles can be discriminated in a cytometer. To optimize the concentration of formamide solution, the PCR products representing the wild type

and mutant alleles were generated in separate amplification reactions, using Cy5 labeled forward and biotin labeled reverse primers and the genomic DNA template derived from a patient carrying one BRCA1 5382 insC allele. The optimal concentration of formamide where the mean fluorescence intensity of the short products decreased almost to background levels while the long PCR products decreased only to approximately 40% of the reference (measured at 57 % formamide) was at 62 % formamide, as shown in **Figure 4B**. Using Cy5-labeled wild type specific and mutation specific forward primers and common biotin labeled reverse primers, a clinical sample with determined heterozygous BRCA1 5382insC mutation and the control DNA of Jurkat cells could be clearly distinguished (**Figure 4C**). The 62 % formamide concentration was somewhat below what was expected based on the calculated T_m -s as shown in **Figure 4D**.

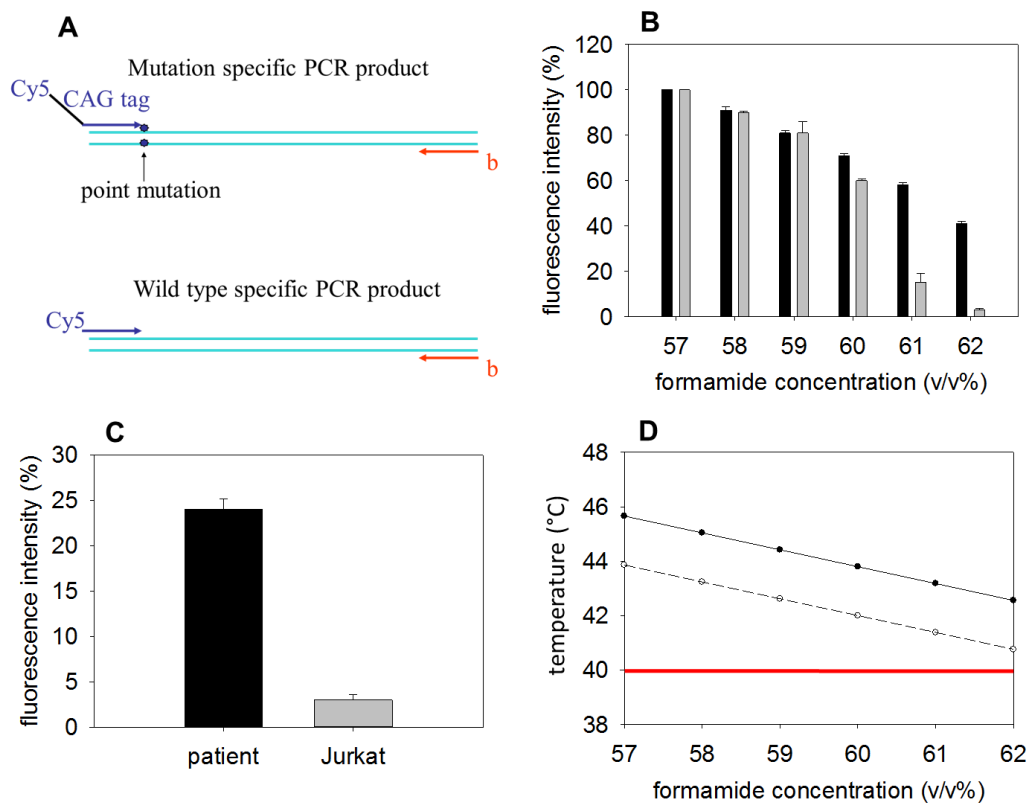


Figure 4. Detection of BRCA1 5382ins mutation.

(A) PCR products applied. The Cy5 labeled wild type specific and mutation specific sense primers containing additional 18 bp CAG tag were used in two separate reactions. The biotin labeled antisense primer was the same in both cases.

(B) Mean fluorescence intensities remaining after heat treatment in the presence of different concentrations of formamide expressed in percentages (%) of the values measured in 57 % (v/v) formamide. Gray columns: wild-type specific PCR products; black columns: mutation specific product.

(C) Detection of BRCA1 5382insC mutation in the genomic DNA derived from of a heterozygous patient. Allele specific PCR reaction was performed in a multiplex mode using a Cy5-labeled mutation specific sense primer containing a 18 bp CAG tag, a Cy5-labeled wild type specific sense primer (with no CAG tag), and a collective biotin labeled antisense primer. The PCR products were immobilized on streptavidine coated microbeads and heat treatment was performed at 57 % (v/v) and 62 % (v/v) formamide concentrations. The columns show the percentage of the mean fluorescent intensity after 62 % (v/v) formamide treatment relative to the values measured at 57 % (v/v) formamide. Black column: patient sample; Gray column: Jurkat cells (wild type control).

(D) Dependence of T_m on formamide concentration. Mutation specific PCR product: continuous line; wild-type allele specific product: dashed line.

Error bars represent the SD of three independent measurements.

A. 2.3. Detection of single-stranded DNA regions

When two, partially complementary strands anneal, the non-complementary regions stay single-stranded. First, ss DNA probes were prepared, using linear amplification; these included a biotinylated sense strand, a 6FAM labeled antisense strand, and a shorter, 6FAM labeled antisense probe. The 6FAM labeled strands with different length were hybridized to the biotinylated strand, yielding homoduplexes and heteroduplexes, as shown in **Figure 5A**. The products were exposed to the Pvu II restriction endonuclease that can cleave the ds DNA carrying the target sequence but not ss DNA. Next, the biotinylated products were bound to streptavidinated microbeads and analyzed in the flow cytometer. We observed a significant decrease of fluorescence only in the case of the microbead bound homoduplexes, just as expected for these ds specific enzymes (**Figure 5B**).

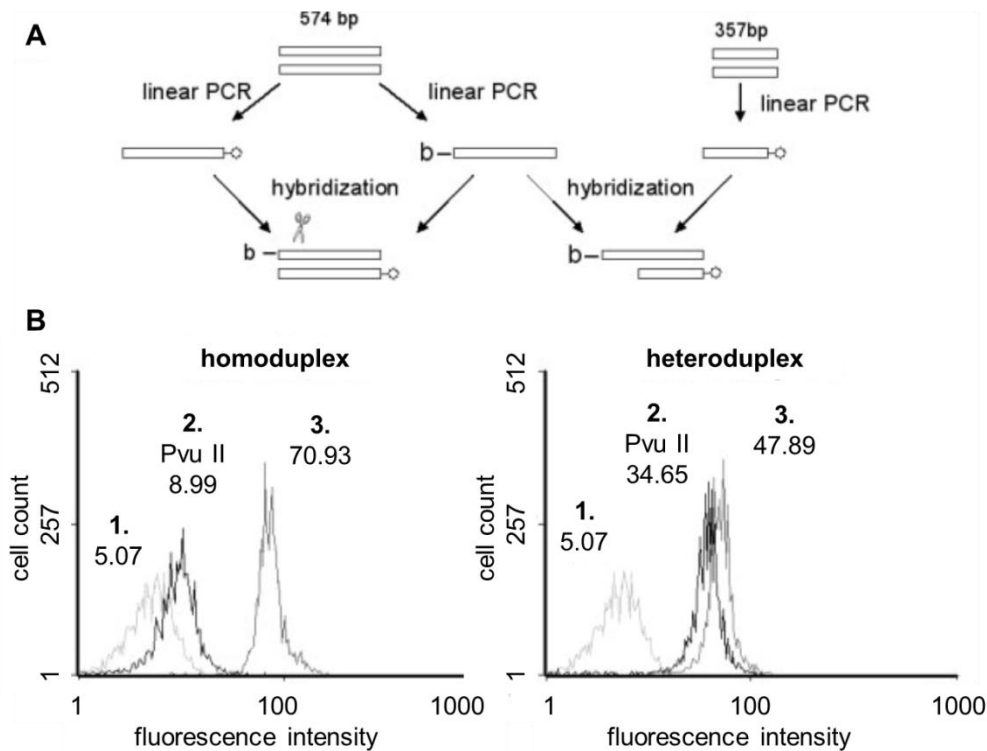


Figure 5. Flow cytometric analyzes of deletions by restriction endonuclease digestion.

(A) Principle of the method. Biotin and 6FAM labeled ss DNA fragments of different length prepared by linear amplification, using 6FAM (star) and biotin labeled (b) primers, were denatured and reannealed and the resultant homo- and heteroduplexes exposed to Pvu II restriction endonuclease. Its recognition sequence is cleaved by the enzyme exclusively in the homoduplex, giving rise to decrease of fluorescence in the microbead-bound homoduplexes only.

(B) Fluorescence intensity distribution histograms of the microbead samples carrying homo- (left) and heteroduplexes (right), before (grey line, peak “3”, left and right) and after (black line, peak “2”, left and right) Pvu II digestion. Background fluorescence of beads: peak “1”, on both panels. The numbers represent the mean fluorescence intensities of the peaks. (Representative data of five independent experiments.)

Single strand DNA was also digested by Pvu II to some extent; we assume that this may be the result of transient hybridization of the separate molecules at these short complementary (palindromic) regions. However, this background cleavage does not appear to significantly affect the sensitivity of the approach.

A. 3. DISCUSSION

The microbead based methods described can be applied for the diagnosis of several genetic disorders where the length or the sequence of a certain genomic segment is changed. Genetic disorders that can be detected include triplet expansions, SNP-s, point mutations, microsatellite polymorphisms, insertion/deletion polymorphisms and rearrangements.

The T_m analyzes may be feasible if the difference between the melting points of the two different length PCR products allows their differential elution upon denaturation. The minimal difference detected by our assay corresponds to a T_m point difference of 1.6°C. The formamide concentration where the difference is maximal is to be empirically determined in a relatively narrow concentration range. The mild conditions of denaturation achieved using formamide are expected to prevent any major nonspecific effect, like molecular aggregation, nonspecific binding of DNA to the beads or adverse chemical reactions, and allow for rather simple experimental procedures.

Microbead-based melting point analyzes was applied successfully both for the detection of the rare Huntington's disease and the frequent 5382insC mutation of BRCA1 gene.

In the case of Huntington's disease the variable length of the CAG repeat in exon 1 of the Huntingtin gene was measured. The smallest difference that could be detected using our standard assay conditions comprised five CAG triplets, i.e. 15 base pairs, present in a heterozygous manner. However, it is likely that this limit could be improved by further optimization. Data obtained through the analysis of ten Huntington's patients with determined CAG repeats and of five healthy donors have demonstrated that the assay is remarkably reliable and can be certainly considered as an initial test in large-scale population screening programs (**Figure 6**). Although a battery of different methods has been introduced for the diagnosis of triplet expansions, neither of these appears to surpass the procedure described herein in simplicity and ease of multiplexing, considering the steps of analyzes. Aside from this potential practical utility, I have demonstrated that flow cytometric differential melting point analyzes can be used to detect rather short length differences of dsDNA molecules.

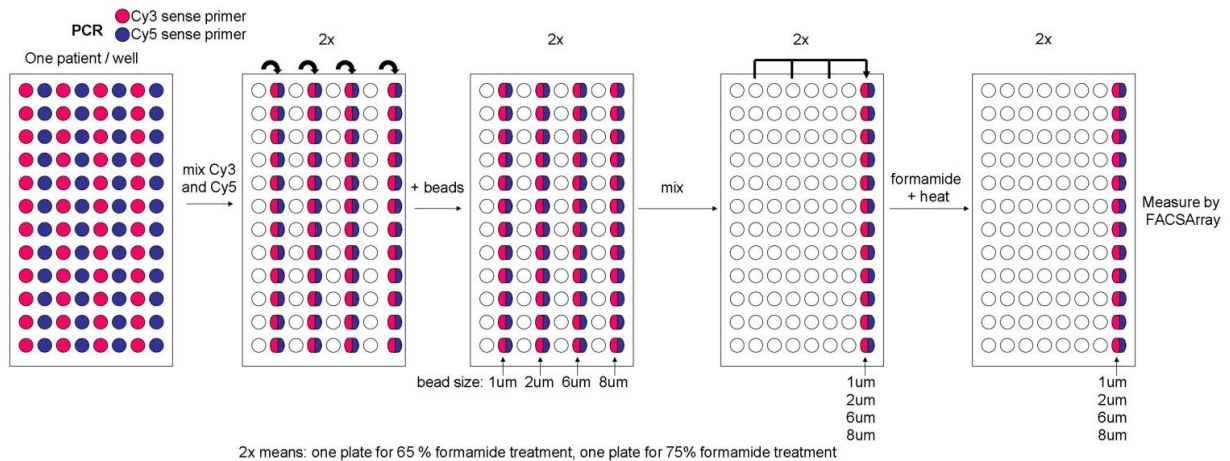


Figure 6. Flow chart of a possible high-throughput screening of CAG triplet expansion.

Using 4 different size commercially available beads (Other beads containing different fluorochromes, or one fluorochrome emitting different intensities of fluorescence can be also used. Instead of biotin-streptavidine linkage other molecular linkers can be also applied however biotin-streptavidine is the strongest one that is known.) and the two fluorochromes already tested, 768 patient samples would yield 96 mixed samples to be measured at two different formamide concentration. In a FACSarray instrument this analysis would take about 60 mins. Such a multiplexed assay (devised for 96 well format below) would not involve any new element as compared to what has already been experimentally tested, except for the application of the different size microbeads.

The same principle was tested as to its utility for the diagnosis of point mutations, when combined with allele specific PCR (Wang et al. 2005). The prevalence of BRCA1 mutation carriers is around 1/800 in the general population, however, it can vary significantly among different countries or ethnic groups (Fackenthal and Olopade 2007; Ramus and Gayther 2009). The approach described can also be used for the detection of any other point mutation and of SNPs, applying allele specific PCR reactions to generate different length mutation/SNP specific and wild type specific PCR products. In the case of the 5382insC mutation of the BRCA1 gene tested, we added a 6-CAG tag to the mutation specific primer to achieve a length difference between the two PCR products that proved to be sufficient for length discrimination in the case of the repeat expansion disease. Based on the fact that the two PCR products of different CAG repeat length were shown not to interfere with each-other at immobilization to, or upon debinding of the non-biotinylated strands from the same bead (see **Figure 2**, panel C), it would seem possible to develop a multiplex microbead assay for the simultaneous detection of all the 14 cancer risk associated BRCA1 mutations (Linger and Kruk 2010) in one single

well of a 96 or a 384 well plate with the combination of three different types of fluorescent dyes linked to the PCR products and six kinds of microbeads with different size and color.

Commonly used techniques to analyze PCR products based on size discrimination include various electrophoresis methods, used in conjunction with Southern-blotting, HPLC and capillary gel electrophoresis-based methods, melting curve analysis (MCA) (Zhao et al. 2017) by real-time PCR systems and next generation sequencing (NGS) (Bahlo et al. 2018). The purpose of my efforts was to test if flow cytometry could also be used for this purpose, offering potential advantages in high-throughput and/or multiplex analyses. The general conclusion reached is clearly positive.

The range of related potential applications include genetic disorders involving insertions, deletions, triplet expansions, microsatellite polymorphisms. In addition, when primers with different length are used (Wang et al. 2005), single nucleotide polymorphisms (SNPs) or point mutations could also be detected. Although melting point analysis by real-time PCR, based on the differential melting kinetics of primers discriminating between two alleles, provide straightforward answers and are routinely used, we have confirmed that a flow cytometric method of comparable sensitivity and multiplicity might offer a valuable alternative platform.

The other approach, involving restriction enzyme digestion of homo- and heteroduplexes, may also provide a sensitive diagnostic tool or assay system in a broad range of genetic disorders or conditions. The ease and cost-effective nature of the assay could make it the test of choice for screening purposes in various applications including basic research, e.g. in the investigation of immunoglobulin gene rearrangement.

B. QUANTITATIVE IMAGING CYTOMETRY FOR EPIGENETIC ANALYSIS

B. 1. INTRODUCTION

Histones are the fundamental units of nucleosome structure in which a histone octamer consisting of four different types of core histones is wrapped around by 146 bp long stretches of the genomic DNA forming the first level of chromatin compactation. The octamer is composed of two H2A-H2B dimers and one (H3-H4)₂ histone tetramer. Neighbouring nucleosome core particles are connected by the linker DNA which is associated with the linker histone (H1). Nucleosomes play essential structural and functional roles in the transition between transcriptionally active and inactive chromatin states. Stability of nucleosomes is of regulatory importance in eukaryotes (Kornberg and Lorch 1991; Andrews and Luger 2011; Teves and Henikoff 2014; Venkatesh and Workman 2015) since the formation of nucleosome free regions (NFRs) is a prerequisite for downstream steps of transcriptional activation. Histone-DNA and nucleosome-nucleosome interactions are affected by histone post-translational modifications (PTMs) that mainly occur on the N- or C-terminal tail of core histone molecules. PTMs form a specific pattern throughout the chromatin, what is often alluded to as the histone code. More than one histone tail can be modified within a particular nucleosome at the same time, and more than one amino acid residue can be modified on the same histone tail; the combinations of histone modifications are major determinants of epigenetic regulation. Lysine, serine, arginine, threonine, tyrosine, histidine residues on the N- or C terminal tail of core histone molecules are the targets of chromatin-modifying enzyme complexes to establish covalently bound modifications, e.g. acetylation, methylation, phosphorylation, ubiquitination, sumoylation, poly-(ADP) ribosylation, crotonylation, succinylation, malonylation, citrullination, formylation, propionylation, butyrylation, hydroxylation and glycosylation (Zentner and Henikoff 2013; Rothbart and Strahl 2014). Histone PTMs are established on the histones by proteins termed as writers (e.g.: histone methyltransferase, histone acetyltransferase), recognized by readers (proteins containing bromodomains, chromodomains, plant homeodomain (PHD) fingers, bromodomain-associated homology (BAH) domains, ATRX-DNMT3-DNMT3L (ADD) domains, Proline-Tryptophane- Tryptophane-Proline (PWWP), and removed by erasers (histone demethylases, histone deacetylases) (Rothbart and Strahl 2014).

Although histones have a high degree of conservation, variants have evolved to assume diverse roles in gene regulation. E.g., H2A.X differs from H2A by its C-terminus containing the serine residue (position 139 in humans), which rapidly becomes phosphorylated upon double-strand break (DSB) induction. Human H2A and H2A.X also

differ by four amino acids including a residue (N39H) located in the interfacial region of the H2A-H2B dimers (Fink et al. 2007; Bonisch and Hake 2012). The phosphorylated form named γ H2A.X is widely known as a DNA repair module and it is extensively used to monitor DNA damage response (DDR) (Bonner et al. 2008). In mammals, many hundreds of histone H2A.X molecules become phosphorylated (in ' γ H2A.X foci') within 10-30 min in the chromatin region flanking each newly formed DSB (up to several Mbs (Rogakou et al. 1999; Redon et al. 2012). DSBs can be formed in the DNA when cells are exposed to exogenous agents such as ionizing or UV radiation and certain chemicals (e. g. the Topoisomerase II (TOP2) inhibitor etoposide). ATM-dependent H2A.X phosphorylation occurs also in the absence of genotoxic stimuli and appears to play a role in transcriptional activation (Singh et al. 2015). Endogenous γ H2A.X was shown to be enriched at the transcription start site (TSS) of actively transcribed genes (Seo et al. 2012).

Epigenetic modifications on the N-terminal or C-terminal tails protruding from the nucleosome core particle and also on the globular domains can determine stability features of nucleosomes regulating histone-histone and histone-DNA interactions. The flexible, highly basic and mostly unstructured histone tails are known to interact with nucleosomal DNA (Mutskov et al. 1998), linker DNA (Angelov et al. 2001) and the regions of the neighboring nucleosomes containing acidic residues (Davey et al. 2002). The role of the epigenetic modifications in chromatin organization and gene regulation, is not completely understood. Histone modifications, such as negatively charged functional groups (acetylation, phosphorylation), can affect nucleosome stability directly by modifying the net charge of the histone proteins thus changing the strength of the histone-DNA interactions. Neutralization of the basic character of histone proteins by acetylation or phosphorylation may facilitate DNA unwinding and the transition from the transcriptionally inactive heterochromatic state to the transcriptionally active euchromatic state. Examples of a direct destabilizing effect of acetylation were observed by magnetic tweezer measurements (Anderson et al. 2001), single molecule force spectroscopy studies revealing that histone acetylation decreases the force required to mechanically unwrap nucleosomes (Brower-Toland et al. 2005), and single-molecule FRET studies indicating that histone acetylation increases nucleosome unwrapping (Lee et al. 2011) in isolated or *in vitro* reconstituted nucleosomes. However, randomly hyperacetylated nucleosomes have been used in most of these studies, which makes it difficult to assign how the different lysines in the tails, and within the folded portion of the histone core, contribute to the overall effects.

Beside PTMs, histone variants can also have direct effect on nucleosome stability. It was reported that H2A.Z can either increase or decrease nucleosome stability depending on the chromatin context. In an *in vitro* chromatin model system which consist of 12 repeats of a 208 bp nucleosome positioning sequence, H2A.Z facilitated intranucleosomal interaction increasing the intrinsic stability of nucleosomes. On the other hand, internucleosomal interactions were inhibited, increasing the sensitivity of the array to MNase digestion and influencing nucleosome positioning *in vitro* (Fan et al. 2002). Stronger H2A-H2B dimer-(H3-H4)₂ tetramer interactions were demonstrated in FRET experiments performed with *in vitro* reconstituted nucleosomes containing H2A.Z rather than canonical (prototypic, expressed in a replication dependent manner) H2A histones (Park et al. 2004). In genome wide studies, unusually labile H2A.Z containing nucleosomes, i.e. sensitive to low concentration of NaCl, were detected at the TSS region of transcriptionally active promoters (Jin et al. 2009). These labile nucleosomes were composed of H2A.Z together with histone variant H3.3 bordering nucleosome free regions. In another study, the hierarchy of stability features of nucleosomes containing different combinations of H2A, H2A.Z, H3 and H3.3 were investigated using isolated mononucleosomes (Jin and Felsenfeld 2007) and the results were interpreted in the context of the structural difference between H2A.Z and H2A in the loop-1 dimerization region. Replacement of H2A with H2A.Z in only one of the two dimers (hence named heterotypic nucleosome) could cause a structural clash sufficient to destabilize a nucleosome. However, no such a sterical hindrance could be observed in a recent crystallographic study (Horikoshi et al. 2016). On the other hand, the H2A.Z/H3.3 nucleosomes were unstable when both dimers were H2A.Z/ H2B (homotypic nucleosome) (Weber et al. 2010). H2A.Z isoform composition can also affect nucleosome stability. Two isoforms of H2A.Z are known to exist, encoded by separate genes, which differ by only 3 amino acids: H2A.Z1 and H2A.Z2. H2A.Z histone variants are indispensable for the survival of *Drosophila* and mice in view of the fact that knock-out animals are not viable; H2A.Z1 and Z2 may have different functions since H2A.Z2 could not compensate for the absence of H2A.Z1 in H2A.Z1 knock-out mice (Dryhurst et al. 2009).

The structural difference of the isoforms in the loop 1 region is assumed to influence the stability of the nucleosomes containing the different isoforms. However, an opposite conclusion on the relative stability features of H2A.Z1 and H2A.Z2 was reached in FRAP (Horikoshi et al. 2013) and in Western blot (Dryhurst et al. 2009) studies.

The effect of PTMs or histone variants on nucleosome stability has been subject to intensive research, via many different methodological avenues. Comparison of these

approaches (see below) has revealed the need for approaches allowing assessment of nucleosome stability features *in situ*, in the original sequence and epigenetic context of the particular nucleosomes to be studied, at a through-put matching the expenses incurred.

The techniques that have proven to provide the most informative data regarding nucleosome stability include biochemical or biophysical measurements on isolated or reconstituted nucleosomes (Ausio et al. 1984; McMurray and van Holde 1986; McMurray et al. 1991; Thambirajah et al. 2006; Gansen et al. 2009; Andrews and Luger 2011; Bohm et al. 2011; Chen et al. 2013), approaches based on metabolic labeling (Zheng et al. 2014; Farrelly et al. 2016), biochemical strategies embedded in genomic approaches (Henikoff et al. 2009; Teves et al. 2012), single-molecule, magnetic tweezer measurements (Chien and van der Heijden 2014; Vlijm et al. 2015), proteomic analyzes (Kimura et al. 2008; Zheng et al. 2014; Farrelly et al. 2016) and microscopic studies using transfected histones fused with fluorescent (Kimura and Cook 2001; Ikura et al. 2007) and photo-activatable proteins (Pang et al. 2013). The above methods assess dissociation of histones from the nucleosomes either in live cells where it occurs spontaneously, or when purified or reconstituted nucleosomes are exposed to different ionic environments, or by evoking changes of superhelicity with the help of mechanical torsion or intercalators. However, none of these methods can readily and rapidly address the stability of histones with a specific post-translational modification, i.e. within a given chromatin context, *in situ*. The biophysical techniques that rely on transfected constructs (Kimura and Cook 2001; Ikura et al. 2007; Pang et al. 2013) provide information on exogenous fusion products, carrying no PTMs, in relatively few cells, limiting their physiological relevance and accuracy. PTM specific information is derived from biochemical or biophysical studies involving *in vitro* modified, isolated or reconstituted nucleosomes without cell-to-cell resolution (Gansen et al. 2009; Lee et al. 2011). Genomics approaches to analyze histone turnover in a PTM specific manner also lack the individual cell's perspective and they are not adequate for screening type studies.

Laser scanning cytometry (LSC) is the technology of choice for automated, quantitative, high-throughput analyzes of samples attached to a surface, such as adherent cells, tissue specimens or agarose embedded cells. The LSC instrument that was used in my experiments is equipped with four lasers: 405 nm, 488 nm, 563nm, 633 nm and four photomultiplier tubes (PMTs), each detecting a specific wavelength range of fluorescence excited by the scanning lasers (for further methodical details see Materials and Methods). As the laser light intersects the sample, scattered or transmitted light is simultaneously directed to one or more photomultiplier tubes. The PMT signals are converted into images and the

events, such as cells, nuclei or other subcellular structures are identified and segmented on the basis of their fluorescence. From the segmented events, a variety of quantitative data are calculated: area, integral fluorescence, maximal pixel intensity, circularity, perimeter, x and y coordinates, and more. The numerical values are displayed in scattergrams and histograms, allowing assessment of relationships among the various features. The utility of this technique was demonstrated earlier by us for the studying of CpG methylation in (Szekvolgyi et al. 2009).

We have developed an assay based on quantitative imaging cytometry which delivers histone type and post-translational modification (PTM) specific information on the stability features of nucleosomes consisting of native endogenous or ectopically expressed histones as well, *in situ*, in the individual nuclei of a cell population, and what is amenable to high-throughput studies. In our method, agarose embedded cells are lysed and exposed to salt or to DNA intercalating agents, and the remaining chromatin-bound histones are detected using specific antibodies and quantitative microscopy conveniently performed by LSC, hence the name coined for the method: Quantitative Imaging of Nuclei after Elution with Salt/Intercalators (QINESIn). Exposure to salt will primarily affect electrostatic histone/histone/DNA interactions (Gloss and Placek 2002; Chien and van der Heijden 2014), while DNA intercalators extend, unwind, and at higher intercalator concentrations overwind the DNA, constraining the histone-DNA contacts (Gunther et al. 2010; Pang et al. 2013). DNA intercalators also increase the DNA melting temperature (Bjorndal and Fygenon 2002) and are expected to affect higher-order chromatin structure (Rabbani et al. 1999; Rabbani et al. 2005).

B. 2. RESULTS

B. 2. 1. PTM-dependence of nucleosome stability

The workflow for QINESIn (shown in **Figure 7A**) involves: 1) elution of histones using either intercalators in the presence of 0.75 M NaCl (see below), or salt alone, to assess DNA superhelicity dependent and overall stability, respectively, and 2) measurement of the fraction of histones remaining chromatin-bound in the individual nuclei using histone type- or PTM-specific antibodies (**Figure 7B, C**). For validation purposes, we reproduced previously published observations on nucleosome eviction by doxorubicin intercalation (Pang et al. 2013; Yang et al. 2013). Eviction of H3K4me3 was confirmed by elution with doxorubicin analyzed in parallel by LSC (**Figure 7B**) and ChIP-Seq (chromatin immunoprecipitation sequencing) (**Figure 7D**) in mES cells (mouse embryonic stem cells).

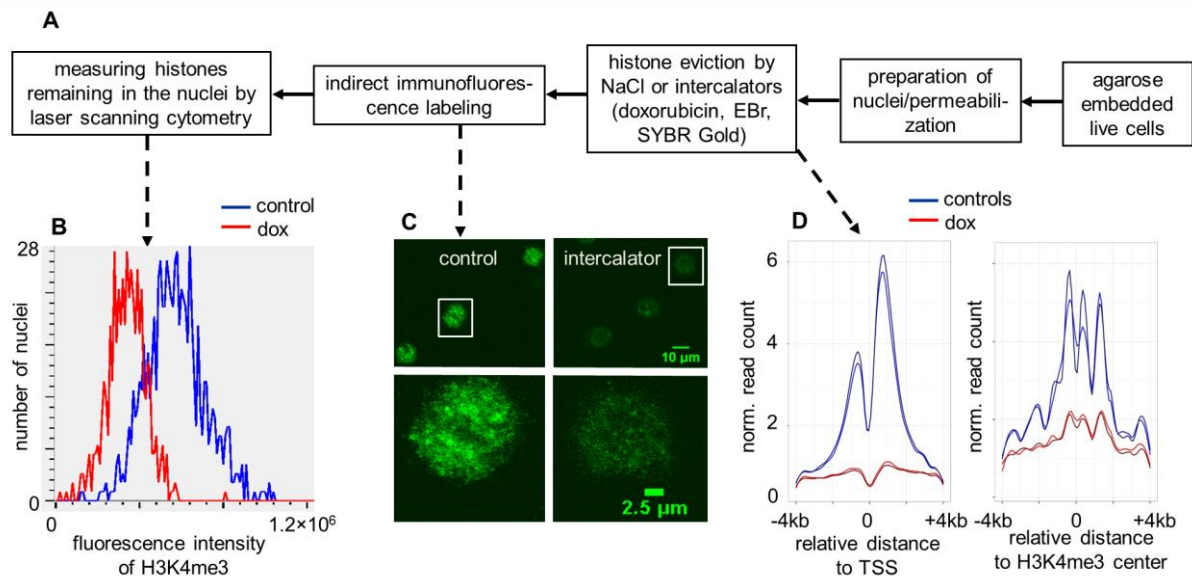


Figure 7. Doxorubicin induced eviction of nucleosomes.

(A) Flow-chart of the method. Histones remaining in the nuclei after treatment with increasing concentration of NaCl or intercalator solutions were detected by indirect immunofluorescence labeling and quantitatively analyzed by laser scanning cytometry (LSC). Arrows with continuous line connect the main steps of the experiment from right to left. Arrows with dashed line point at the results of the LSC (left), confocal microscopic (CLSM, middle) and ChIP-Seq studies (right).

(B) Immunofluorescence intensity distribution histograms of H3K4me3 marked nucleosomes in the nuclei of control (blue) and doxorubicin treated (18 μM ; red) G1 phase mES cells. Integral fluorescence values for ~ 400 G1 nuclei were measured by LSC.

(C) H3K4me3 immunofluorescence staining of mES nuclei: representative CLSM images, before (control) and after (dox) intercalator treatment.

(D) ChIP-Seq density profiles in the samples analyzed by LSC (see panel (B)). H3K4me3 ChIP-seq analyzes were performed in two technical replicates of the doxorubicin treated (red) and control (blue) samples. Anchor-plots of H3K4me3 sites around transcription start sites (TSSs; left) and around H3K4me3 positive non-TSS sites (right) are shown. ChIP-Seq signals were plotted in a ± 4 kb window. The Y axis shows the averaged read counts of the detected regions (tags normalized to 10 million). The ChIP-Seq data were obtained in collaboration with Zoltán Simándi and Attila Horváth.

In agreement with ref. (Pang et al. 2013), the H3K4me3 carrying promoter-proximal nucleosomes were more sensitive to doxorubicin treatment than bulk H3 histones (**Figure 8**).

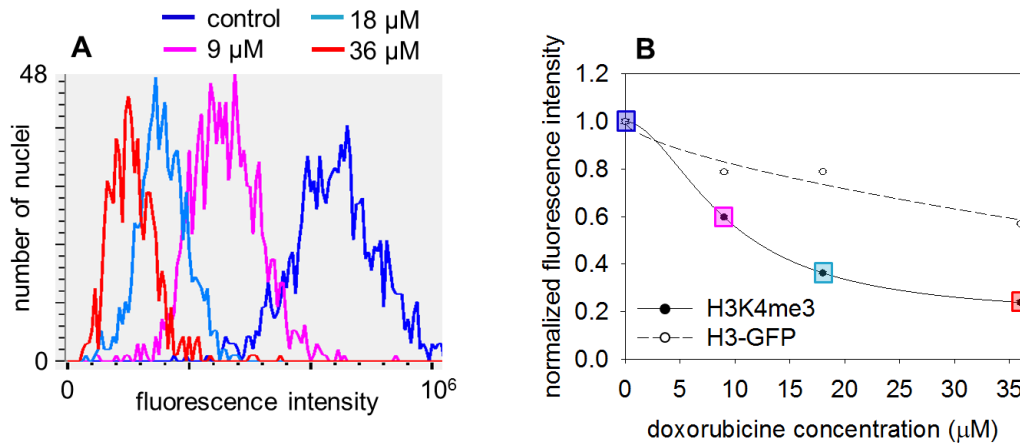


Figure 8. H3K4me3 and bulk H3 elution profiles obtained upon doxorubicin treatment of live HeLa cells.

(A) Immunofluorescence intensity distribution histograms of H3K4me3 in the nuclei of control (blue) and doxorubicin treated G1 phase HeLa cells, using the following concentrations of the drug: 9 μM (magenta), 18 μM (light blue) and 36 μM (red). Integral fluorescence values for ~ 600 G1 nuclei were measured by LSC. Doxorubicin treatment was performed on H3-GFP expressing HeLa cells. The means of the H3-GFP signal (not shown in this panel) are plotted together with those of immunofluorescence on panel B.

(B) Elution profiles constructed from the fluorescence distribution histograms generated by LSC. The curves demonstrate the decreasing levels of chromatin bound H3K4me3 (according to the color code used on panel A) and of the H3-GFP, used as internal reference, as a function of doxorubicin concentration. The curves refer to G1 phase cells gated according to their DNA fluorescence distribution. Error bars represent SEM of ~ 600 G1 nuclei measured by LSC.

H3K4me3 marked nucleosomes were evicted completely from the TSS at most of the active genes (~ 6000 genes) when the intercalator doxorubicin was used at concentrations close to the plasma levels reached in cancer chemotherapy (Greene et al. 1983); (**Figure 7D**, left panel). The H3K4me3 signals were also decreased by the intercalator treatment in regions outside TSSs (**Figure 7D**, right panel). These results were further validated using ChIP-qPCR conducted at different doxorubicin concentrations carried out on a pair of genes known to be

expressed and non-expressed in mES cells, respectively (data obtained in collaboration with Zoltán Simándi, published in (Imre et al. 2017)).

It was also demonstrated that doxorubicin itself was sufficiently washed out from the samples in the course of the experiment so as not to inhibit amplification and subsequent steps of the ChIP-Seq or ChIP-qPCR workflow (data obtained in collaboration with Zoltán Simándi, published in (Imre et al. 2017)), a potentiality, stemming from an elevated melting temperature (Bjorndal and Fyngenson 2002), not considered and ruled out before (Pang et al. 2013).

GFP-tagged versions of histones H2B and H3 also exhibited differential doxorubicin sensitivity (**Figure 9A**), as expected (Pang et al. 2013). The difference between the binding stability of the H2A-H2B dimer and that of the (H3-H4)₂ tetramer within the nucleosome was much more pronounced when another intercalator dye, EBr was used (note the log scale and the ~100-fold difference in **Figure 9B**). The elution profiles obtained with EBr were very similar at 4 °C and at RT.

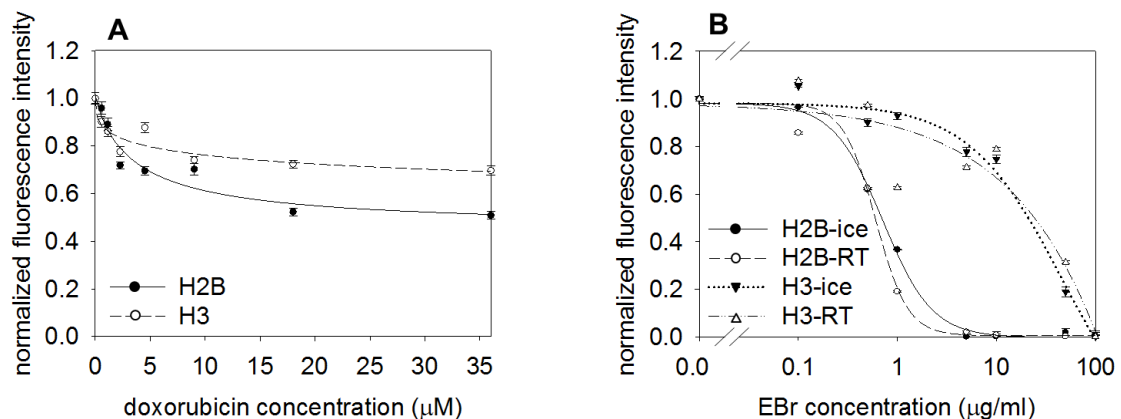


Figure 9. H2A-H2B dimer and (H3-H4)₂ tetramer exhibit different intercalator sensitivity.

(A) Doxorubicin induced H2B-GFP and H3-GFP elution in histone-GFP expressor HeLa nuclei.

(B) EBr induced elution of H2B-GFP and H3-GFP performed on ice and at room temperature (RT) in histone-GFP expressor HeLa nuclei. EBr was applied in the presence of 0.75 M NaCl.

The curves refer to G1 phase cells gated according to their DNA fluorescence distribution. Error bars represent SEM of ~600 G1 nuclei measured by LSC.

The dynamic range of EBr titration was best when it was added in the presence of 0.75 M salt (**Figure 10**).

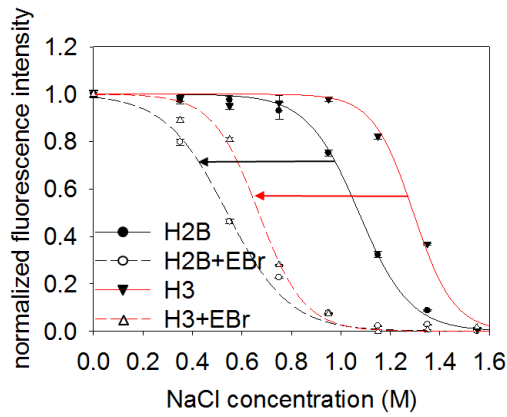


Figure 10. Effect of co-treatment with EBr and salt. The arrows show the shift of elution curves in the presence of 100 µg/ml EBr. The curves refer to G1 phase cells gated according to their DNA fluorescence distribution. Error bars represent SEM of ~600 G1 nuclei measured by LSC.

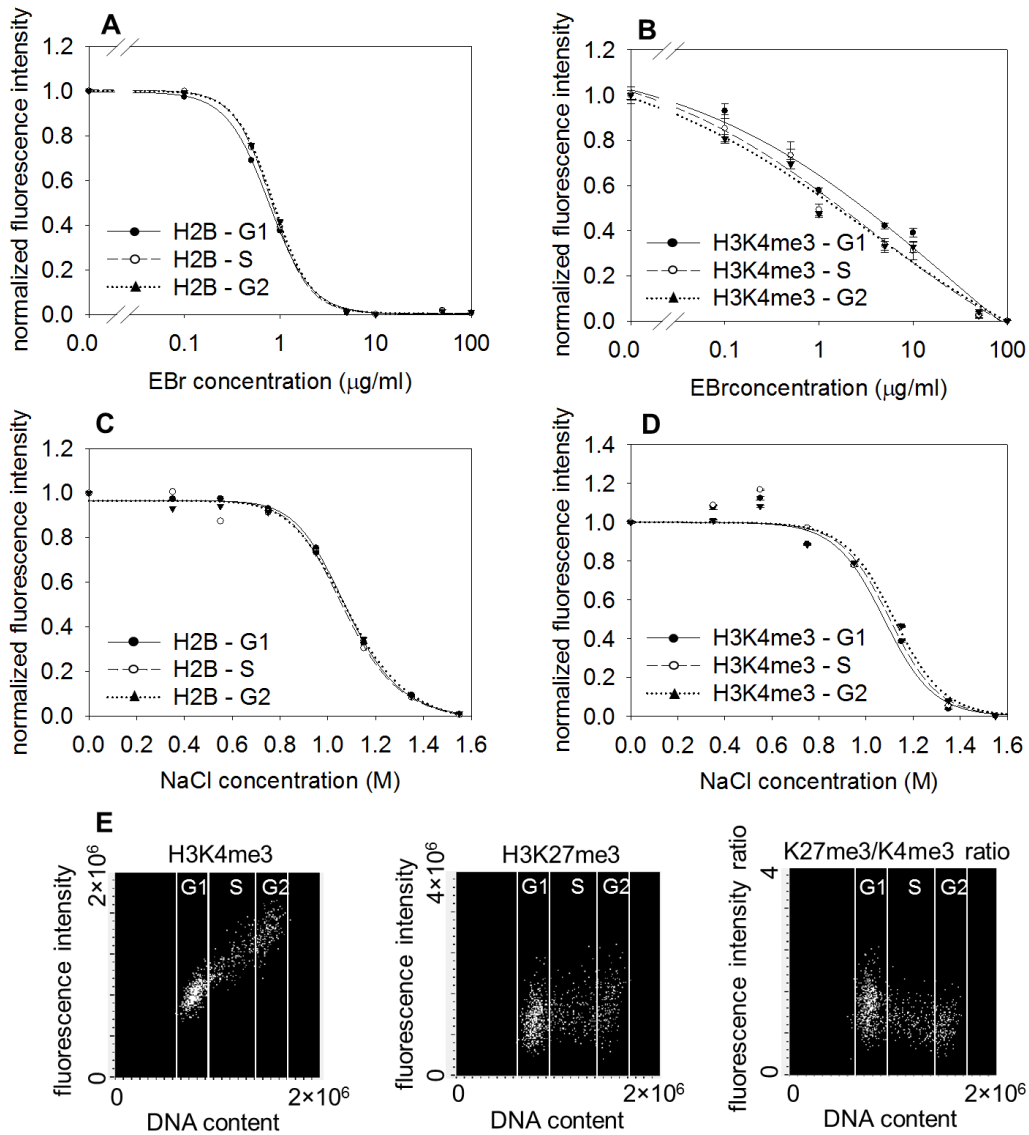


Figure 11. Histone elution analyzed according to different cell cycle phases.

EBr elution profiles of H2B-GFP (A) and H3-GFP (B), and NaCl elution profiles of H2B-GFP (C) and H3-GFP (D) in the nuclei of G1, S and G2 phase HeLa cells identified by gating on the DNA fluorescence distributions within non-synchronized cell populations.

Error bars represent SEM of ~600 G1 nuclei measured by LSC.

(E) Scattergrams of H3K4me3 (left panel), H3K27me3 (middle panel) immunofluorescence, and of the H3K27me3/K4me3 ratio values (right panel) of the individual nuclei as a function of DNA content. Each dot on the scattergrams represents a single nucleus co-labeled with mouse monoclonal anti-H3K4me3 and rabbit monoclonal anti-H3K27me3, stained by the appropriate dye-conjugated secondary antibody.

As shown in **Figure 11**, QINESIn was able to resolve the cell cycle distribution of the nuclei analyzed, yielding cell cycle phase-specific information on the stability features studied as well as on the overall modification levels.

The differential eviction of H3K4me3 and H3K27me3-containing nucleosomes reported earlier (Pang et al. 2013) could also be reproduced by QINESIn in intercalator elution using EBr (**Figure 12A**). Similar elution profiles were determined for H3K27me3 and H3-GFP, while H3K4me3 was significantly destabilized relative to H3-GFP, using H3-GFP as an internal control for both experiments (compare **Figure 12A** and **B**). The difference in the stability features of the H3K4me3 and H3K27me3-containing nucleosomes were also observed in mES and in neural progenitor cells (NPC) differentiated from mES (**Figure 12C**).

The patterns and extent of nuclear H3K4me3 and H3K27me3 signals were different. H3K23me3 showed peripheral while H3K4me3 showed intranuclear localization (**Figure 12D**).

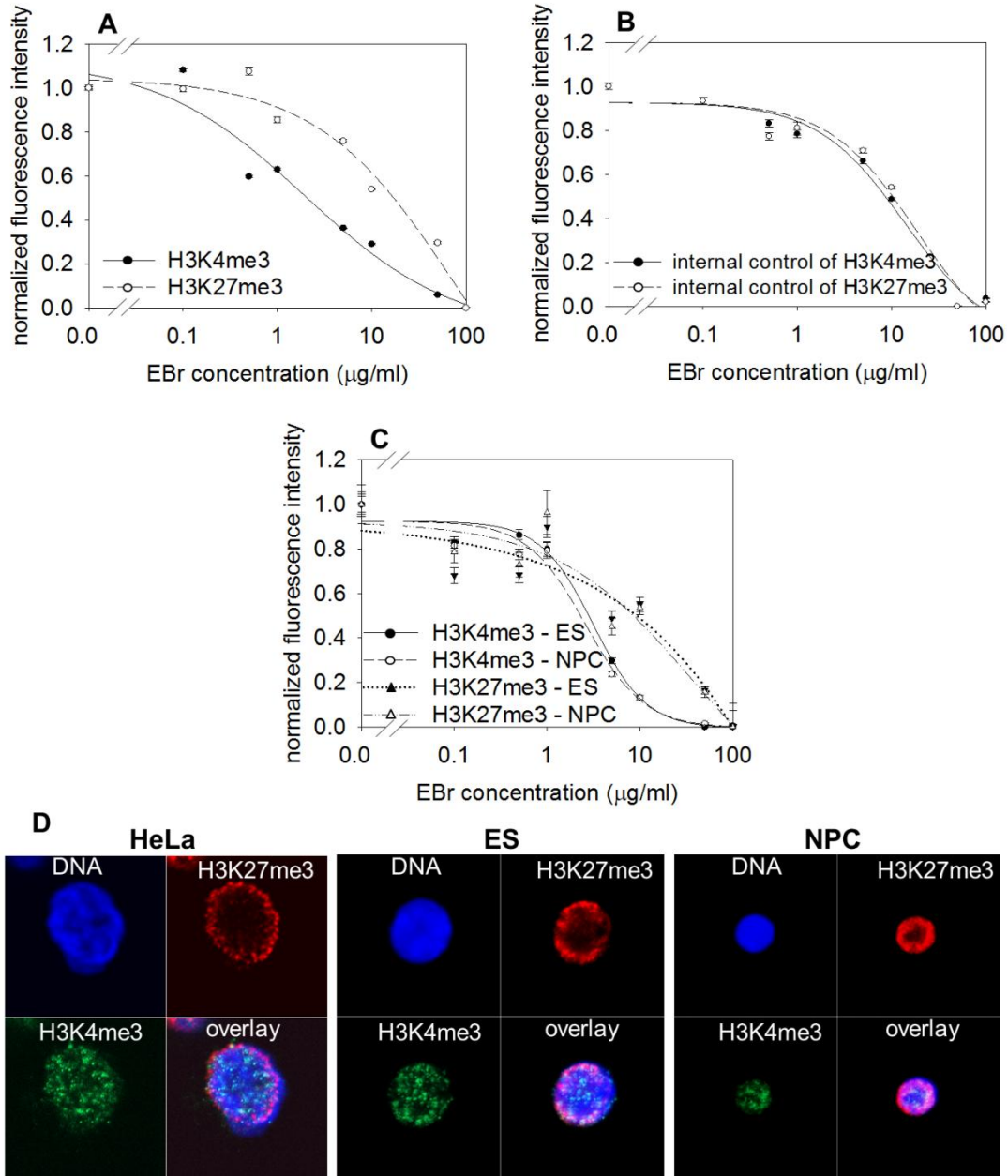


Figure 12. Intercalator induced elution is PTM-dependent.

(A) EBr elution profiles of H3K4me3 or H3K27me3 in HeLa nuclei.

(B) H3-GFP (used as internal control) elution curves in the experiment on panel (A).

(C) EBr elution profiles of H3K4me3 or H3K27me3 in mES and NPC nuclei.

(D) Nuclear localization of H3K4me3 and H3K27me3 fluorescence signals in HeLa, mES and NPC nuclei (CLSM images).

The curves refer refer to G1 phase cells gated according to their DNA fluorescence distribution. Error bars represent SEM of ~600 G1 nuclei measured by LSC.

The relatively destabilized character of the H3K4me3 nucleosomes was detected using two different monoclonal antibodies, and the specificity of antibody binding was verified in competition experiments using a H3K4me3 derived peptide. Moreover, using the H3K4me3 reader TAF3-derived recombinant protein (Lauberth et al. 2013; Kungulovski et al. 2014) it was also shown that reader-unbound as well as the reader-engaged H3K4me3 epitopes (such as that of TAF3) become labeled by the antibody in our protocol.

Next, we tested if the well-known differential dissociation of the H2A-H2B dimer vs. the (H3-H4)₂ tetramer from the nucleosome by *salt* could also be monitored by the QINESIn platform. As shown in **Figure 13A**, the assay was able to clearly distinguish between these two histone complexes. The dimer-tetramer differences seen by intercalator elution, and the differences between H3K4me3 and H3K27me3 EBr elution profiles were also observed via salt elution, in HeLa (**Figure 13B**; using H3-GFP as an internal control, shown in **Figure 13C**), in mES as well as in NPC (**Figure 13D**).

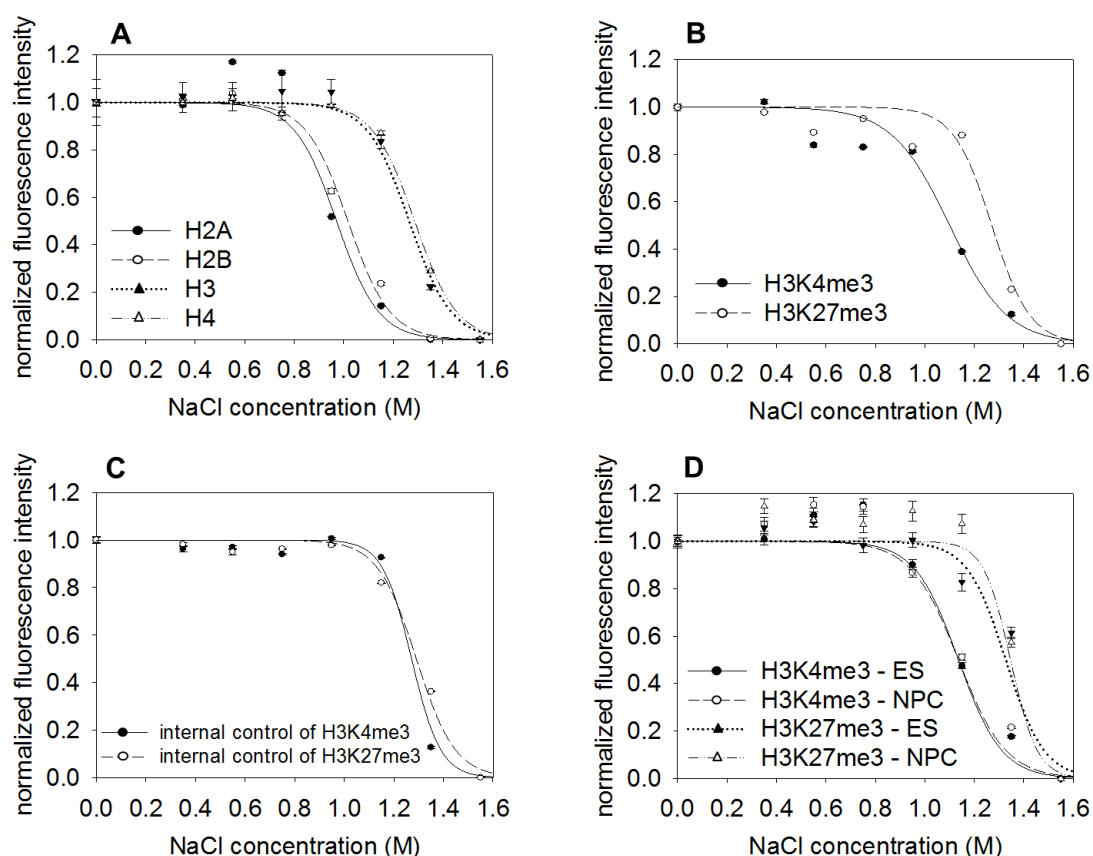


Figure 13. Salt induced elution is histone type and PTM-dependent.

(A) Salt elution profiles of antibody detected H2A, of H2B-GFP, H3-GFP and H4-GFP in histone-GFP expressor HeLa nuclei.

(B) Salt elution profiles of H3K4me3 and H3K27me3 in HeLa nuclei.

(C) H3-GFP elution curves (internal control) in the experiment of panel (B).

(D) Salt elution profiles of H3K4me3 and H3K27me3 in mES and NPC nuclei.

The curves refer to G1 phase cells gated according to their DNA fluorescence intensity distribution and the error bars represent SEM of ~600 G1 nuclei measured by LSC.

In summary, the above observations confirm that the results obtained by QINESIn, used in either salt elution or intercalator elution format, are in good agreement with what is expected based on published data generated by various other approaches. The utility and sensitivity of the current approach is exemplified below by analyzing first the stability of nucleosomes containing H2A.Z histone variants, then the effects of H2A.X phosphorylation.

B. 2. 2. Effect of histone variants on nucleosome stability

To investigate the effect of histone variants on nucleosome stability, first H2A.Z containing nucleosomes were analyzed by QINESIn using anti-H2A.Z antibodies from different manufacturers. (Those on H2A.Z below are unpublished data.) The two antibodies that were used to measure H2A.Z eviction gave different results in the salt elution assay (**Figure 14A**). Surprisingly, the elution profile of H2A.Z, detected by an anti-H2A.Z antibody from Abcam (ab 97966, hereafter: Abcam1) was similar to that obtained for bulk H3, while the other antibody purchased from Thermo Fisher Scientific (TFS) revealed H2A-like stability features. (**Figure 14B**),

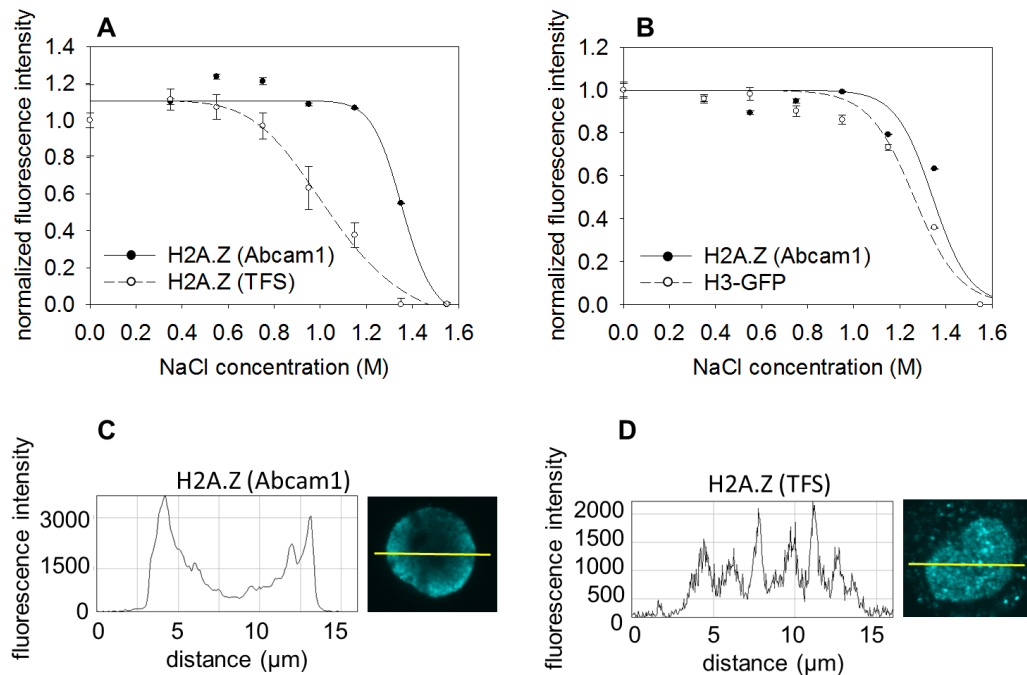


Figure 14. Salt elution curves of histone variant H2A.Z and GFP-tagged “bulk” H3.

(A) Elution curves of H2A.Z in nuclei treated with different concentrations of salt solutions detected by indirect immunofluorescence labeling using H2A.Z specific polyclonal antibodies from different manufacturers: Abcam, catalogue number: ab 97966; TFS catalogue number: PA5-17336.

(B) Comparison of the salt elution profiles of H2A.Z detected by Abcam1 antibody and H3-GFP (used as internal control).

(C and D) Nuclear localization of H2A.Z recognized by (C) the Abcam1 antibody or (D) the TFS antibody.

The elution curves refer to G1 phase cells gated according to their DNA fluorescence intensity distribution and the error bars represent SEM of ~600 G1 nuclei measured by LSC.

Analyzing the nuclear localization of H2A.Z recognized by antibodies from different manufacturers, differences in the distribution patterns could be observed: H2A.Z visualized by the Abcam1 antibody was more peripheral (**Figure 14C**), while H2A.Z detected by the TFS antibody was distributed all over the nucleus, defining numerous distinct foci (**Figure 14D**). These observations were in line with the microscopic images in the the manufacturers' datasheets of the antibodies.

The salt elution curves measured by the Abcam1 antibody raised against the C-terminus of H2A.Z was similar to that of the heterochromatic histone marks, suggesting that this antibody may recognize H2A.Z molecules ubiquitinated on the C-terminus and known to localize preferentially in heterochromatic regions. To analyze the effect of ubiquitination on H2A.Z stability, salt elution assays were performed after treatment of live cells with PYR-41, a membrane permeable inhibitor of the ubiquitin-activating enzyme E1. No significant changes after PYR-41 treatment were detected, either in the mean fluorescence intensities (showing expressions levels) or in the elution curves (**Figure 15**).

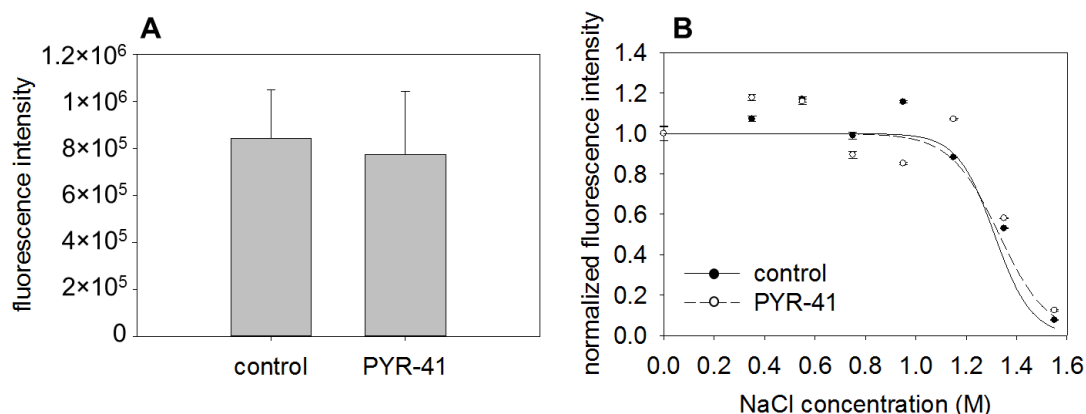


Figure 15. Effect of PYR-41 inhibitor.

(A) Effect of PYR-41 inhibitor on the nuclear levels of H2A.Z detected by the Abcam1 antibody. Error bars represent SD of ~600 G1 nuclei measured by LSC.

(B) Effect of PYR-41 inhibitor on the eviction of nucleosomes containing H2A.Z measured by salt elution using the Abcam1 antibody. Error bars represent SEM of ~600 G1 nuclei measured by LSC.

The bar chart and the elution curves refer to G1 phase cells gated according to their DNA fluorescence intensity distribution.

To test if the two antibodies might recognize different isoforms of H2A.Z, plasmid-derived, transfected H2A.Z isoforms expressed as fluorescent fusion proteins were analyzed. Comparing the CFP-tagged H2A.Z1 and the YFP-tagged H2A.Z2, no difference in salt elution could be observed (**Figure 16A**) and the elution profiles were similar to bulk H2A (**Figure 16B**), and to H2A.Z detected with the TFS antibody (**Figure 14A**).

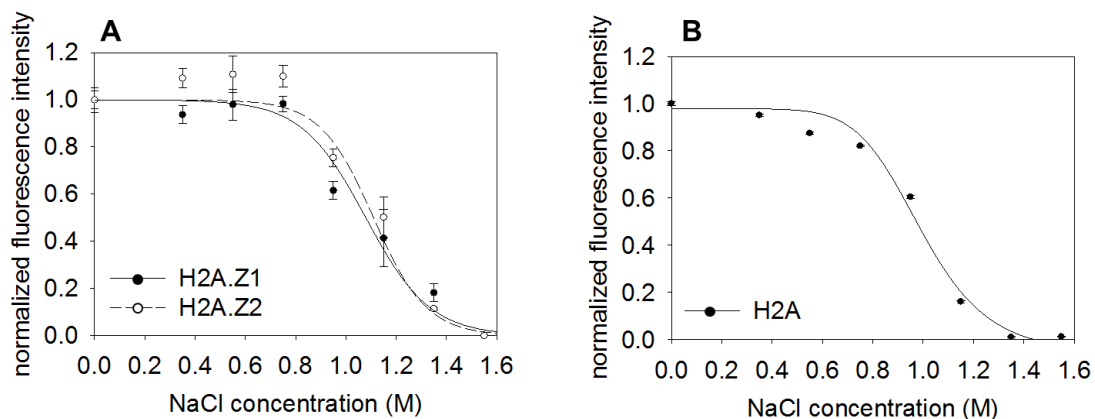


Figure 16. Salt elution profile of H2A.Z isoforms compared with bulk H2A.

(A) Elution curves of the CFP-tagged H2A.Z1 and YFP-tagged H2A.Z2 isoforms.

(B) Salt elution curve of bulk H2A detected by indirect immunofluorescence labeling.

The elution curves refer to G1 phase cells gated according to their DNA fluorescence intensity distribution and the error bars represent SEM of ~600 G1 nuclei measured by LSC.

Measurements were also performed on endogenous, native H2A.Z1 and H2A.Z2 histones using H2A.Z1 KO or H2A.Z2 KO cells (Matsuda et al. 2010). The Abcam1 antibody recognized both Z1 and Z2 isoforms and no difference could be detected in the elution profiles. These results were verified using another antibody (ab4147) from Abcam (hereafter: Abcam2) as well (**Figure 17**).

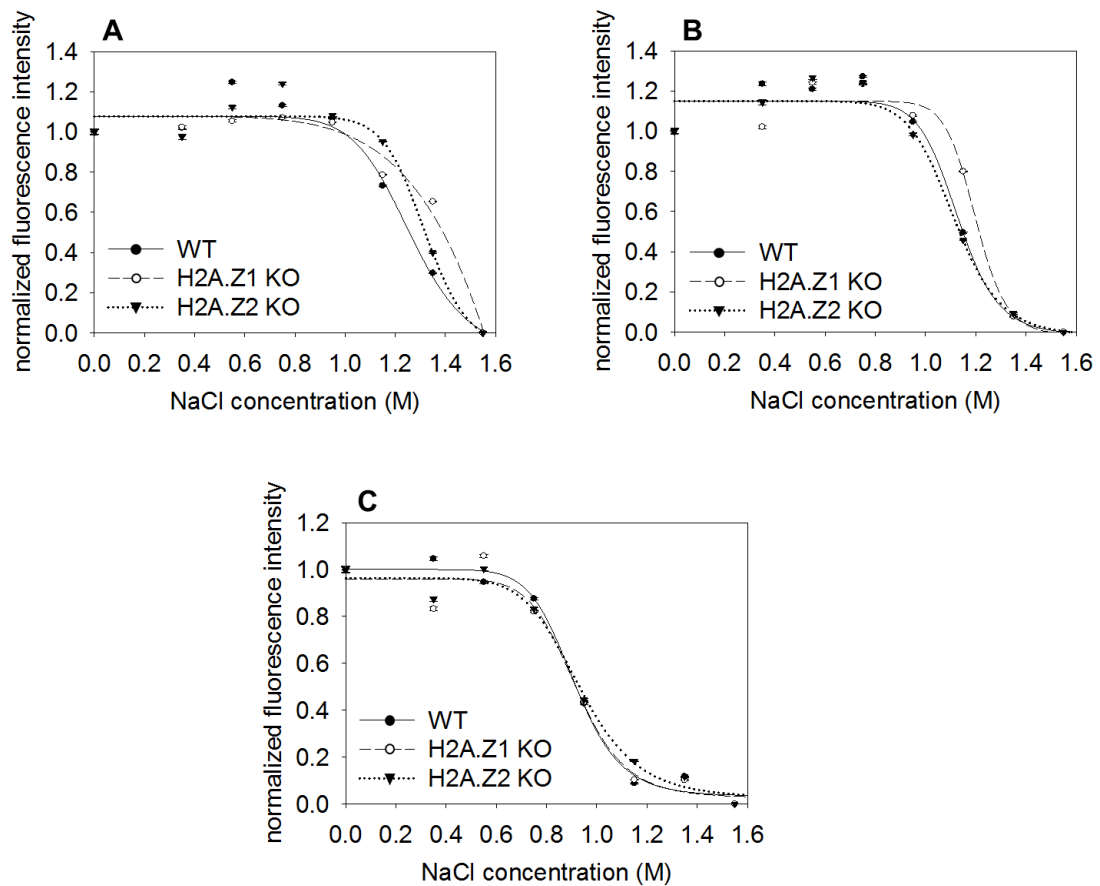


Figure 17. Salt elution profile of endogenous, native H2A.Z isoforms.

(A) Salt elution measurement of H2A.Z using Abcam1 antibody.

(B) Salt elution measurement of H2A.Z using Abcam2 antibody.

(C) H2B co-labeled with Abcam1 was used as internal control.

The curves refer to G1 phase cells gated according to their DNA fluorescence intensity distribution. Error bars represent SEM of ~600 G1 nuclei measured by LSC.

In further experiments, I tested H2A.Z mutants in which (1) the C-terminal tail was deleted (ΔC) removing the binding site of the H2A.Z reader protein PWWP2A, or (2) the lysines of the N-terminal tail that can be acetylated were changed to arginine (5KR). These mutant histones were expressed in H2A.Z1/Z2 double knock out cells (Punzeler et al. 2017). The salt elution curve of the ΔC mutant was shifted to the left, showing that the H2A.Z ΔC containing dimers become as destabilized as the canonical dimers (**Figure 18**). Based on these data, PWWP2A has got a major role in the regulation of the stability of nucleosomes containing H2A.Z. Measuring the salt elution curve of the 5KR mutant lacking acetylation had no effect on nucleosome stability (**Figure 18**).

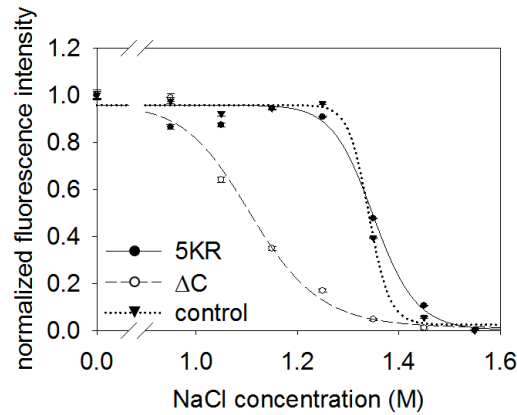


Figure 18. Salt elution profile of H2A.Z mutants.

Salt elution profile of H2A.Z 5KR and H2A.Z Δ C mutants compared with control cells, using the H2A.Z-specific Abcam1 antibody.

The curves refer to G1 phase cells gated according to their DNA fluorescence intensity distribution. Error bars represent SEM of ~600 G1 nuclei measured by LSC.

Using EBr as a destabilizing agent, the H2A.Z (detected by Abcam1) elution profile was similar to that of the canonical H2B. However, a major intercalator-resistant fraction remained **Figure 19**.

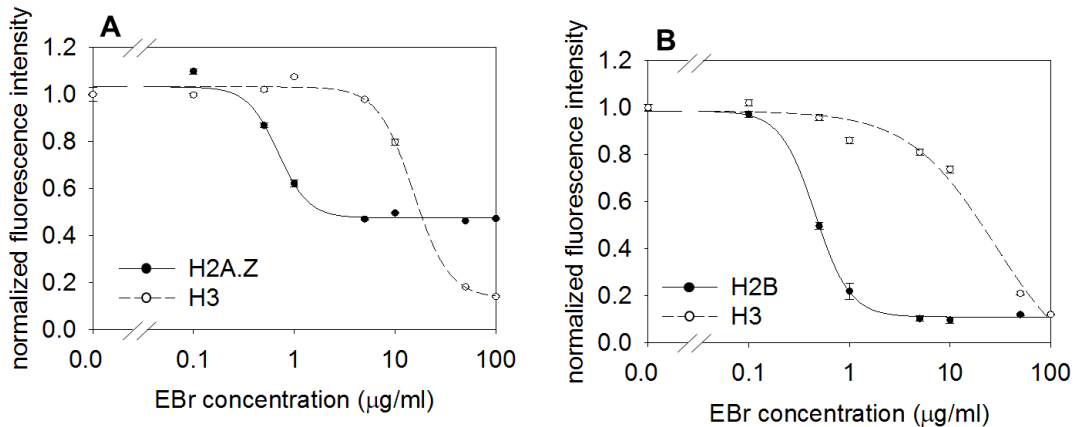


Figure 19. EBr elution profile of the Abcam1-detected H2A.Z (Abcam1) compared with the canonical histones H2B and H3.

(A) EBr elution profile of H2A.Z compared to GFP-tagged H3 used as internal control.

(B) EBr elution profile of GFP-tagged H2B and H3 demonstrates almost complete eviction of dimers and tetramers containing canonical histones in the same conditions as in (A).

Normalization was done only to “1” but not to “0” value of the Y axis (see Methods) to show the fraction of residual histons at maximum intercalator concentration. The curves refer to G1 phase cells gated according to their DNA fluorescence intensity distribution. Error bars represent SEM of ~600 G1 nuclei measured by LSC.

The levels of H2A.Z remaining after intercalator treatment were lower in the absence of PWWP2A binding, showing that the difference between H2A.Z and canonical H2A is PWWP2A-related also in the case of EBr elution. (**Figure 20.**)

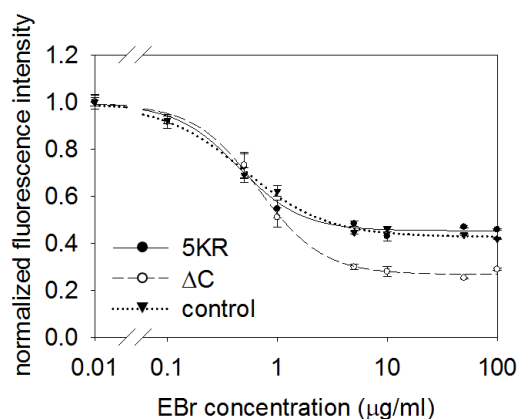


Figure 20. EBr elution profiles of H2A.Z mutants.

EBr elution profile of H2A.Z 5KR and H2A.Z Δ C mutants compared with control cells, using the H2A.Z-specific Abcam1 antibody.

The curves refer to G1 phase cells gated according to their DNA fluorescence intensity distribution. Error bars represent SEM of \sim 600 G1 nuclei measured by LSC.

Analyzing intercalator resistance of nucleosomes at different cell cycle phases, no difference could be observed between G1, S and G2 **Figure 21.**

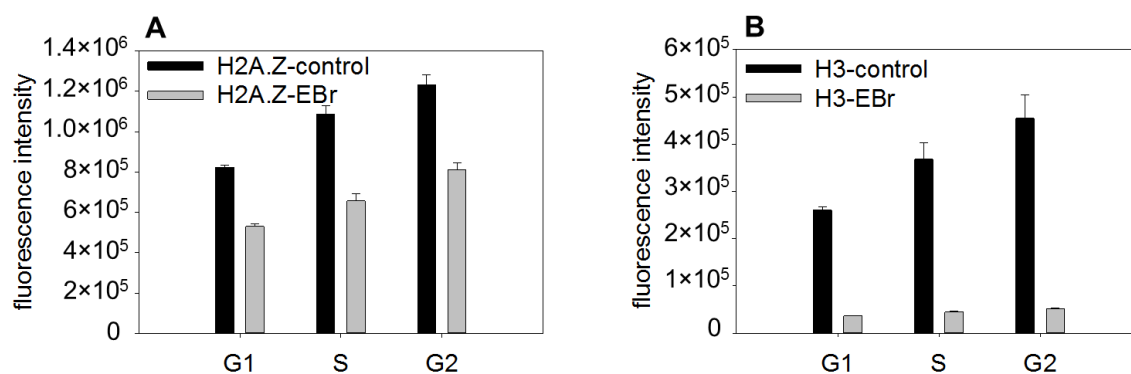


Figure 21. Comparison of the intercalator resistance of Abcam1-detected H2A.Z and H3-GFP in the different phases of the cell-cycle.

(A) Partial eviction of H2A.Z elicited by 100 μ g/ml EBr in all the phases of the cell-cycle.

(B) The degree of H3-GFP eviction elicited by 100 $\mu\text{g/ml}$ EBr is near-complete in the different phases of the cell-cycle

Cell cycle phases were gated according to their DNA fluorescence intensity distribution and the error bars represent SEM of ~ 600 G1 nuclei measured by LSC

H2A.Z (Abcam1) was eluted almost completely and homogenously upon high salt treatment (**Figure 22A**); intercalator resistant H2A.Z molecules were present in distinct foci after elution with the highest concentration (100 $\mu\text{g/ml}$) of EBr (**Figure 22B**).

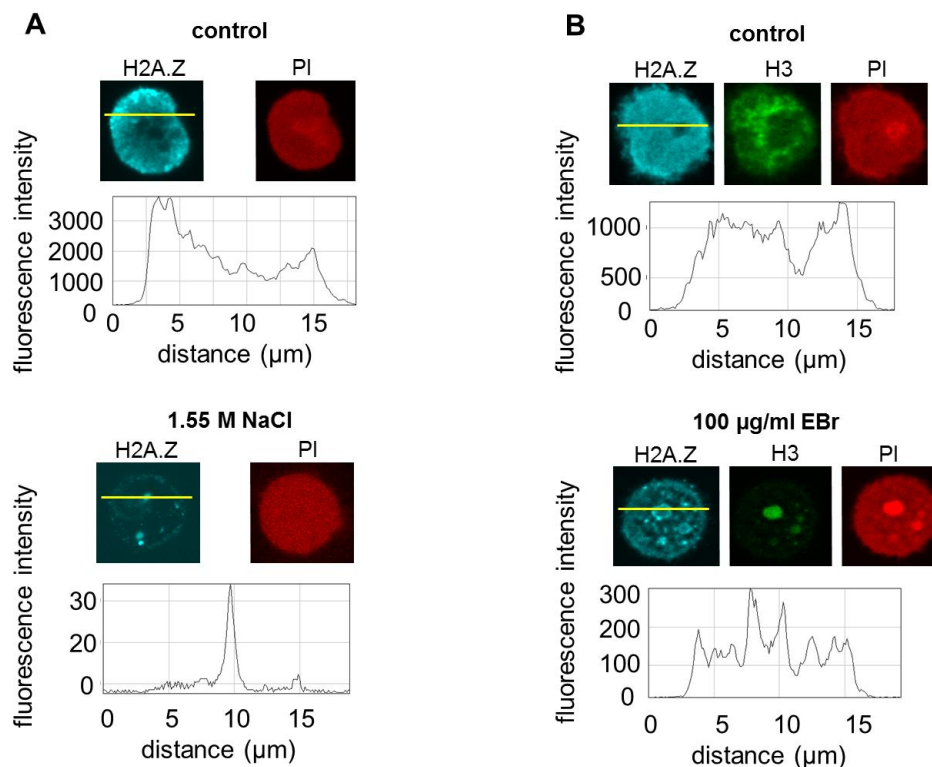


Figure 22. Nuclear localization of H2A.Z (Abcam1) before and after eviction by salt or intercalator.

(A) CLSM images and line scans of H2A.Z in the absence (control) and in the presence of 1.55 M salt.

(B) CLSM images and line scans of H2A.Z in the absence (control) and in the presence of 100 $\mu\text{g/ml}$ EBr. EBr elution was performed in the presence of 0.75 M NaCl. H3GFP was used as internal control.

The intercalator resistant H2A.Z (Abcam1) population was further investigated by salt elution. After removing the intercalator sensitive fraction of H2A.Z, the nucleosomes that remained in the chromatin were treated with increasing concentrations of salt solutions and

elution curves were recorded. Comparing the salt elution profiles of intercalator resistant H2A.Z (pre-treated with 100 $\mu\text{g/ml}$ EBr) and all H2A.Z (EBr non-treated control), no significant difference could be measured in any of the cell-cycle phases (**Figure 23**).

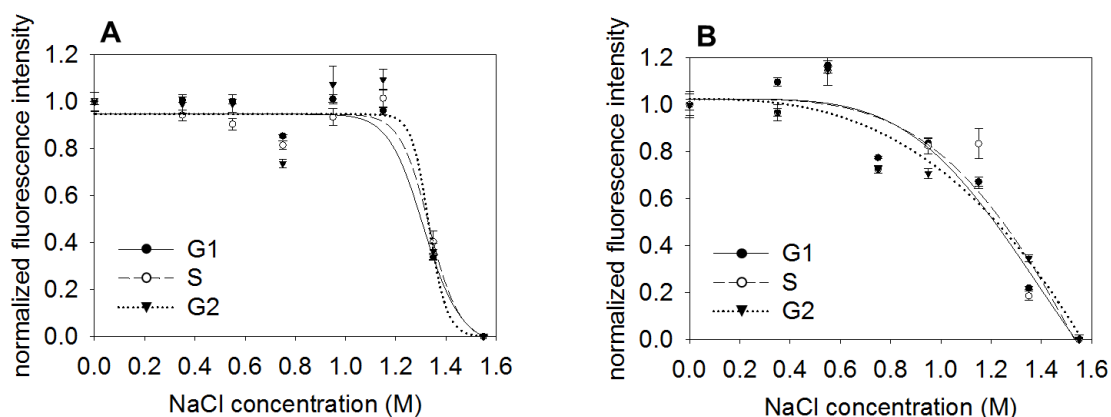


Figure 23. Salt elution curves of H2A.Z (Abcam1): all vs. intercalator resistant nucleosomes.

(A) Salt elution curves of all H2A.Z in the different phases of the cell-cycle.

(B) Salt elution curves of intercalator resistant H2A.Z in the different phases of the cell-cycle.

Nuclei were pretreated with 100 $\mu\text{g/ml}$ EBr to remove the intercalator sensitive fraction of H2A.Z before salt elution. The intercalator was washed out from the nuclei (at 4°C, overnight) before the salt elution curves were obtained.

The curves refer to G1 phase cells gated according to their DNA fluorescence intensity distribution. Error bars represent SEM of ~ 600 G1 nuclei measured by LSC.

There was a difference in the avidity of the anti-H2A.Z antibody (Abcam1) binding to the EBr sensitive vs. resistant subpopulation of H2A.Z. The K_d of antibody binding to the H2A.Z epitopes still available after EBr treatment was ~ 3 times smaller than that of its binding to all of the epitopes recognized by the same polyclonal antibody (**Figure 24**). In view of the results implicating PWWP2A binding in conferring intercalator resistance to a subpopulation of H2A.Z (**Figure 20**), these observations are best interpreted by assuming that the reader protein masks certain epitopes and allows others to be recognized by the polyclonal antibody.

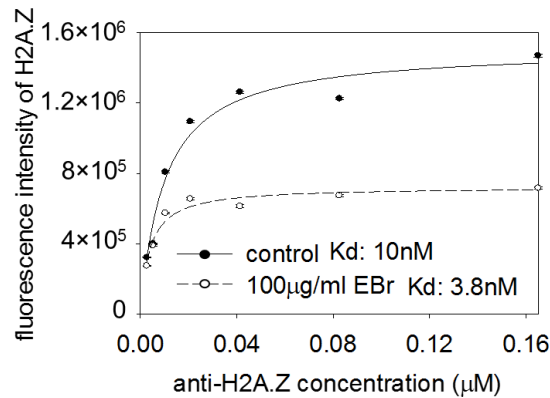


Figure 24. Determination of the dissociation constants (K_d) of anti-H2A.Z antibody (Abcam1) in nuclei containing total H2A.Z (control) and nuclei containing only the intercalator resistant H2A.Z species. The intercalator sensitive H2A.Z subpopulation was evicted by treatment with 100 µg/ml EBr. The curves refer to G1 phase cells gated according to their DNA fluorescence intensity distribution and the error bars represent SEM of ~600 G1 nuclei measured by LSC.

The intercalator resistant fraction was further characterized after elution by high salt. SDS-PAGE was performed and the resultant bands were analyzed by MS **Figure 25**.

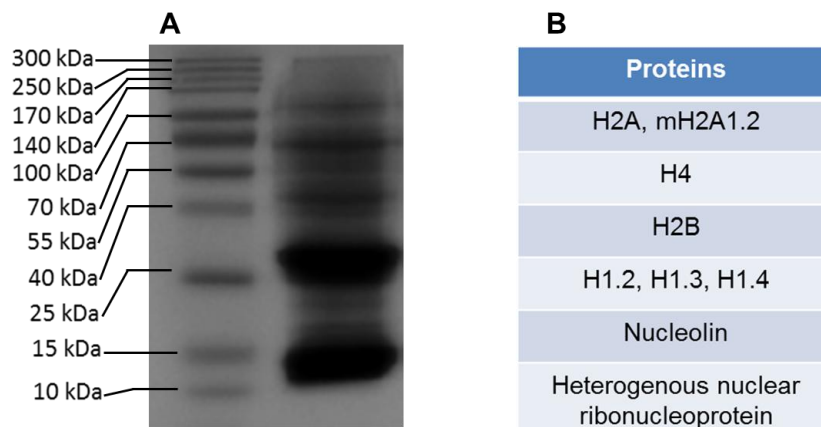


Figure 25. Proteomic characterization of the intercalator resistant fraction of proteins.

(A) SDS-PAGE analysis of the intercalator resistant fraction of proteins remaining chromatin-bound after treatment with 100 µg/ml EBr. Intercalator resistant proteins were eluted by 2 M NaCl.

(B) Bands detected on SDS-PAGE (panel A) were cut out and further analyzed by MS. Proteins detected by MS are listed in the table. (Gel electrophoresis and MS were performed by the Proteomics Core Facility of the Department of Biochemistry and Molecular Biology, University of Debrecen)

The histone variants H2A.X and γ H2A.X (phosphorylated H2A.X) were also analyzed by QINESIn (Imre et al. 2017). Significant destabilization of nucleosomes containing H2A.X was observed in salt elution but not in EBr elution experiments following phosphorylation of the histone variant by brief exposure of cells to etoposide (**Figure 26A, B**; focusing on a narrower intercalator concentration range to increase precision).

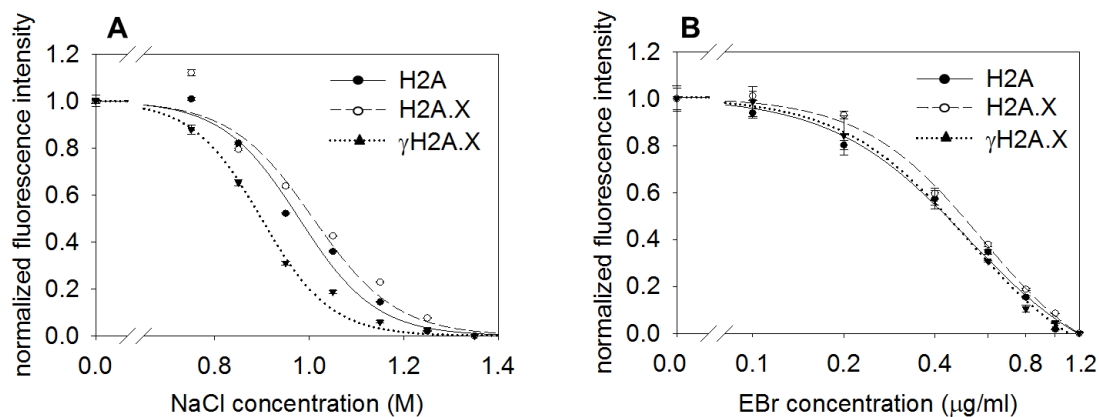


Figure 26. Stability features of histone variant H2A.X.

(A) Salt elution profiles of γ H2A.X, H2A.X and H2A, measured in parallel in the nuclei of HCT116 cells exposed to 25 μ M etoposide.

(B) EBr elution profiles of γ H2A.X, H2A.X and H2A measured in parallel, in the nuclei of etoposide treated HCT116 cell sample.

The curves refer to G1 phase cells gated according to their DNA fluorescence intensity distribution. Error bars represent SEM of \sim 600 G1 nuclei measured by LSC.

For maximal accuracy, the experimental set-up was such that γ H2A.X was measured simultaneously with H2A or H2A.X in the same sample (**Figure 27A**). Etoposide increased the phosphorylated H2A.X levels above those of endogenous γ H2A.X (**Figure 27B**); the elution curves were similar at different time points of the early phase of the DNA damage response (**Figure 27C-E**).

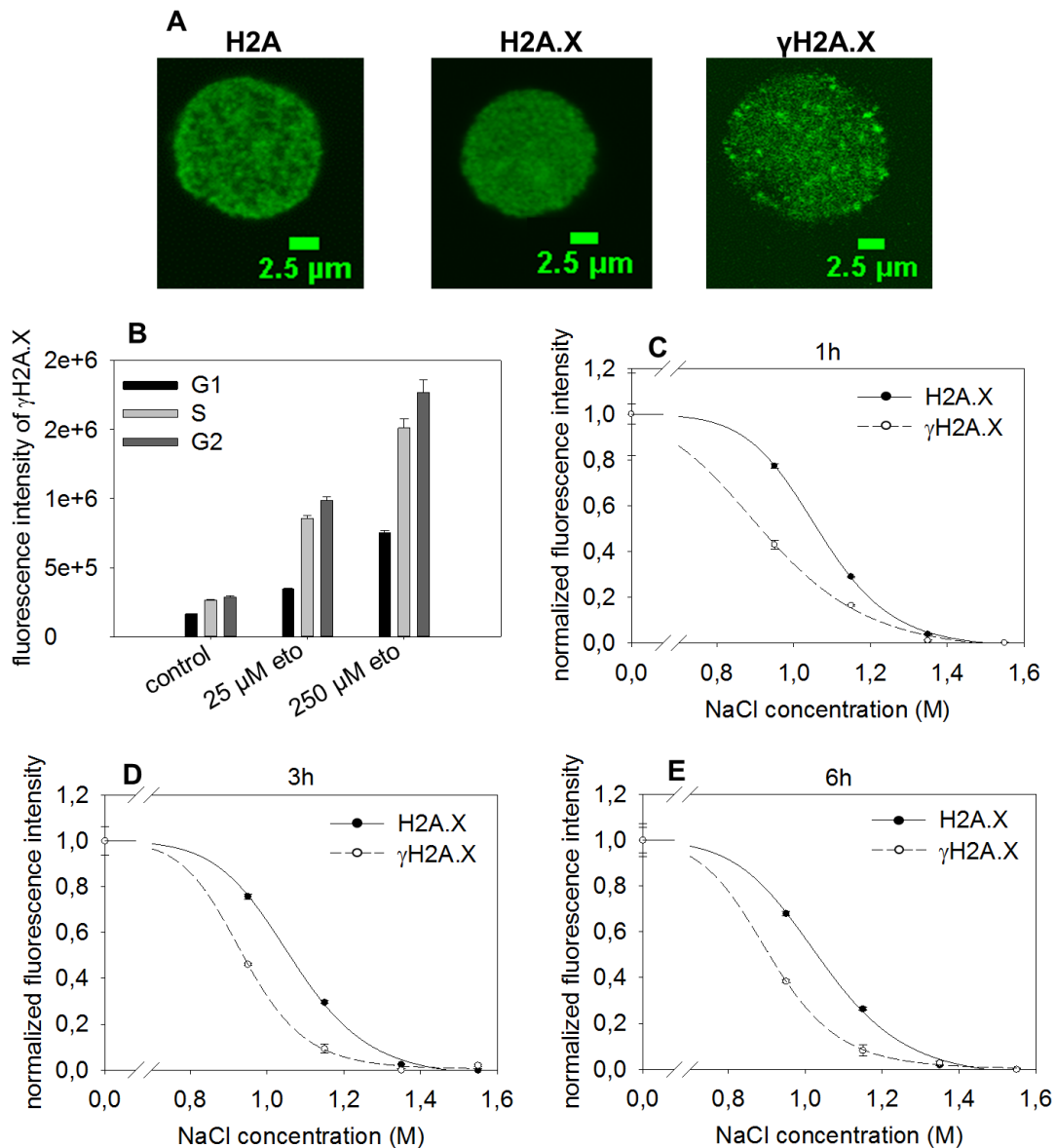


Figure 27. H2A, H2A.X and γ H2A.X localization, expression and stability features.

(A) Nuclear localization of H2A, H2A.X and γ H2A.X. CLSM immunofluorescence images of HCT116 nuclei.

(B) LSC evaluation of nuclear γ H2A.X immunofluorescence intensities after exposure of HCT116 cells to different concentrations of etoposide, for 1 h. Mean fluorescence intensities in the different cell cycle phases gated according to their DNA fluorescence distribution are shown. Error bars represent SEM of \sim 600 G1 nuclei measured by LSC.

(C-E) Salt elution curves of H2A.X and γ H2A.X recorded after 1 h (C), 3 h (D) and 6 h (E) treatment of the cells with 25 μ M etoposide. γ H2A.X was labeled together in the same sample with either H2A or H2A.X, using species-specific secondary antibodies.

The curves refer to G1 phase cells gated according to their DNA fluorescence distribution. Error bars represent SEM of \sim 600 G1 nuclei measured by LSC.

B. 2. 3. Superhelicity dependence of nucleosome stability

Our method proved to be highly instructive in demonstrating the intimate relationship between DNA superhelicity and nucleosomal stability: When random nicks (single stranded breaks) or DSBs were introduced into the genomic DNA using a frequent cutter nickase enzyme, or by DNase I respectively, the exogenous breaks significantly decreased nucleosomal binding of the H2A family members (H2A, H2A.X and H2A.Z) during salt elution (**Figure 28A-E**), but not in intercalator elution (**Figure 29A-D**), (except for a minor effect in the case of H2A.Z intercalator elution (**Figure 29E**)). On the contrary, intercalator elution profiles were, salt elution profiles were not shifted upon nickase treatment in the case of H3 (**Figure 28F and 29F**).

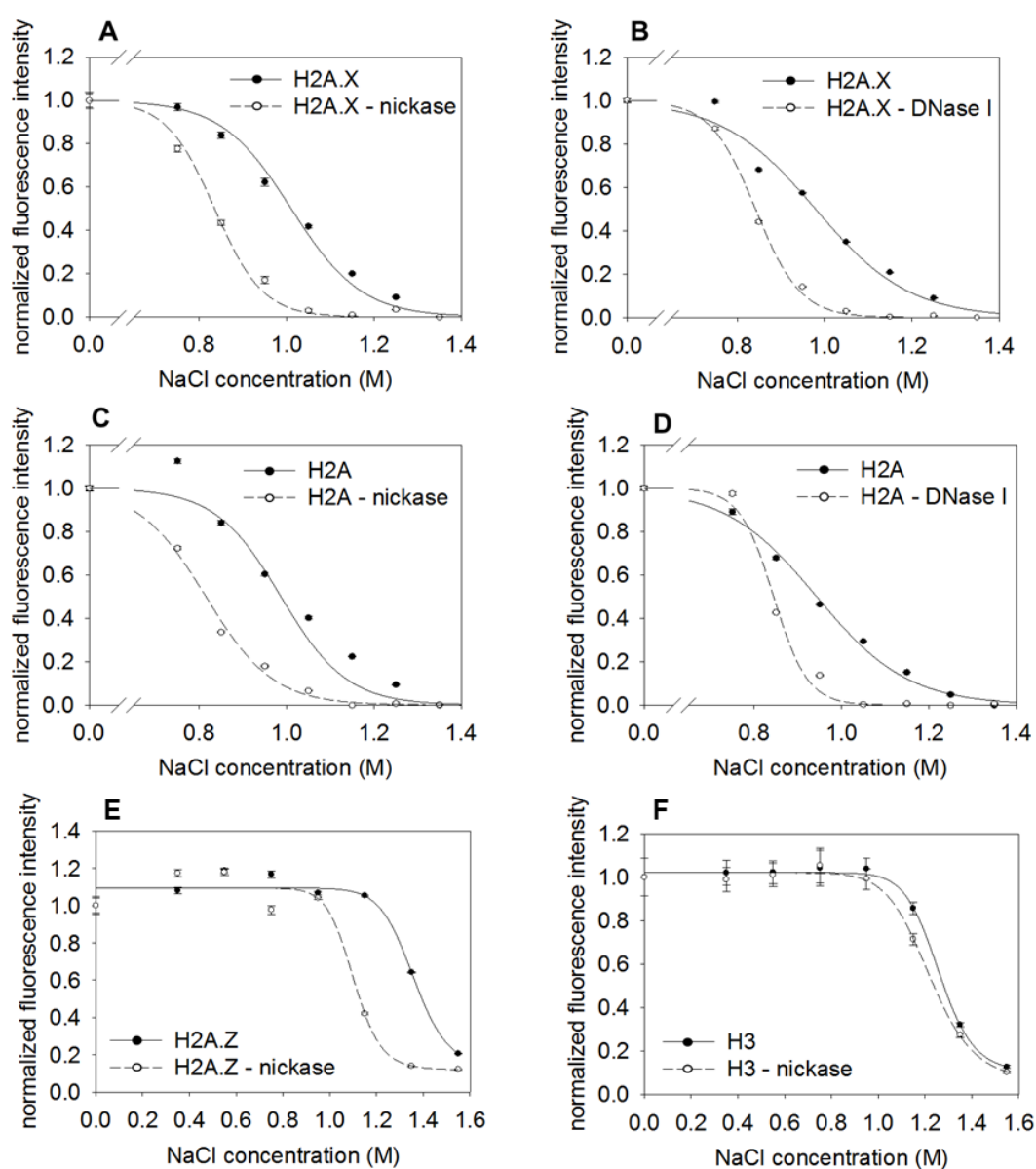


Figure 28. DNA superhelicity dependent stability features of nucleosomes containing histone variant H2A.X, H2A.Z and canonical H2A, as revealed by the NaCl elution assay.

(A) Effect of nickase treatment on H2A.X salt elution in HCT116 nuclei.
 (B) Effect of DNase I treatment on H2A.X salt elution in HCT116 nuclei.
 (C) Effect of nickase treatment on H2A salt elution in HCT116 nuclei.
 (D) Effect of DNase I treatment on H2A salt elution in HCT116 nuclei.
 (E and F) Elution profiles of H2A.Z and GFP-tagged bulk H3 in supercoiled chromatin or in nickase relaxed chromatin, measured by salt elution. H3-GFP was used as internal control. The elution curves refer to G1 phase cells gated according to their DNA fluorescence intensity distribution and the error bars represent SEM of ~600 G1 nuclei measured by LSC.

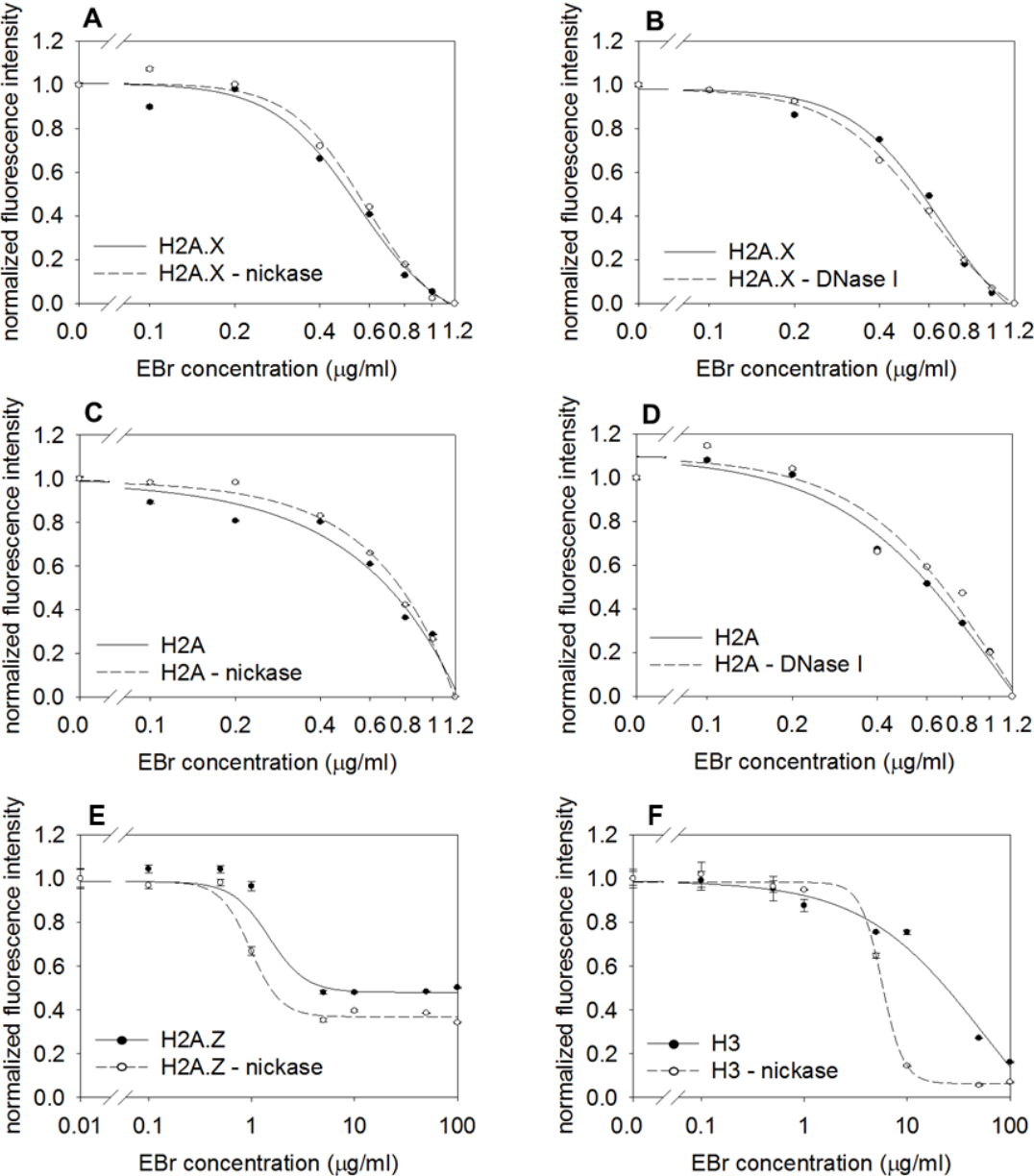


Figure 29. Effects of nuclease elicited DNA relaxation on nucleosome stability, as revealed by the EBr elution assay.

(A and B) EBr elution curves of H2A.X after nickase (A) or DNase I (B) treatment of the nuclei (compare with **Figure 28A, B**).

(C and D) EBr elution curves of H2A after nickase (C) or DNase I (D) treatment of the nuclei (compare with **Figure 28C, D**).

(E and F) Elution curves of H2A.Z and GFP-tagged bulk H3 in supercoiled chromatin or in nickase relaxed chromatin, measured by intercalator elution. H3-GFP was used as internal control. (compare with **Figure 28E, F**)

The curves refer to G1 phase cells gated according to their DNA fluorescence distribution. Error bars represent SEM of ~600 G1 nuclei measured by LSC.

The spectacular histone mobilizing effect of nicking treatments allowed us to determine the distance range of propagation of nucleosome destabilization along the supercoiled chromatin loops. If nucleosome-proximal nicking were required for facilitated H2A-H2B eviction then we would expect approximately one nick per ~200 bp to occur when most of the dimers are released. In contrast with this expectation, gel electrophoretic analyzes of the ds fragments obtained after S1 nuclease digestion (converting the nickase-elicited nicks to ds breaks) have revealed their surprisingly infrequent incidence: The nicks, generated at nickase concentrations where nucleosome eviction already involves the majority of nucleosomes (0.05 U/ml), delimit ≥ 10 kb fragments, and this is the case even at 10x lower nickase concentrations (**Figure 30**).

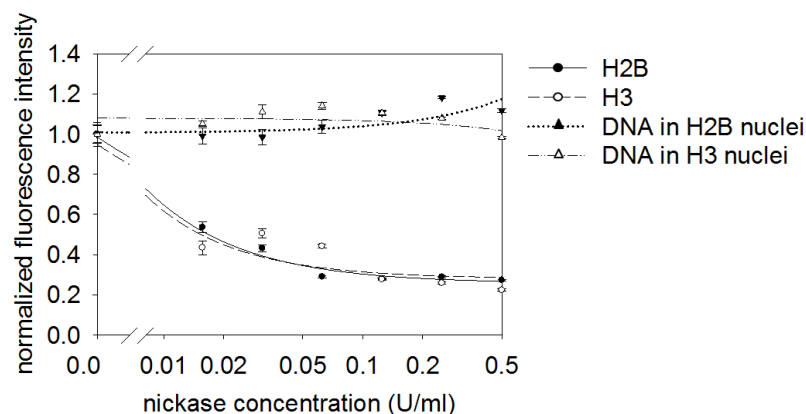


Figure 30. Eviction of H2B-GFP and H3-GFP in nuclei treated with different concentrations of nickase. H2B-GFP and H3-GFP HeLa nuclei were treated with 0.95 M NaCl, or 10 μ g/ml EBr in the presence of 0.75 M NaCl, respectively, after treatment with nickase used at the concentrations indicated in the Figure. Fluorescence of EBr indicating nuclear DNA content was recorded in parallel with the GFP signal. The curves refer to G1 phase cells gated

according to their DNA fluorescence intensity distribution. Error bars represent SEM of ~600 G1 nuclei measured by LSC.

The results of **Figure 31**, obtained at S1 concentrations where most of the nicks were converted into double-strand breaks (Varga et al. 1999), were confirmed by urea-agarose denaturing gel electrophoresis (Hegedus et al. 2009) in **Figure 32**.

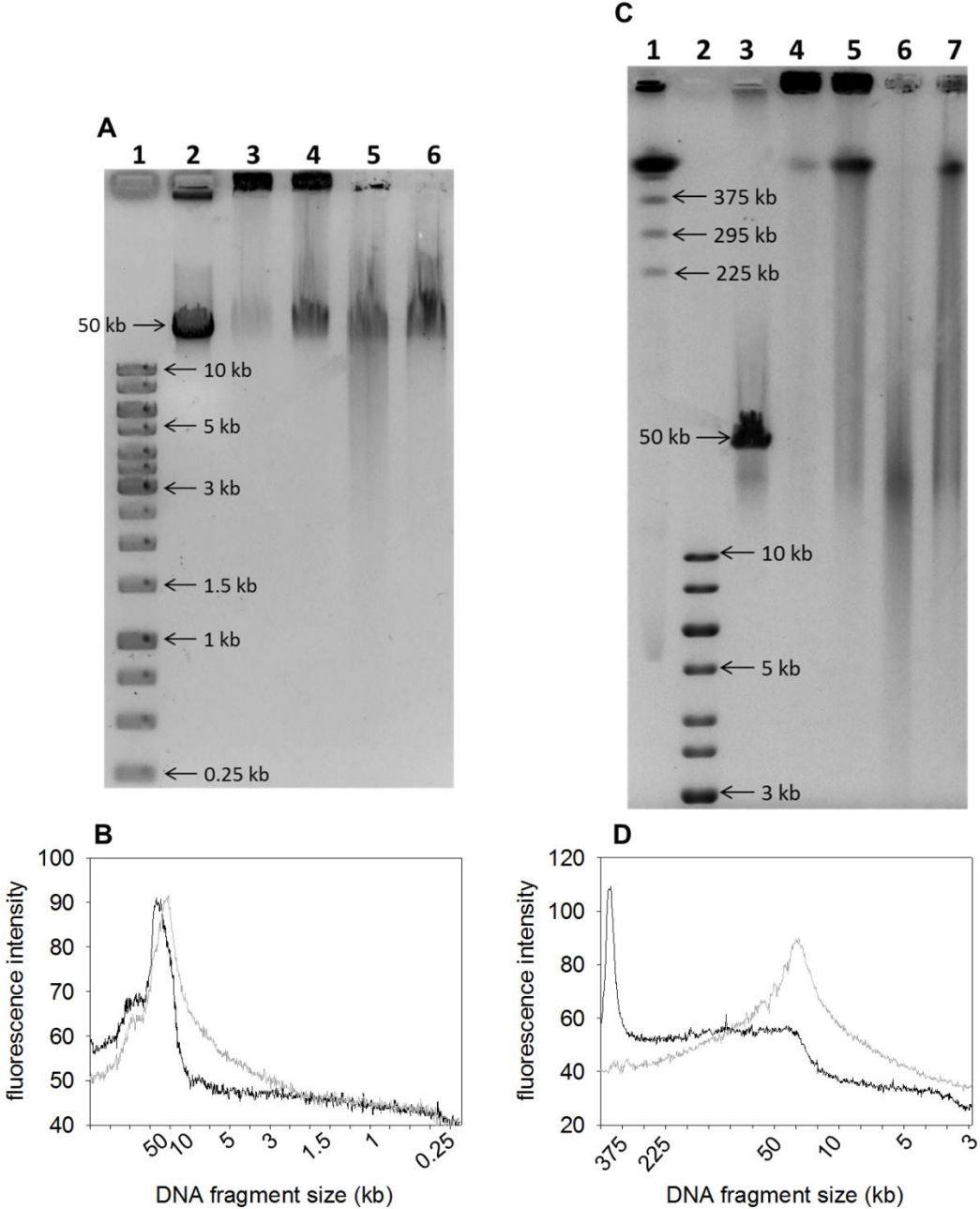


Figure 31. Comparison of nick distribution after nickase digestion.

(A-D) Double-strand fragment size distribution of the DNA prepared from the H2-GFP HeLa nuclei after the nicks were converted to double-strand breaks by S1 nuclease (see Methods). The size distribution of the DNA samples was analyzed by conventional agarose gel

electrophoresis (A, B) or by CHEF (C, D). Lanes on panel A: Lane 1, 1 kb DNA ladder; lane 2, lambda DNA; lane 3, untreated control; lane 4, 0.5 U/ml nickase; lane 5, 0.5 U/ml nickase + 1000 U/ml S1; lane 6, 1000 U/ml S1. Line-scans on panel B correspond to lane 4 (black line) and lane 5 (grey line) of panel A. Lanes on panel C: Lane 1, 225-2200 kb Pulse marker; lane 2, 1 kb DNA ladder; lane 3, lambda DNA; lane 4, untreated control; lane 5, 0.5 U/ml nickase; lane 6, 0.5 U/ml nickase + 1000 U/ml S1; lane 7, 1000 U/ml S1. Line-scans on panel D correspond to lane 5 (black line) and lane 6 (grey line) of panel C.

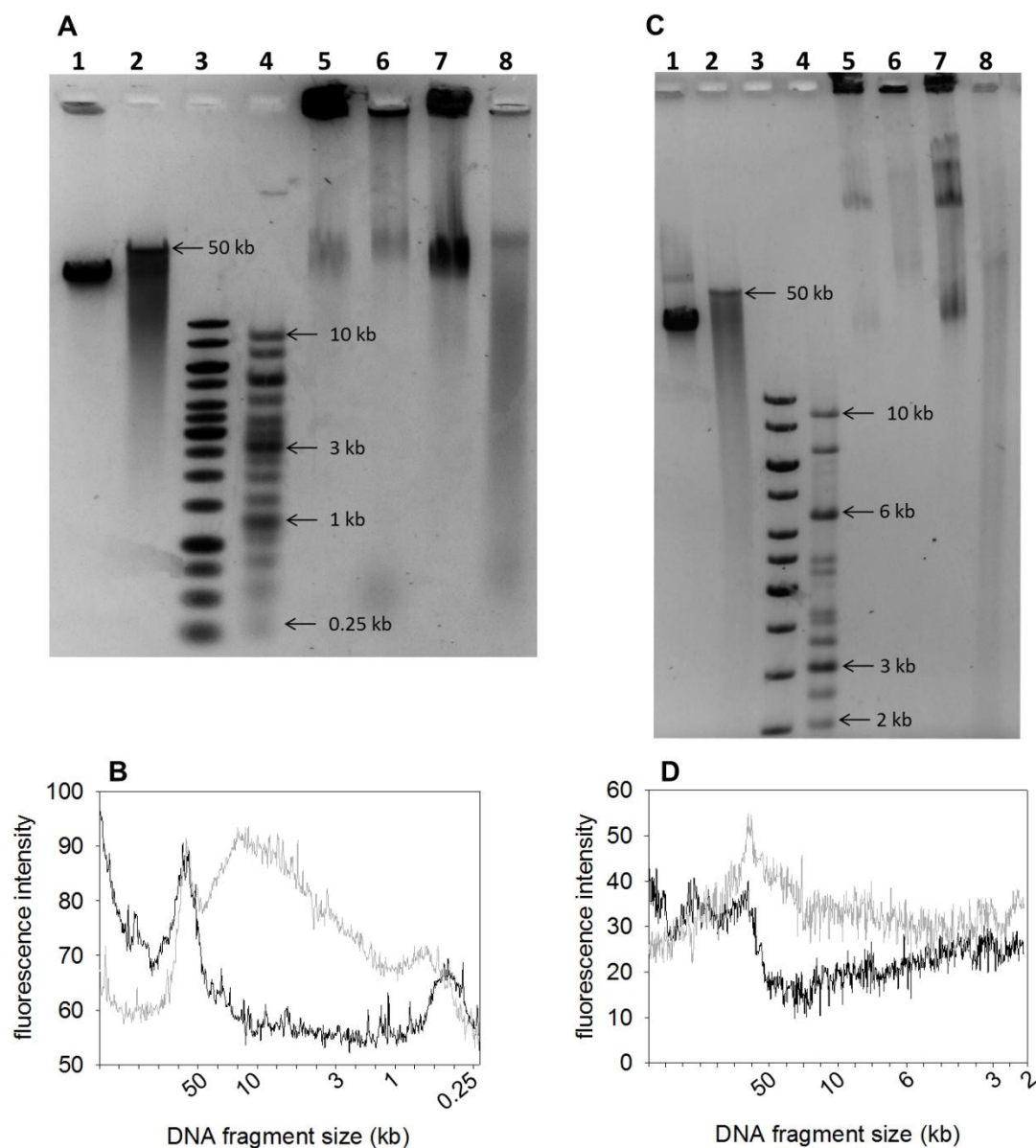


Figure 32. Standard and pulsed-field urea/agarose gel electrophoresis (ref. (Hegedus et al. 2009)) of the deproteinized DNA of agarose-embedded nickase treated H2B-GFP HeLa nuclei.

(A and B) DNA fragment size distribution analyzed by standard gel electrophoresis of non-denatured and urea/heat-denatured samples after digestion of nuclei with nickase. Lanes on

panel A: Lane 1, lambda DNA; lane 2, denatured lambda DNA; lane 3, 1 kb DNA ladder; lane 4, denatured 1 kb DNA ladder; lane 5, nickase untreated, non-denatured control; lane 6, nickase untreated, denatured control; lane 7, non-denatured DNA of 0.5 U/ml nickase treated nuclei; lane 8, denatured DNA of 0.5 U/ml nickase treated nuclei. Line-scans on panel B correspond to lane 6 (black line) and lane 8 (grey line) of panel A.

(C and D) DNA fragment size distribution analyzed by FIGE of non-denatured and urea/heat-denatured samples after digestion of nuclei with nickase. Lanes on panel C: Lane 1, lambda DNA; lane 2, denatured lambda DNA; lane 3, 1 kb DNA ladder; lane 4 denatured 1 kb DNA ladder; lane 5, nickase untreated, non-denatured control; lane 6, nickase untreated, denatured control; lane 7, non-denatured DNA of 0.5 U/ml nickase treated nuclei; lane 8, denatured DNA of 0.5 U/ml nickase treated nuclei. Line-scans on panel D correspond to lane 6 (black line) and lane 8 (grey line) of panel C.

B. 2. 4 General characteristics of the elution assays

To test whether the elution curves are independent of the expression levels of histones examined, nuclei of H2B-GFP expressing cells were gated according to the fluorescence intensity of GFP and elution curves were recorded in the nuclei showing low, medium and high GFP signals. (**Figure 33A**) The elution curves measured on nuclei with different H2B-GFP levels were similar to each other.

Reproducibility of the method from experiment-to-experiment was demonstrated by calculating the average and standard deviation of three independent measurements in the case of canonical H2B and H3 and also in the case of H3K4me3 and H3K27me3 modifications using salt elution or intercalator elution assays (**Figure 33B-F**).

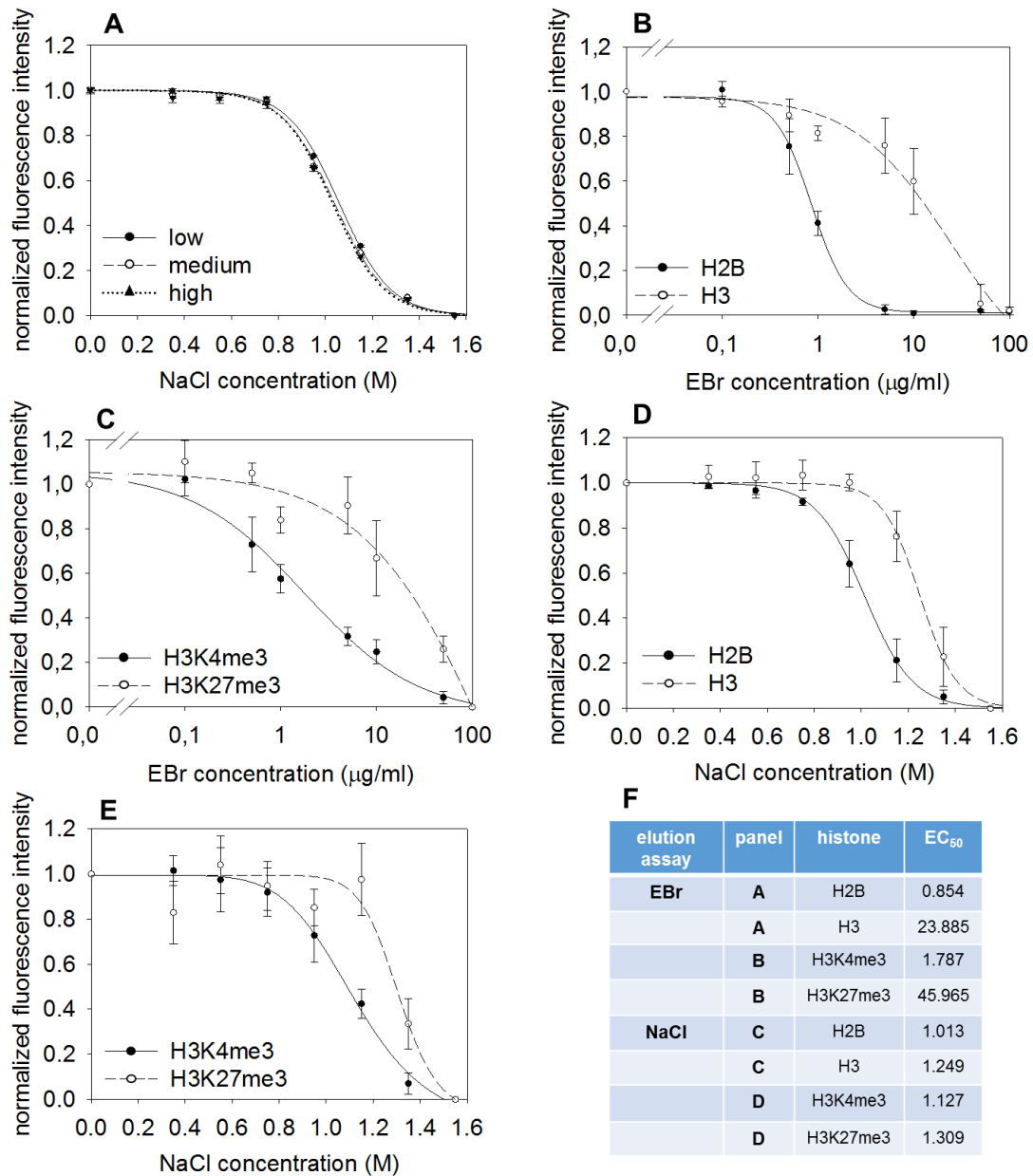


Figure 33. Comparison of H2B NaCl elution at different expression levels and the assessment of reproducibility.

(A) Salt elution curves of low, medium and high H2B-GFP expressor cells gated before adding the salt solutions indicated on the X axis, measured by LSC. Error bars represent SEM of ~600 G1 nuclei measured by LSC.

(B-E) Elution curves constructed from three independent experiments performed using histone-GFP expressor HeLa cells (panels B and D) or HeLa cells without histone-GFP construct (panels C and E). The mean fluorescence intensity values of ~600 G1 nuclei of the three samples were averaged at each eluent concentration to obtain the data points and the SDs (error bars) on the Figure.

(F) EC_{50} values, representing the treatment conditions where the normalized mean fluorescence intensity decreases to 50 % relative to the untreated nuclei, corresponding to the curves in panels B-E.

The curves refer to G1 phase cells gated according to their DNA fluorescence distribution.

To assess that the elution profile of a particular histone may reflect the effects of its intra- or internucleosomal interactions immuno-cross-linking experiments were performed in the case of H2A.Z found to be unusually stable. The H3-like stability of H2A.Z containing dimers, mediated by its PWWP2A binding domain, may be the consequence of the interaction between H2A.Z C-terminal tail and the tetrasome which could be facilitated by increasing ionic strength. Nuclei were pretreated with different concentrations of salt solutions (in a range where H3 histones remain chromatin bound, see **Figure 33D**), then H2A.Z histones were X-linked by antibody labeling. Increasing amounts of H3 histones remained chromatin-bound as a result of immuno-X-linking of H2A.Z (**Figure 34**).

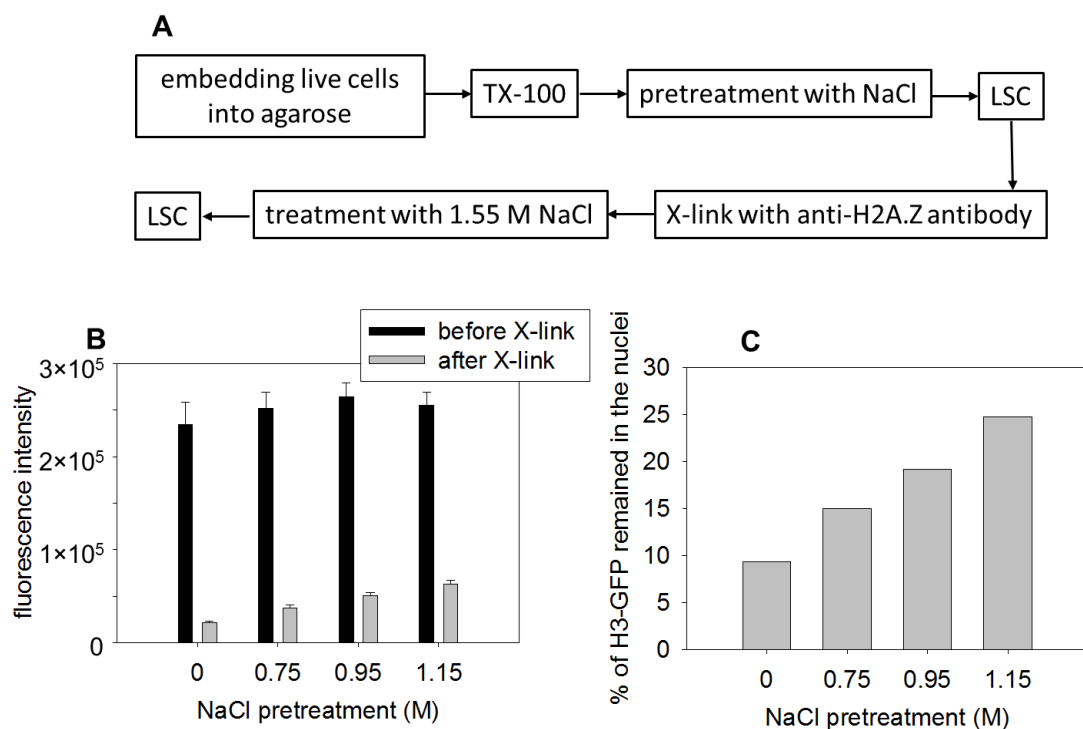


Figure 34.

Assessment of the possible salt dependent binding of Abcam1 anti-H2A.Z antibody to H3.

(A) Flow-chart of the experimental design.

(B) Bar chart of the fluorescence intensities of GFP-tagged H3 histones before and after X-linking using the Abcam anti-H2A.Z. The bar chart refers to G1 phase cells gated according to

their DNA fluorescence intensity distribution and the error bars represent SEM of ~600 G1 nuclei measured by LSC.

(C) Percentage of the immobilized fraction of GFP-tagged H3 histones.

In contrast, a the two members of the dimer within the nucleosomes was independently dissociated from the chromatin measured in immuno-X-linking experiments using salt or intercalator as nucleosome destabilizing agents. Doxorubicin was used as intercalator applied at physiological salt concentration (**Figure 35**).

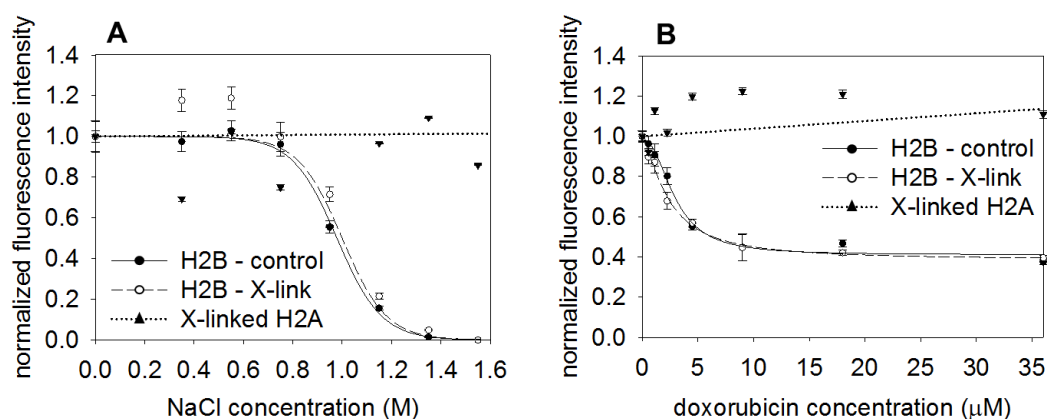


Figure 35. Effect of H2A immuno-cross-linking by bivalent antibodies on the salt (A) and intercalator (B) elution profiles of H2B-GFP and of the cross-linked H2A measured in histone-GFP expressor HeLa nuclei. Control: samples with no cross-linking. For antibody X-linking, labeling of histones with primary and secondary antibodies was performed prior to salt or intercalator treatment.

The curves refer to G1 phase cells gated according to the DNA fluorescence distributions.

Error bars represent SEM of ~600 G1 nuclei measured by LSC.

B. 3. DISCUSSION

The chapter below summarizes the main features of QINESIn together with a few examples of questiones raised in the wake of the observations made by the technique.

Our slide-based cytometric method offers a simple means to assess and compare stability features of nucleosomes consisting of native histones *in situ*. Its novelty stems in its combinative features, exploiting the advantages of cytometric analyzes in measurements based on exposure of chromatin to various destabilizing agents. Its features are compared to those of the most common alternative approaches in **Table 2**.

	QINESIn	Proteomic analyses Refs. (A)	Assays on isolated/reconstituted nucleosomes Refs. (B)	Genomics approaches Refs. (C)	Plasmid derived tagged histones Refs. (D)
Quantitative analysis of nucleosome stability	+	+	+	+	+
Histone PTM specificity	+	+	+/-	+	-
Histone variant specificity	+	+	+	+	+
Overall expression or modification levels assessed	+	+	-	+/-	-
Measurement targets endogenous histones	+	+	+	+	-
Measurement of nucleosome stability <i>in situ</i>	+	-	-	-	+
Analyses according to cell cycle phases, without synchronisation	*	+	-	-	-
Assessment of superhelicity effects <i>in situ</i>	**	+	-	-	-
Detection of molecular interactions by X-linking	***	+	-	-	+
High-throughput screening.	+	-	-	-	-
Comparison of different cell types in mixed-cell experiments	****	+	-	-	-
Analysis according to cell surface markers in mixed-cell experiments	+	-	-	-	-
Cell-by-cell analyses	+	-	-	-	+
Sensitivity to heterogeneity (e. g. gating for different expression levels)	*****	+	-	-	+
Picturing genome-wide distribution	-	-	-	+	-

Table 2. Comparison of QINESIn with other methods available for the examination of molecular features related to nucleosome stability. “+” indicates that the particular approach has proved to be applicable for the corresponding purposes listed in the left column. “+/-” indicates that the particular approach provides semiquantitative or not readily extractable information. The asterisks refer to the data demonstrating the QINESIn features: * **Figure 11 and 23**; ** **Figure 28 and 29**; *** **Figure 35**; **** **Figure 13D**; ***** **Figure 33A**
References:

(A): (Kimura et al. 2008; Pang et al. 2013; Zheng et al. 2014; Farrelly et al. 2016; Wierer and Mann 2016),

(B): (Ausio et al. 1984; McMurray and van Holde 1986; McMurray et al. 1991; Thambirajah et al. 2006; Gansen et al. 2009; Andrews and Luger 2011; Bohm et al. 2011; Lee et al. 2011; Chen et al. 2013; Chien and van der Heijden 2014; Taguchi et al. 2014; Vlijm et al. 2015; Wei et al. 2015; Harada et al. 2016; Krietenstein et al. 2016; Ordu et al. 2016; Rudnizky et al. 2017),

(C): (Henikoff et al. 2009; Heyse et al. 2009; Teves et al. 2012; Ramachandran and Henikoff 2016),

(D): (Kimura and Cook 2001; Ikura et al. 2007; Pichler et al. 2012; Pang et al. 2013; Liu et al. 2015)

The main advantages of QINESIn over the other methods listed in the table are the following. The conduct of nucleosomes containing fluorescent protein-tagged histones may be very different from that of the endogenous complexes: **Table 3** shows that the C.V. values calculated for the distribution of H2B-GFP or H3-GFP in the absence of any treatment tend to be larger than those obtained for the antibody detected histones.

treatment	labeling	cell to cell C.V.	sample to sample C.V.
EBr	H3-GFP	0.51	0.25
	H2B-GFP	0.75	0.13
	H3K4me3 IgG	0.24	0.11
	H3K27me3 IgG	0.36	0.25
	K27me3/K4me3	0.25	—
	H3K4me3 Fab	0.31	—
NaCl	H3-GFP	0.41	0.15
	H2B-GFP	0.94	0.16
	H3K4me3 IgG	0.29	0.15
	H3K27me3 IgG	0.49	0.16
	K27me3/K4me3	0.24	—

Table 3. Coefficient of variation (C.V.= S.D./mean) values calculated for the distribution of IgG labeled H3K4me3 and H3K27me3, Fab labeled H3K4me3 and of H2B-GFP or H3-GFP, based on the distribution histograms of HeLa cells recorded by LSC. The measured points closest to EC₅₀ on the normalized elution curves were chosen for calculation.

Regarding topological effects, although the degree of supercoiling can be directly assessed by measuring the extent of psoralen cross-linking of the complementary DNA strands by genomic approaches (Kouzine et al. 2013; Naughton et al. 2013), they allow insight neither into the consequences of these changes on nucleosome stability nor the propagation of these effects along the loops. Furthermore, they cannot reveal cell-to-cell differences and are much more labour intensive. The effect of particular PTMs on nucleosome stability can be analyzed using reconstituted systems, if the enzyme complex generating that PTM is also available (see e.g. (Lee et al. 2011)), but such measurements would address nucleosomes outside their chromatin context and would require the *in vitro* production of the modifying complex and a detailed understanding of its functioning. Furthermore, in

reconstituted systems, the stability parameters determined may be highly sensitive to the length of the DNA used for reconstruction (Nikitina et al. 2017). Our method is uniquely suitable for rapid screening of several features at the same time (e.g. to compare the stability of nucleosomes distinguished by different PTMs (**Figure 12**), or to determine the size of supercoiled loops in different PTM context (comparing H3K4me3 and H3K27me3 e.g., as it was done for bulk H3 in **Figure 30**). Measurements can be readily conducted in microplates providing the method with high-throughput potential, sharply distinguishing QINESIn from the other approaches.

The nucleosomal subpopulation measured by the QINESIn approach may be rather homogenous. Since TSS proximal H3K4me3 comprises ~95 % of all the H3K4me3 signals (based on our ChIP-Seq data), the elution profile of H3K4me3 reflects the overall stability features of active promoters, i.e. a rather well-defined subpopulation of the nucleosomes. In the case H3K27me3, overall stability features of a more heterogeneous population of nucleosomes belonging to facultative heterochromatin (Saksouk et al. 2015) are revealed *en masse*, cell-by-cell. It is also possible to investigate localized chromatin domains *in situ* by QINESIn (Imre et al. 2017), what may include nuclear subregions or nuclear bodies.

Since the released nucleosomal components diffuse out of the measured volumes (**Figure 7C**, **Figure 25**), the relative sensitivity to salt or intercalators is assumed to be proportional to the off-rate of the equilibrium dissociation constants involved in histone-histone and nucleosome-DNA interaction. Thus, an aspect of nucleosome stability which is pertinent to the principle of de-repression underlying gene regulation is addressed. The elution curves are independent of the expression levels of histones (**Figure 33A**) and are highly reproducible from experiment-to-experiment (see **Figure 33B-F**).

The permeabilized, hence ATP depleted, state of the nuclei is obviously incompatible with active chromatin remodelling processes, which is also evidenced from the lack of sensitivity of the method to temperatures between 0-22 °C during the elution and washing steps (**Figure 9B**). The latter observation demonstrates the stability of the measuring conditions (see also sample-to-sample C.V. listed in **Table 3**).

The non-equilibrium conditions of the experimental setting upon elution rule out the possibility of any repositioning of the released histones, which is a potentiality shown to occur upon supravital doxorubicin treatment (Pang et al. 2013; Wojcik et al. 2013). The sensitivity of the method to structural changes of the histones is apparently determined by the effect of these changes on nucleosome stability; H2A.X, without phosphorylation, was indistinguishable from H2A in spite of the structural differences described in Introduction.

The elution characteristics of a particular histone may reflect the effects of its molecular associations: Regarding the H3-like salt-elution profiles of H2A.Z demonstrated above (and detected also earlier (Thambirajah et al. 2006)), a fraction of H3-GFP could be prevented from salt elution by previous antibody cross-linking of H2A.Z (**Figure 34**). This observation suggests that H2A.Z may be bound to the nucleosome via stronger dimer-tetramer interaction than H2A (Park et al. 2004), an effect induced by salt pretreatment. We speculate that the H2A.Z reader PWWP2A might mediate this interaction. Salt preincubation could allow the release of the canonical H2A, making room for the variant histone. In contrast, a remarkable independence of the two members of the dimer within the nucleosomes was corroborated by the immuno-cross-linking experiments shown in **Figure 35**.

The H3-like stability of H2A.Z could be a trivial consequence of a possible cross-reactivity of the (Abcam) antibody with the tetrasome. However, this is a ChIP-grade antibody and the deletion of the PWWP2A binding site of H2A.Z had a remarkable destabilizing effect on the dimers in the absence of any alteration in the tetrasome status and antigenicity. Thus the possibility that the H3-like elution characteristics of H2A.Z may be due to cross-reactivity of the Abcam antibody with an epitope of the tetrasome is highly unlikely.

Our simple and versatile strategy to measure nucleosome stability is capable of resolving possible cell-cycle differences (**Figure 11A-E**); however, such differences have not been observed in the case of the particular histones investigated in this study, suggesting that the degree of stability is a stable feature of the nucleosomes involved. The about twofold elevation of H3K4me3 levels in G2 cells (**Figure 11E**) suggests that this PTM is copied over to the new nucleosomes upon DNA replication (as opposed to H3K27me3 that shows no change in expression level across the cell cycle phases). Thus, the lack of any cell cycle dependence of the elution profiles implies that the stability of the new H3K4me3 nucleosomes is similar to or identical with that of the old ones.

As shown in **Table 3**, the sample-to-sample variability of average nuclear immunofluorescence is 1.5-6x smaller than cell-to-cell variability. The latter values were very similar when whole IgG or its Fab fragments were used, suggesting that the widths of the intensity distribution is unrelated to chromatin accessibility issues, in line with the fact that histone deacetylase inhibition didn't increase labeling or change the C.V. significantly either (**Table 4**). The width of the distribution of the ratio of two immunofluorescence signals, calculated separately for each cell, which is a parameter expected to be independent from potential cell-to-cell differences in antibody accessibility and binding, was very similar to

those of the individual signals; this observation suggests that variability is more of biological than technical origin.

treatment	labeling	cell to cell C.V.
EBr	H3K4me3 IgG	0.16
	H3K27me3 IgG	0.29
	H3K4me3 Fab	0.31
NaCl	H3K4me3 IgG	0.17
	H3K27me3 IgG	0.24

Table 4. Coefficient of variation (C.V.= S.D./mean) values calculated for the distribution of IgG labeled H3K4me3 and H3K27me3, Fab labeled H3K4me3, based on the distribution histograms of TSA treated HeLa cells recorded by LSC. The measured points closest to EC₅₀ on the normalized elution curves were chosen for calculation.

The effect of EBr exhibits strong salt dependence (**Figure 10**), which may be the reason why eviction induced by EBr remained unrevealed in (Pang et al. 2013). In an earlier work demonstrating EBr induced destabilization at low salt (McMurray and van Holde 1986), intercalator concentration exceeded that used by us. Additive destabilization of chromatin DNA-protein complexes by EBr and NaCl was also observed earlier (Schroter et al. 1985).

The salt dependence of EBr effects could in part be explained by interactions mediated by the H1 histone expected to be completely released at 0.35 M salt (together with non-histone proteins (Sanders 1978; Yager et al. 1989)). However, doxorubicin destabilized nucleosomes upon treatment of live cells (**Figure 8**), i.e. in normotonic intranuclear milieu, in line with what has been described for daunomycin (Wojcik et al. 2013). Interestingly, the salt concentration found to be optimal for EBr elution (0.75 M; **Figure 10**) exactly coincides with the concentration above which the dimers and tetramers are evicted in a successive manner (Yager et al. 1989), and also where the dimers undergo a conformational transition (Bohm et al. 2011).

We have validated QINESIn with reference to published data (Pang et al. 2013) and have confirmed them with the intercalator sensitivity of qPCR and ChIP-Seq being taken into account. The preferential sensitivity of H3K4me3 containing nucleosomes to doxorubicin eviction described in that publication (using MelJuSo cells and patients' AML blasts) is corroborated by our method using HeLa, mES cells as well as NPC (**Figure 12**). These results indicate that the phenomenon is not unique to certain cell types and differentiation/proliferation states. The destabilized character of the H3K4me3 containing

nucleosomes is in agreement with their high *in vivo* turnover (Zheng et al. 2014), suggesting that a physiologically relevant chromatin feature can be detected and analyzed by QINESIn.

The enhanced release of H3K4me3 upon intercalator treatment is apparently not due to the presence of a reader protein (data obtained with a recombinant reader protein, TAF3), although the modification itself is not expected to exert any direct effect on nucleosome structure and stability (Bowman and Poirier 2015). Nucleosomes decorated with the same modification but outside TSSs were affected by doxorubicin in the same sample to a lesser degree (**Figure 7D** right panel), suggesting that factors determined by the molecular environment of this PTM have a role in H3K4me3 nucleosome destabilization. (In contrast with our findings on H3K4me3, the reader of H2A.Z has got a strong impact on the stability of nucleosomes containing this variant.) The data on the cell-cycle expression pattern of H3K4me3 shown in **Figure 11**, panel **E**, and the lack of any difference in stability features assessed by QINESIn (**Figure 11A-D**) gain an interesting perspective in this context.

It is remarkable that γ H2A.X, residing in repair foci (**Figure 27A**), doesn't become immobilized (**Figure 27C-E**) in these molecular aggregates similarly to how histones become stabilized by cross-linking with bivalent antibodies prior to elution (**Figure 26**). This is in line with the model that these foci are rather loose structures allowing access for the multitude of repair factors accumulating within the foci (Price and D'Andrea 2013). Moreover, γ H2A.X is bound less tightly within nucleosomes than H2A.X, a difference detected only via salt elution (compare **Figures 26A** and **28B**). Thus, QINESIn confirms the conclusion drawn from sedimentation velocity analyzes (Li et al. 2010) indicating that phosphorylation on the C-terminus of H2A.X has a destabilizing effect on the nucleosome (Heo et al. 2008; Cheema and Ausio 2015), resolving a prevailing controversy (Bonisch and Hake 2012). Due to the fact that nucleosome stability is measured *in situ* rather than on reconstituted nucleosomes, the observed features may reflect the effect of several factors cooperating in determining nucleosome stability *in vivo*. Since the long stretches of chromatin packed with γ H2A.X are generally visualized as being initiated at a double-strand break (Martin et al. 2014), the destabilized nature of γ H2A.X nucleosomes may be due to these breaks, in line with the observations presented here. Although the degree of destabilization was smaller in the case of γ H2AX as compared to the effect of nicking (compare **Figures 26A** and **28A**), this may be due to heterogeneities within the γ H2AX nucleosomes (Siddiqui et al. 2015), and/or the structural complexities of the repair foci. Destabilization may also be due to direct effects of the negative charge of the phosphate in γ H2A.X, to the presence of protein factors bound on this platform (Price and D'Andrea 2013), to the PTMs associated with these variant histones

(acetylation, ubiquitination; (Ikura et al. 2007; Chen et al. 2013)), or any combination of the above. Destabilization of H2A.X nucleosomes after phosphorylation may be a medically relevant observation in the sense that DNA damage response could be further attenuated as a consequence of treatment with intercalating agents. Accurate comparison of the binding strength of H2A.X and γ H2A.X was not possible in the context of the methodology applied in the study first reporting decreased DDR in the wake of doxorubicin treatment (Pang et al. 2013).

Salt and intercalator elution appear to detect different aspects of nucleosome stability based on the experiments with nickase treatment comparing bulk H2B and H3 histones (**Figure 28C, F and 29C, F**). As a further example, H2A.Z nucleosomes detected by Abcam1 antibody behaved H3-like in salt elution, but H2B-like in intercalator elution. This is in line with the stabilizing effect of this variant in reconstituted nucleosomes (Park et al. 2004) and further suggests that supercoiling related effects may be independent from, i.e. not being influenced by, the intrinsic stability. As **Figure 19** shows, a fraction of H2A.Z nucleosomes exhibits resistance to high concentrations of the intercalator, likely reflecting the fact that this variant is present in both repressed and actively transcribing regions of chromatin, exerting its biological roles in a context-specific manner (Cheema and Ausio 2015).

Intercalators are known to aggregate chromatin (Rabbani et al. 1999), thus intercalator resistance could be related to this aggregation. However, intercalator resistant H2A.Z could be eluted by salt where the salt elution profile was similar to that of H3, and deletion of the PWWP2A binding site decreased the fraction of salt resistant H2A.Z, suggesting that resistance to the intercalator is due to the change of dimer stability rather than to a reduced accessibility of aggregated chromatin to eluents. Also, the intercalator resistant histone molecules were readily accessible even for antibodies.

Nuclear localization of intercalator resistant H2A.Z nucleosomes was mainly peripheral and perinucleolar suggesting associations with lamina-associated domains (LAD) and nucleolar-associated domains (NAD) containing heterochromatic regions of chromatin. In line with this observation, salt elution profile of intercalator resistant fraction of H2A.Z containing dimers was still unusually stable, similar to (H3-H4)₂.

Analyzes of a H2A.Z mutant lacking the C-terminal reader binding site has revealed that the unusual stability of H2A.Z containing nucleosomes is likely the consequence of the interaction between the PWWP2A binding domain of H2A.Z and the tetrasome (**Figure 18 and 20**). This mechanism is also supported by the observation where the presence of a green fluorescent protein on the C-terminus of H2A.Z1 or Z2 results in less stable H2A.Z dimers,

similarly to the effect of the deletion of the PWWP2A binding domain. We propose that binding of the reader protein prevents the interaction between the C-terminus and the tetrasome, an interaction described in ref. (Wrattin et al. 2012), leading to nucleosome destabilization. Based on genome wide analysis PWWP2A localizes to the promoter region of actively transcribed genes (Link et al. 2018; Zhang et al. 2018) that are known to co-occur with H3K4me3, a PTM characteristic for destabilized nucleosomes (Pang et al. 2013; Imre et al. 2017).

This finding may lead to a novel paradigm regarding the role of histone variant composition and PTMs in transcriptional regulation with nucleosome destabilization taking central stage.

The PTM-specificity of the stability parameters detected with QINESIn is a powerful advantage of the approach. It will be of interest to extend the analysis to the characterization of nucleosomes containing other histone PTMs. It will be important to determine how broadly conserved is the remarkable dichotomy of H3K27me3 compared to H3K4me3 marked nucleosomes across different cell types (**Figure 12A, C**) and whether the destabilized nature of H3K4me3 marked, promoter proximal nucleosomes is related to the simultaneous presence of additional PTMs, e.g. acetylation, or to the topological factors discussed below. It will be highly interesting to further develop the methodical platform demonstrated herein making it amenable to ChIP-Seq studies; this will require upscaling of the current chamber based protocol so as to allow for ChIP on the agarose block-derived samples.

DNA relaxation ensuing after either nickase or DNase I treatment results in a highly significant destabilization of the nucleosome (**Figure 28; Figure 29F; Figure 30**), with different sensitivity to nicking in the salt and in the intercalator elution for H2A, H2A.X (**Figure 28**), compared to H3 (**Figure 29F**). These observations emphasize that different determinants of nucleosome stability can be addressed by the two elution protocols. The QINESIn results are in line with biophysical data demonstrating that nucleosomes containing relaxed DNA exhibit enhanced sensitivity to salt (Elbel and Langowski 2015). Binding of an intercalator to the DNA relaxes and also extends superhelical DNA (Gunther et al. 2010; Pang et al. 2013); if the DNA is already relaxed (by nickase treatment), only extension is possible. Different contributions of these topological aspects to the binding strength of the different histones could explain the primarily salt- or intercalator-sensitivity of the response to nicking.

The dramatic effect of nicking on nucleosome stability (**Figure 28; Figure 29F**) suggests that regulation of superhelicity may be exploited by the cell for gene regulatory purposes as contemplated in (Levens and Benham 2011; Wong et al. 2018). Relaxation of

superhelical loops by nicking only once at ≥ 10 kb regions is apparently sufficient to destabilize most nucleosomes among our experimental conditions along the entire superhelical domain affected. Since the majority of the nucleosomes become released from the relaxed chromatin loops even at a tenfold lower nickase concentration (**Figure 30**), the incidence of nicks necessary for nucleosome eviction likely overlaps the size of the supercoiled chromatin loops ((Szekvolgyi et al. 2007) and references therein). Thus, local topological changes under physiological conditions, such as those arising from topoisomerase action, may also have important effects on the stability of a relatively large number of nucleosomes. It is tempting to speculate that such a loop-wide nucleosomal destabilization could be “read” by the cell at specific nucleosomes in a site-specific manner with the help of locally acting reader proteins or chromatin remodelers.

In view of the above findings, I draw the conclusion that QINESIn can be readily applied to quantitatively analyze the effect of different endogenous histone PTMs or histone variants on nucleosome stability, in *in situ* screening studies distinguishing between intrinsic and superhelicity dependent stability. The method can assess the overall expression or modification levels and it is suitable for the detection of molecular interactions by immuno cross-linking. Analyzes can be performed on mixed cell populations for the comparison of different cell types or according to cell surface markers or cell-cycle phases cell by cell, on a large cell population.

C. CYTOMETRIC MICROBEAD ASSAYS FOR EPIGENETIC ANALYZIS

C. 1. INTRODUCTION

We could make good use of our experience acquired in flow cytometric microbead analyzes to answer some of the questions related to the epigenetic research projects of our lab, studying the occurrence of different PTMs on the same nucleosome.

To analyze PTM co-occupancy on the same nucleosome, Western blot analyzes of mononucleosomal samples is used as a general tool (Kimura et al. 2008; Hayashi-Takanaka et al. 2015). In this approach, mononucleosomes generated by sonication or by MNase digestion are immunoprecipitated by a PTM specific antibody and histones of the resulting nucleosomes are analyzed on Western blots using antibodies against various other PTMs. A similar strategy was used for histone variants as well (Sarcinella et al. 2007; Dryhurst et al. 2009). Neither this approach, nor the other more specialized methods applicable for this purpose (Voigt et al. 2012; Kinkley et al. 2016; Shema et al. 2016; Weiner et al. 2016) allow high-throughput and/or multiplex measurements. Using a flow cytometric platform, I have developed a method that may offer advantages over the above techniques regarding these limitations, in terms of versatility of possible applications as well as simplicity. I will demonstrate that detection of intranucleosomal combinations of epigenetic modifications is possible by capturing of mono-nucleosomes on microbeads via PTM-specific antibodies and subsequent analyzes of the bead-bound nucleosomes for other modifications, using immunofluorescence labeling. These data are contained in chapter C.2.1.

The success of the above experiments prompted us to test the approach in the analyzes of endogenous or exogenous ss DNA breaks (nicks), and their specific chromatin environment (histones carrying certain post-translational modifications, RNA/DNA-hybrids (R-loops), epigenetic traits in the focus of interest in our lab. The idea was to detect the presence of particular histone modifications and R-loops on fragmented chromatin captured on microbeads via biotinylated antibodies.

Transient, endogenous single- or double-strand DNA breaks are generated in the nucleus of a living cell in a programmed manner in the context of physiological molecular mechanisms such as transcription. During transcriptional elongation, e.g., the movement and rotation of RNA Pol II along the DNA results in the generation of positive supercoils in front of the polymerase and negative supercoils behind it (Liu and Wang 1987; Puc et al. 2017), thus torsional stress-resolving enzymes, topoisomerases, are essential components of transcription machinery. Human topoisomerase I (TOP1) relaxes the double helix by generating transient nicks, while topoisomerase II enzymes (TOP2 α and TOP2 β) induce

transient single- and double-strand breaks. Both classes of the enzyme rejoin the cleaved DNA ends, whereupon they dissociate from the DNA (Puc et al. 2017). On the other hand, promoter-proximal, transient ds breaks accompany gene activation, relying on TOP2 β (e. g. early-response genes involved in neuronal activity (Madabhushi et al. 2015). These latter phenomena seem to be closely related to a long-standing basic research project of our group, stemming from the observation that the chromatin of non apoptotic human and yeast cells contain endogenous nicks with an average incidence of ~50 kb, probably at the bases of the supercoiled DNA loops (Szekvolgyi et al. 2007). It was also shown by genome wide analyzes that nicks co-occur with histone modifications characteristic for the transcriptional start sites of the active promoters (our unpublished data) and that these sites also contain RNA/DNA hybrids (R-loops) in their molecular vicinity (Szekvolgyi et al. 2007). R-loops are by-products of transcription (Santos-Pereira and Aguilera 2015; Puc et al. 2017), containing an RNA/DNA hybrid and a single-stranded DNA displaced by the RNA strand. The proposed physiological functions of R-loops involve class switch recombination of the immunoglobulin loci, protection of high GC content-promoters from DNA methylation and the facilitation of transcription termination at terminators of certain genes (Santos-Pereira and Aguilera 2015). Increased accumulation of R-loops can lead to genomic instability (Tubbs and Nussenzweig 2017). Co-localization of nicks, R-loops and certain histone PTMs observed in ChIP-Seq experiments (our unpublished data together with L. Székvolgyi) was to be confirmed and further studied using independent technology, also because of technical issues of nick-labeling.

C. 2. RESULTS

An MMA assay was developed to reveal intranucleosomal or intramolecular PTM combinations, as well as the presence of histone variants, on microbead immobilized mononucleosomes or single histone molecules (**C.2.1.**).

Cytometric microbead analyzes was implemented to detect nicks at transcriptionally active promoters (colocalization of nicks and RNA Pol II Ser2-P) and to confirm our earlier observations suggesting that R-loops may be in the close proximity of free 3'OHs in genomic DNA. (**C.2.2.**) These free termini can be detected via nick-translation or terminal deoxynucleotidyl transferase (TdT) reaction. Antibodies specific for RNA Pol II Ser2-P or RNA/DNA-hybrids enabled us to detect RNA Pol II Ser2-P or R-loops in the microbead captured DNA fragments.

C. 2. 1. Detection of PTM-specific histone associations

A microbead based cytometric method was developed to detect the co-occupancy of different histone PTMs on the same nucleosome or on the same histone molecule. To determine the association of two histone modifications, biotin conjugated antibody specific for one of the PTMs is required. After immobilization of this antibody on streptavidinated microbeads, the antibody coated beads can be used to capture mono-nucleosomes carrying the PTM of interest from sonicated or MNase fragmented chromatin samples or isolated histones. Using fluorophore conjugated antibodies, the presence of the second PTM on the immobilized nucleosomes or histones can be detected by cytometry (**Figure 36A**).

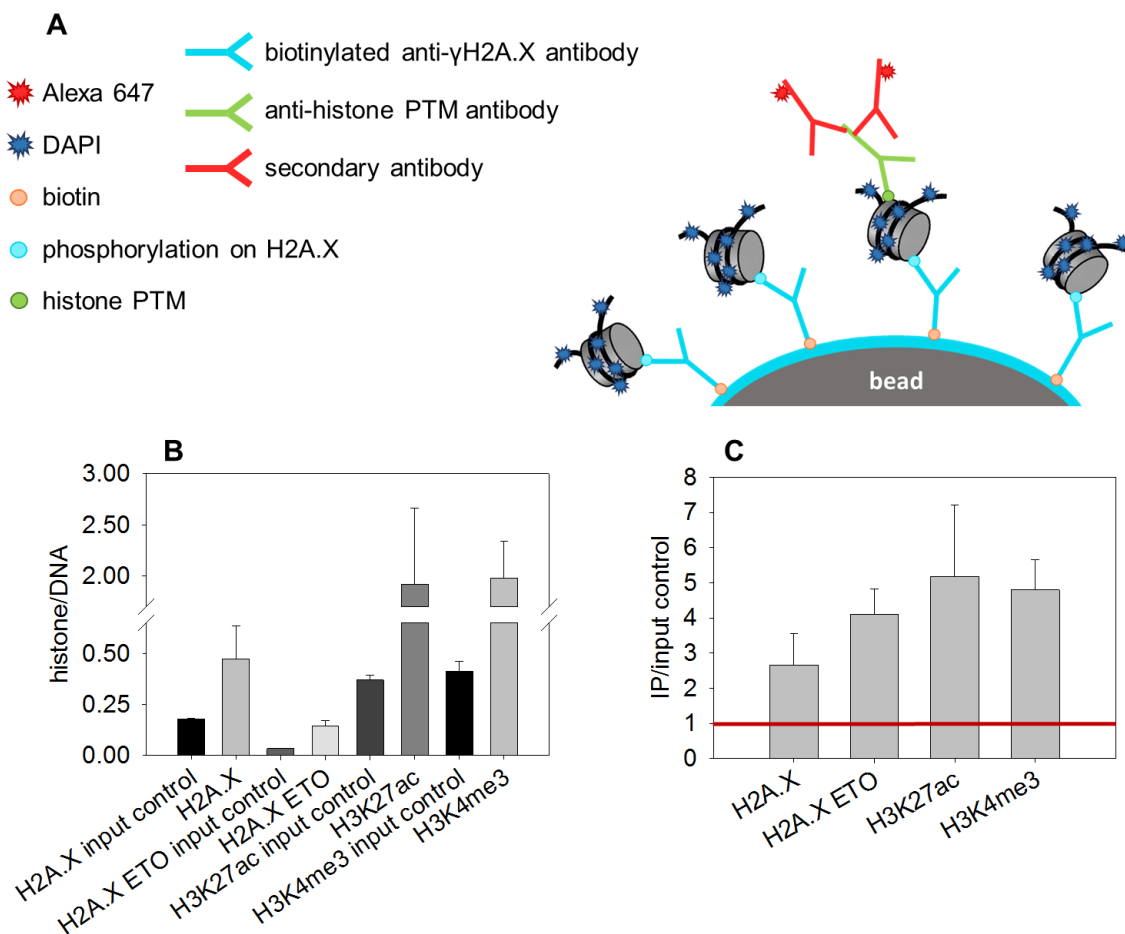


Figure 36. Detection of histone PTM associations.

(A) Scheme of immunofluorescence labeling of microbead-bound nucleosomes.

(B) Nucleosomes isolated from Jurkat cells were immobilized on anti- γ H2A.X coated microbeads. In the case of input control, the same amount of isolated nucleosomes were added to non-coated beads. Parallel samples containing aliquots of beads carrying the γ H2A.X containing nucleosomes were labeled with anti-H3K4me3, anti-H3K27ac or anti-

H2A.X primary antibodies and an A647 conjugated secondary antibody. Fluorescence intensities were normalized to the fluorescence of DNA detected by DAPI.

(C) DNA normalized fluorescence intensities of antibody labeled histones calculated as the ratio of specific signal measured on anti- γ H2A.X coated beads (IP; from panel (B)) over the nonspecific signal measured using non-coated beads (input control; from panel (B)). Values reflect the fold change of IP compared to input; values above 1 (red line) were considered indicative of co-localizing PTM and γ H2A.X.

Nucleosomes isolated from Jurkat cells treated with etoposide (H2A.X ETO) were used as the positive control demonstrating that the amount of γ H2A.X containing nucleosomes immobilized on beads was increased as a result of etoposide treatment, compared to samples derived from Jurkat cells not exposed to etoposide (H2A.X). Error bars represent SD of the beads in one representative measurement.

To test this strategy, PTMs associated with endogenous γ H2A.X histone variant were investigated. Streptavidinated microbeads were coated with biotinylated γ H2A.X specific mouse antibodies and the chromatin was fragmented to 200-750 bp by sonication. The captured nucleosomes were labeled with H3K4me3 and H3K27ac specific primary antibodies and fluorophore-conjugated secondary antibody, and quantified by flow cytometer. As a control, the H2A.X histone variant was also measured in the etoposide-treated and non-treated, control samples. In line with our expectations, in the samples derived from cells exposed to etoposide, the level of immobilized H2A.X containing nucleosomes was higher. It was also shown that endogenous γ H2A.X histone variants co-occur with H3K4me3 and with H3K27ac on the same nucleosome (**Figure 36B**). The co-localization of H3K4me3 and γ H2A.X was confirmed by superresolution STED microscopic analysis of agarose embedded and permeabilized nuclei labeled with the same antibodies that were used in the microbead assay (**Figure 37**).

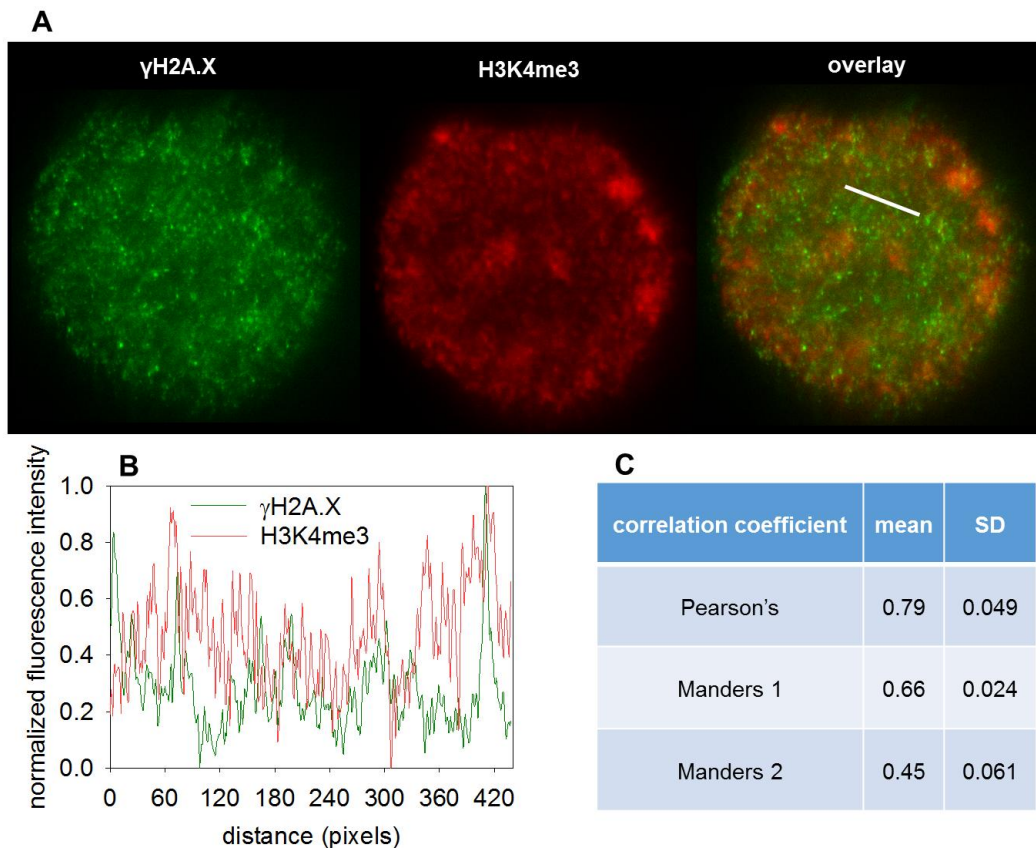


Figure 37. Microscopic analyzes of γ H2A.X - H3K4me3 co-localization.

(A) High resolution microscopic images of nuclei co-labeled with anti- γ H2A.X (green) and anti-H3K4me3 (red) antibodies measured by STED microscopy (pictures taken by Dr. Péter Nánási).

(B) Line scan of nuclear γ H2A.X and H3K4me3 immunofluorescence. Fluorescence signals along the white line indicated on the overlay image above are shown. Fluorescence intensities were normalized so as to set the lowest and highest values between 0 and 1, respectively.

(C) Co-localization of γ H2A.X and H3K4me3 was quantified calculating the Pearson's and Manders correlation coefficients. Average correlation coefficient values of four nuclei are shown in the table.

C. 2. 2. Detection of nick-proximal RNA Pol II and R-loops

Based on the above, the polymerase based nick-labeling strategy was used to confirm our genomic data showing enrichment of endogenous nicks at active promoters of *Saccharomyces cerevisiae* genomic DNA (Hegedüs et al. 2018).

I performed a global „ChIP-on-beads” analyses of nick – RNA Pol II co-localization as shown in **Figure 38A**. After nick-labeling, the chromatin samples were fragmented,

captured on microbeads and embedded into agarose. The agarose embedded beads were labeled using antibodies specific for RNA Pol II phosphorylated on Ser5 or Ser2 characteristic for transcriptional initiation or elongation, respectively.

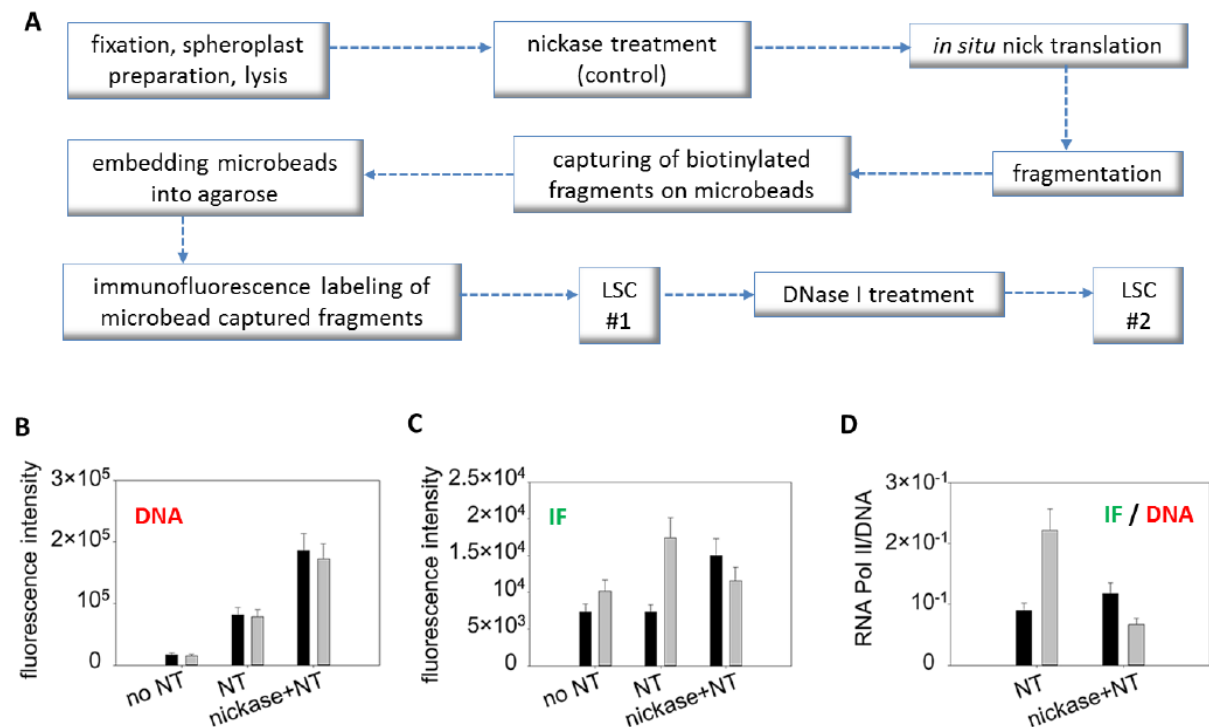


Figure 38. Global „ChIP-on-beads” analysis of nick – RNA Pol II co-localization.

(A) Flow-chart of the experiment: Nicks were labeled by incorporating biotinylated nucleotides using *in situ* nick-translation in fixed, permeabilized yeast nuclei, and fragmented chromatin was captured on streptavidinated microbeads. The beads containing chromatin fragments on their surface were embedded into agarose, then the different RNA polymerase species characteristic for initiation and elongation/termination were detected by immunofluorescence labeling and quantified by LSC. Background fluorescence was determined in a second LSC measurement of the same sample after removal of the chromatin fragments from the beads by DNase I treatment. See details in Materials and methods.

(B) Fluorescence intensity of DNA of microbead-captured, nick-translated chromatin fragments with (nickase+NT) or without (NT) nickase treatment, or chromatin fragments without nick-translation (no NT), labeled with RNA Pol II Ser2-P specific (black columns), or RNA Pol II Ser5-P specific antibodies (grey columns). The differences of the first and the second LSC measurement (see Materials and Methods) were plotted.

(C) Mean fluorescence intensities of RNA Pol II Ser2-P (black columns) and Ser5-P (grey columns) labeling of microbead-captured, nick-translated chromatin fragments with (nickase+NT), without (NT) nickase treatment, or without nick-translation (no NT).

(D) Mean fluorescence intensities of RNA Pol II Ser2-P (black columns) and Ser5-P (gray columns) labeling of microbead-captured, nick-translated chromatin fragments with (nickase+NT) and without (NT) nickase treatment, normalized to the DNA content captured by the microbeads. Nearly identical Ser-P/Ser-2 ratio was determined in independent measurements of the same immunoprecipitate. Error bars represent SD of ~2000 beads measured by LSC.

Nickase was used to introduce random nicks to the samples that served as negative control exhibiting no RNA Pol II enrichment. Agarose embedded beads were measured by a slide based imaging cytometric device (Laser Scanning Cytometer (LSC)) to analyze the samples according to similar parameters as in the case of flow cytometry. The advantage of imaging cytometry was that the DNA-specific signals could be distinguished from background by measuring the same beads before and after DNase I treatment (as described in Materials and Methods).

Compared to non-nick-translated samples, the mean DNA signals increased when endogenous nicks were biotinylated and were increased further when exogenous nicks were generated by nickase, in line with our expectations (**Figure 38B**). In the nick-translated samples (NT) Ser5-P signals were higher than Ser2-P signals and this difference was eliminated if random nicks were generated by nickase before nick-translation (**Figure 38C**).

The DNA-normalized RNA Pol II immunofluorescence was similar in the samples with and without nickase treatment in the case of Ser2-P, while the Ser5-P signals were much higher when the endogenous nicks were labeled only (compare the gray and black bars representing the two RNA Pol species in the nickase+NT and NT bar pairs of **Figure 38D**).

These data confirmed the conclusions of our “ChIP-on-chip” measurements that endogenous nicks are preferentially associated with active promoters in *S. cerevisiae* (Hegedüs et al. 2018).

Based on the favorable experience described above, I tested the microbead-based cytometric approach to detect R-loops in the close proximity of endogeneous single-strand DNA discontinuities at the whole genome level, in an attempt to confirm and further analyze earlier observations of the group (Szekvolgyi et al. 2007). The scheme of the assay is shown in **Figure 39**.

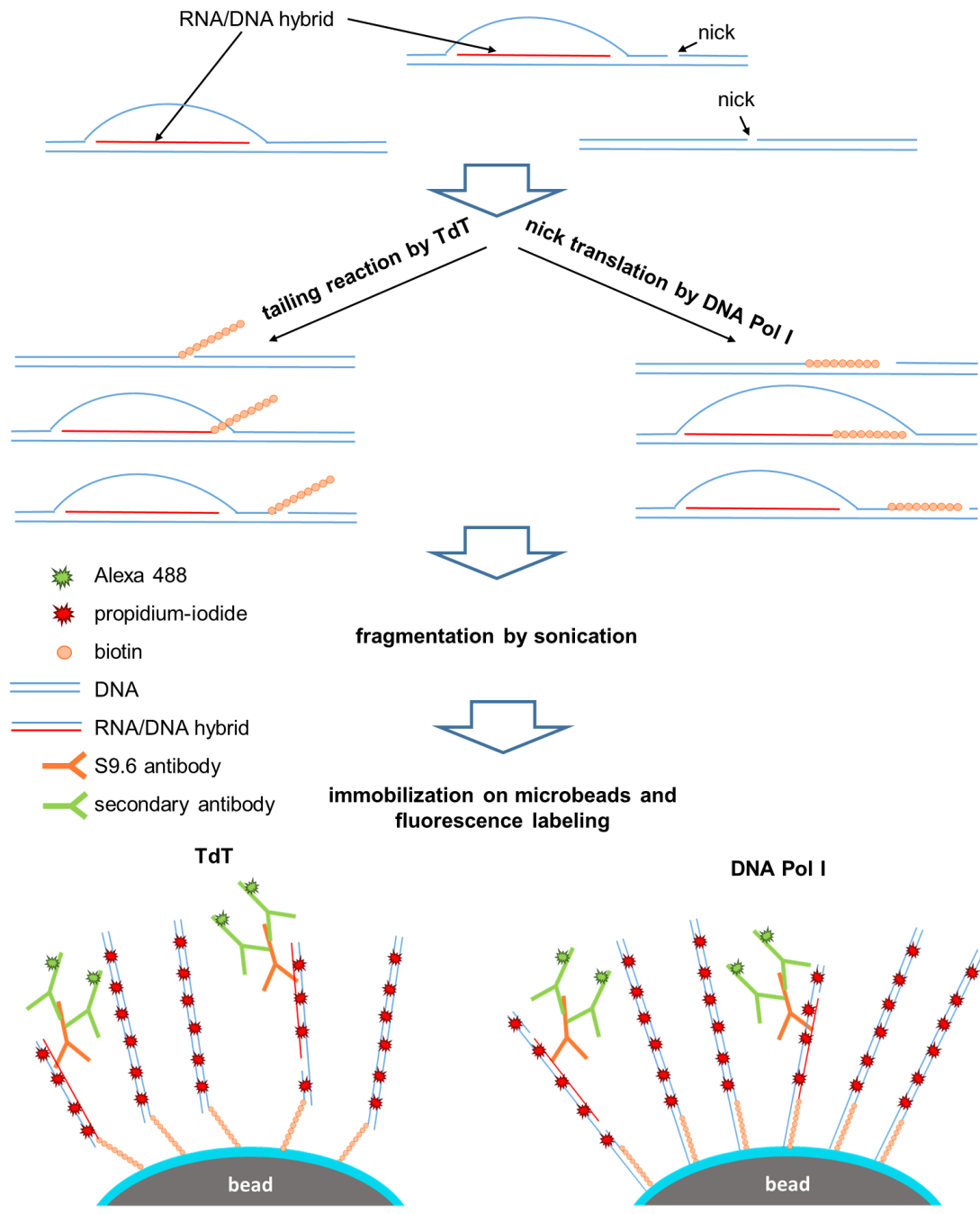


Figure 39. Flow cytometric detection of nicks and nick-proximal R-loops. Experimental design elaborated to distinguish the three scenarios shown: (a) when the labeled 3'OH belongs to the nick in the DNA and the R-loops are nearby, (b) when the labeled 3'OH belongs to the nick in the DNA and the R-loops are more than one nucleosome away from the nicked site, and (c) when the labeled free 3'OH belongs to the R-loop itself. Scheme of the method: limited nick-translation, fragmentation and immobilization of DNA on microbeads. Labeling of immobilized DNA fragments was performed by a DNA specific dye (propidium-iodide) and an RNA/DNA hybrid- (R-loop-) specific antibody (S9.6).

To test this strategy, pilot experiments were performed where live human peripheral blood lymphocytes (HPBLs) were embedded into agarose plugs, then the cells were fixed, lysed and deproteinized. The nicks were labeled by *in situ* nick-translation or tailing reaction using biotinylated nucleotides. To avoid the spreading of biotinylation to long distances, both reactions were terminated by dideoxy nucleotides so that it is only the 100-200 bp vicinity of the nicks that are labeled (referred to as limited nick-translation; method worked out by Éva Hegedüs; (Hegedüs et al. 2018)). After nick-labeling, the agarose plugs were melted and digested with β -agarase. Then the genomic DNA was sonicated to approximately 200-500 bp fragments, which were isolated and immobilized on streptavidinated microbeads. Propidium-iodide staining was used to measure the amount of microbead bound DNA, and the S9.6 anti-RNA/DNA-hybrid antibody was applied to assess R-loops. For nick-translation and tailing reaction DNA polymerase I (Pol I) and terminal deoxynucleotidyl transferase (TdT) were used, respectively (**Figure 40**).

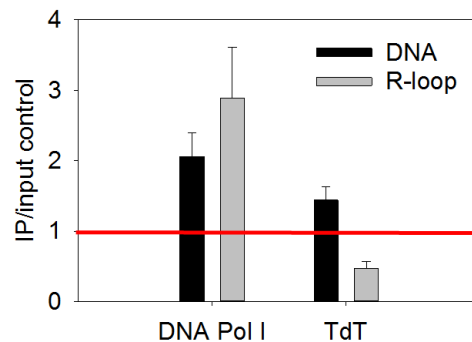


Figure 40. Detection of nicks and nick-proximal R-loops.

Biotinylated DNA fragments were immobilized on streptavidinated microbeads. Biotinylation was by limited nick-translation using DNA Pol I or via tailing reaction using TdT. DNA was quantified by propidium-iodide staining. R-loops detected by S9.6 primary antibody and A488 conjugated secondary antibody were measured in parallel with DNA. In the case of the input control, the same amount of non-biotinylated DNA was added to the beads, to take the nonspecific DNA binding to microbeads into account. Fluorescence intensities were corrected for the background of the empty beads. Values reflect the fold change of IP compared to input; values above 1 (red line) were considered indicative of R-loops co-localizing with free 3'OH ends. Error bars represent the SD of microbeads in a single experiment.

The data show that the efficiency of nick-translation was higher in the case of Pol I labeling as reflected by the higher fluorescence signal of microbead bound DNA. TdT labeling did not yield immunoprecipitates above the threshold. R-loops were detected in the vicinity of nicks with 3'OH, when biotin labeling was performed with Pol I (**Figure 40**). The observations are compatible with scenarios (a) and (c) in **Figure 39**. and argue against (b). The combined RNase treatment tested in (Hegedüs et al. 2018) will be used to distinguish (a) and (c).

C. 3. DISCUSSION

The above observations demonstrate that cytometric microbead assays can give an independent assessment of co-localizing epigenetic marks, what can be used in conjunction with, or as an alternative approach to, sequential ChIP (re-ChIP) procedures. The method was verified detecting co-occurrence of endogenous γ H2A.X either with H3K4me3 or H3K27ac confirming published data (Shema et al. 2016).

As a positive control, etoposide treated cells were used. In these samples the γ H2A.X level is elevated mainly due to the ds DNA breaks elicited by TOP2 inhibition. An increased amount of γ H2A.X was detected on the beads derived from the positive control by an anti-H2A.X antibody (which recognizes both phosphorylated and unphosphorylated H2A.X). Although the anti-H2A.X antibody could compete with the bead captured anti- γ H2A.X, elevated level of H2A.X could be detected on beads carrying nucleosomes captured by anti- γ H2A.X after etoposide treatment. This is in line with data published in (Shema et al. 2016), where co-labeling of PTMs on the same N-terminal tail was performed on biotinylated histones immobilized on streptavidinated surfaces. Thus, sterical hindrance may not be a decisive factor in our experiments.

The co-localization of γ H2A.X and H3K4me3 was further confirmed by superresolution STED microscopy. Based on Pearson's and Manders correlation coefficients calculated from the images, a large fraction of the endogenous γ H2A.X molecules resides in close proximity to H3K4me3, while a smaller fraction of H3K4me3 is localized to γ H2A.X positive regions.

In the experiments above, the γ H2A.X specific antibody used to coat the microbeads was biotinylated. Applying biotin conjugated secondary antibodies, the method can be applied in a versatile manner. Using a panel of antibodies specific for histone PTMs or histone variants, this assay can serve as a feasible tool to perform simple, time- and cost-effective screening studies for the evaluation of histone PTM and histone variant combinations present

on nucleosomes. In contrast with other methods, such as the commonly used Western blot (Kimura et al. 2008; Hayashi-Takanaka et al. 2015), ChIP-Seq (Kinkley et al. 2016; Weiner et al. 2016), or the specialized TIRF microscopic methods (Shema et al. 2016), the microbead assays are much less demanding and are suitable for high-throughput screening. The assay is also able to detect if different PTMs co-occur on the same histone molecule.

The assay could also be used to investigate if endogenous nicks and R-loops on the one hand, and nicks and RNA Pol II species on the other are in molecular proximity. The presence of R-loops in the immunoprecipitates when DNA Pol I was used for nick-labeling extends our earlier data (Szekvolgyi et al. 2007) by suggesting proximity of the two entities within a nucleosomal distance. However, molecular interpretation of this proximity needs further studies, to discern true nick-labeling from that of the free 3'OH of R-loop-derived RNA. The mechanisms behind juxtaposition are yet to be elucidated: one of the possibilities implies TOP2 β , in line with the free 3'OH end configuration and with literature alike (Puc et al. 2017), while R-loop formation may be a downstream effect as nicks are known to promote R-loop formation (Roy et al. 2010). On the other hand, accumulation of the nick signal near sites of RNA Pol II Ser 5-P enrichment detected by the “ChIP-on-beads” approach in the *S. cerevisiae* genome is in line with the possibility that the ss breaks appear in concert with RNA Pol II-related transcriptional activity.

These observations illustrate the utility of the “ChIP-on-bead” approaches described in epigenetic research. The flow and laser scanning cytometric platforms could be interchangeably applied in the assays demonstrated.

GENERAL DISCUSSION AND CONCLUSIONS

GENERAL DISCUSSION

In view of the data presented here, flow cytometry can be utilized for the detection of local genetic alterations. Introduction of this strategy for routine diagnostic purposes may be facilitated by the readily available instrumentation and the wealth of relevant experience already present in many laboratories. Due to its relative simplicity, the method may find its place among the molecular genetic approaches routinely used for such purposes. It may be offered in the case of demand for high-throughput multiplex assays for the simultaneous analyzes of a limited number of genetic conditions in large populations of human and non-human biological samples. The assay based on the differential melting of PCR products of different length was patented in the Hungarian Intellectual Property Office as „Cytometric process for comparative analysis of PCR products lengths and the use of this process”, with an application number: P0800760.

Quantitative microscopy has proved useful in the epigenetics field as a tool of global analyzes (Szekvolgyi et al. 2009; Simandi et al. 2015); the analytical platform described here (based on ref. (Imre et al. 2017)) greatly extends its utility yielding data of direct functional relevance. QINESIn is a very promising approach with high-throughput screening potential what could be exploited e.g. for the chemical profiling of the genome in search of intercalators with PTM, or histone variant specific effects (Pang et al. 2015).

The peculiar stability of H2A.Z containing nucleosomes presented herein provide a good example for the utility of QINESIn in assessing nucleosome stability features affected by reader proteins. These observations not only call the attention to the unexpected differences between different polyclonal antibodies specific for the same histone variant, but also to the heterogeneity of nucleosomes containing the same variant. I think that QINESIn fills in a gap in the spectrum of methods, between ChIP-Seq and immunofluorescence detection of PTMs, providing an approach with functional relevance.

The assay was registered in the Hungarian Intellectual Property Office as „Quantitative *in situ* measurement of histone-DNA interaction.”, application number: P1200081.

It was also demonstrated that flow and laser scanning cytometric analyzes can be extended to the field of epigenetics. ChIP combined with MMA could be a relevant alternative of Western blot or re-ChIP techniques offering multiplex high-throughput analyzes of histone PTM or histone variant combinations of nucleosomes. This aspect may gain special importance in view of the fact that histone PTMs act not only as single modifications but in a combinatorial manner as well, e.g. the H3K4me3/H3K27me3 double-positive nucleosomes

seem to define the poised state of developmental genes (Voigt et al. 2012). Using our method, it will be possible to answer the question how the simultaneous presence of these seemingly antagonistic effects together determine the stability of these „bivalent” nucleosomes.

CONCLUSIONS

1. Methodical. The array of methods elaborated greatly extend the methodical possibilities of cytometry, could serve as the bases for the development of high-throughput tests of genetic and epigenetic alterations and constitute a versatile platform for investigations, realizing the concept of a „lab-on-beads”.
2. Biological. A number of conclusions of biological relevance have been reached that are listed below to illustrate the wide spectrum of problems that can be efficiently addressed using these approaches:
 - 2.1. The relatively destabilized nature of H3K4me3 modified nucleosomes is a general feature, independent of cell type and differentiation state, and it is limited to the promoter-proximal nucleosomes.
 - 2.2. Relaxation of superhelicity by nicks have a major effect on nucleosome stability.
 - 2.3. The destabilizing effect of nicks spreads to loop size distances.
 - 2.4. Phosphorylation decreases the intrinsic stability of dimers containing histone variant H2A.X.
 - 2.5. The majority of H2A.Z containing dimers are unusually stably associated with the tetrasomes.
 - 2.6. Stability of H2A.Z containing dimers does not depend on the isotypes of H2A.Z
 - 2.7. H2A.Z containing dimers comprise an intercalator resistant subpopulation.
 - 2.8. The unusually salt- and intercalator-resistant characteristics of H2A.Z are due to the binding of the PWWP2A reader protein.
3. A number of new questions of biological significance have been raised in the wake of our studies:
 - 3.1. Are there any other PTMs that affect nucleosome stability?

- 3.2. Does the destabilizing role of PWWP2A represent an example of a paradigm for other other histone variants and perhaps for PTM sas well?
- 3.3. What is the exact relationship between free 3'OH groups of R-loop origin and those defining bona fide endogenous nicks?

MATERIALS AND METHODS

Chemicals

All reagents were from Sigma-Aldrich (St. Louis, Missouri, USA) unless otherwise stated.

Plasmids

The plasmids carrying different length CAG repeats (Scherzinger et al. 1999) or different isoforms of the histone variant H2A.Z were transformed into *Escherichia coli* DH5 α by heat shock and selected on LB plates containing 100 μ g/ml ampicillin.

DNA isolation

Genomic and plasmid DNA were prepared by the Intron G-DEX Genomic DNA Extraction Kit and DNA-midi Plasmid DNA Purification Kit (Intron Biotechnology, Seongnam-Si, South Korea) following the manufacturer's instructions.

Cells and clinical samples

HeLa cells expressing H2B-GFP, H3-GFP and H4-GFP fusion proteins (Kimura and Cook 2001), and HCT116 cells (Developmental Therapeutics Branch, National Cancer Institute, Bethesda, Bethesda, MD, 20892) were cultured in DMEM supplemented with 10% FCS, 2 mM l-glutamine, 100 μ g/ml streptomycin, 100 U/ml penicillin. Jurkat cells were cultured in RPMI1640 medium supplemented with 10% FCS, 2 mM l-glutamine 100 μ g/ml streptomycin, 100 U/ml penicillin, Wild type, H2A.Z1 knock-out, H2A.Z2 knock-out, double knock-out and mutant H2A.Z1 expressing DT-40 chicken B cells (provided by Masahiko Harata (Kusakabe et al. 2016; Punzeler et al. 2017)) were cultured in DMEM supplemented with 2% chicken serum, 8% FCS, 2 mM l-glutamine, 100 μ g/ml streptomycin, 100 U/ml penicillin.

Genomic DNA derived from anonymous patients diagnosed with Huntington's disease, confirmed by sequence analyzes and polyacrylamide gel electrophoresis using two different sets of primers, were isolated at the Department of Medical Genetics, School of Medicine, University of Pécs. Genomic DNA with BRCA1 5382 insC mutation was from the Department of Clinical Biochemistry and Molecular Pathology, Medical and Health Science Center, University of Debrecen. Genomic DNA derived from peripheral blood lymphocytes of healthy volunteers were isolated in our laboratory.

PCR reactions

Huntington's disease:

PCR reactions were performed in 50 µl of 1× reaction buffer (7.5 mM Tris-HCl, 20 mM (NH₄)₂SO₄, 0.1 % Tween 20, pH 8.8) containing 2.5 mM dNTP-solution (Promega Life Sciences, Madison, Wisconsin, USA), 200 ng template DNA, 10 pmole of each primer, 1.5 mM MgCl₂, 1 mM β-mercaptoethanol, 3 % formamide, 0.2 mg/ml BSA (Promega Life, Sciences, Madison, Wisconsin, USA) and 2.5 U Taq polymerase (Fermentas, Vilnius, Lithuania). The primers used for amplification of the CAG repeats in the exon 1 of the Huntingtin gene (IT15/HTT/HD) were purchased from Integrated DNA Technologies (Coralville, Iowa, USA). Forward primer, Hunt1: biotin-5'-CAT GGC GAC CCT GGA AAA GCT G-3', reverse primer, Hunt2: Cy5-5'-GGC GGT GGC GGC TGT TGC TGC TGC TG-3' and reverse primer, Hunt3: Cy3-5'-GGC GGT GGC GGC TGT TGC TGC TGC TG-3' (Margolis and Ross 2003). The PCR reactions were performed as described in ref. (Muglia et al. 1996). The products were analyzed on 3% agarose gels run in 1× TAE (40 mM Tris, 20 mM acetic acid, 10 mM EDTA, pH 8.0).

5382 insC point mutation BRCA1:

Allele-specific PCR reactions were performed in 50 µl of 1× reaction buffer containing 2.5 mM dNTP-solution (Promega Life Sciences, Madison, Wisconsin, USA), 200 ng template DNA, 10 pmole of each primer, 1.5 mM MgCl₂, and 2.5 U Taq polymerase (Fermentas, Vilnius, Lithuania). The wild type allele specific forward primer (BRCA1: Cy5-5'-AAA GCG AGC AAG AGA ATC GCA-3'), the mutation specific forward primer (BRCA2: Cy5-5'-CAG CAG CAG CAG CAG CAG CAC CTT AGC GAG CAA GAG AAT CAC C-3', containing a 5' tag of a 18 bp CAG repeat) and the common reverse primer (BRCA3: biotin-5'-AGT CTT ACA AAA TGA AGC GGC CC-3') were used together in a multiplex reaction (Chan et al. 1999). The primers determine a 126 bp long fragment of the human BRCA1 gene, including the site of the 5382 insC point mutation. PCR reaction was performed using the following profile: 1 × 95°C: 12 s; 37 × 94°C: 15 s, 62°C: 15 s, 72°C: 30 s; 1 × 72°C: 5 min, 4°C. The products were analyzed on 3% agarose gels run in 1× TAE (40 mM Tris, 20 mM acetic acid, 10 mM EDTA, pH 8.0).

Heteroduplex analysis:

PCR was performed using 2.5 U Taq polymerase in 50 µl of 1× reaction buffer containing 200 ng template DNA, 20 pmol of each primer, 2.5 mM of dNTP, and 1.5 mM

MgCl₂. The template was the pMEP4 plasmid DNA containing the breakpoint cluster region of the human MLL gene (from Peter Aplan, NIH, Bethesda; see **Figure 41**), throughout the experiments. All primers (pIL1 forward 5'–ATA TGA ATA CTC ATC ACT GAG TGC CTT TGG C–3'; pIL1-biotin forward 5'–(biotin)-ATA TGA ATA CTC ATC ACT GAG TGC CTT TGG C–3'; pM3 forward 5'–GCT GGA GTG TAA TAA GTG CCG A–3'; pM6 reverse 5'–AGC GAA CAC ACT TGGTAC AGATC–3'; pM6-6FAM reverse 5'–(6FAM)-AGC GAA CAC ACT TGG TAC AGA TC–3') were purchased from Integrated DNA Technologies (Coralville, IA; positions of the primers are shown in **Figure 41**). In the first reaction cycle, denaturation was at 94°C for 3 min, annealing was for 2 min, polymerization at 72°C for 1.5 min; this was followed by 35 cycles, 50 s each. In the case of the PCR reaction defined by pIL1–pM6 (574 bp), and pM3–pM6 (357 bp), the annealing temperatures were 56, and 61°C, respectively. The PCR products were cleaned with QIAquick PCR Purification Kit (Qiagen, Valencia, CA), eluted in 50 µl sterile TE (10 mM Tris, 2 mM EDTA, pH 8) and analyzed on 2% agarose gels run in 1× TAE (0.04 M Tris, 0.02 M acetic acid, 0.01 M EDTA, pH 8) and stained with ethidium bromide.

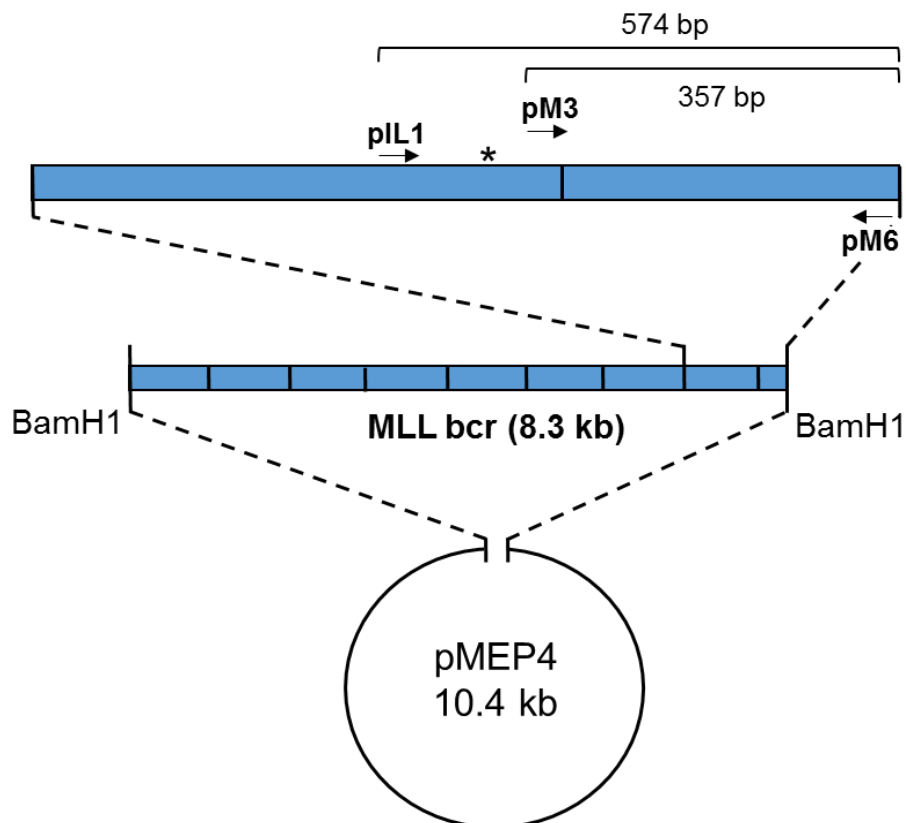


Figure 41. Position of PvuII restriction site (*) and primers (arrows) defining the amplified regions within the MLL bcr of the pMEP4 plasmid.

Preparation of single-stranded DNA by linear amplification:

Amplification was performed at the conditions described above but using either the pIL1-biotin (sense) or the pM6-6FAM (antisense) primer alone. Unlabeled ds PCR products of 574 or 357 bp length were used as template DNA in these experiments.

Hybridization of PCR products and cleavage by Pvu II

The longer 6FAM- and, in a separate test tube, the shorter 6FAM-labeled linear amplicons were mixed with equal amounts of the biotin labeled linear longer product, (as indicated on **Figure 5A**) in TE supplemented with 1 M NaCl. The two samples were denatured at 95°C for 5 min, then annealed at room temperature (RT) for 2 h.

Two hundred nanograms of the hybrids formed between the 6FAM- and biotin labeled PCR products were digested with 10 U Pvu II restriction endonuclease (Fermentas, Life Sciences). Restriction site is shown in **Figure 41**.

Binding of PCR products to beads

Biotinylated and fluorescently labeled PCR products were added to 10 000 polymeric streptavidin coated beads (6 µm diameter, purchased from Polysciences Inc., Warrington, Pennsylvania, USA) in 200 µl 1×PBS (150 mM NaCl, 3.3 mM KCl, 8.6 mM Na₂HPO₄, 1.69 mM KH₂PO₄, pH 7.4) and incubated at RT for 40 min in the dark. After incubation, the beads were washed 3 times in 1×PBS and centrifuged at 20 000 g for 10 min.

Heat treatment in formamide

The beads carrying PCR products on their surface were treated with a concentration series of formamide diluted in ddH₂O. In the experiments related to Huntington's disease the concentration of formamide was titrated between 65-75 v/v % to find the optimal concentration where the PCR products with different length can be distinguished. In the case of the BRCA1 5382insC point mutation, formamide was titrated between 57-62 v/v %. Heat treatment was performed in a total volume of 200 µl, in a PCR tube containing approximately 10 000 beads. The beads were incubated with formamide at 40°C in the dark for 3 min, washed in 600 µl of 1×PBS 3 times and analyzed by flow cytometry

Coating of beads by biotinylated anti- γ H2A.X antibody

10 μ g of the biotinylated mouse monoclonal anti- γ H2A.X (Merck-Millipore, Darmstadt, Germany; 1 mg/ml) antibody was immobilized on the surface of 0.1 mg streptavidinated magnetic Dynabead (Thermo Fisher Scientific, Waltham, Massachusetts, USA), by rotating overnight at 4°C in 1 ml 1×PBS. After immobilization, beads were washed three times with 500 μ l 1×PBS.

Detection of combinatorial histone PTMs

Jurkat cells were washed three times with 5 ml 1×PBS and fixed in 5 ml 1% formaldehyde diluted in 1×PBS/EDTA for 10 min at room temperature on a rotator. After fixation, formaldehyde was quenched by adding 2 ml 2.5 M glycine to the sample. Cells were washed three times with 5 ml 1×PBS/EDTA and resuspended in IP buffer (1% SDS, 50 mM Tris-HCl pH 8, 10 mM EDTA, 1mM PMSF) at a concentration of 10^7 cells/ml. Lysis was achieved by pipetting the cells up and down several times. The cell lysates were centrifugated (12 000 g, at 4°C), and the pellet was resuspended in 1ml of ice-cold IP buffer and sonicated (Bioruptor, Diagenode, New Jersey, USA) for 20 min at 4°C with maximum intensity. The sonicated samples were centrifugated and resuspended in ice-cold IP buffer. 20 μ l aliquots equivalent to 200,000 cells were removed, DNA was isolated and analyzed by agarose gel electrophoresis to control the efficacy of sonication. The sonicated samples were divided to aliquots equivalent of 10^7 cells. 500,000 Dynabeads previously coated with anti- γ H2A.X antibody were added to the sonicated samples and incubated overnight at 4°C on a rotator. The beads were washed 5 times with 500 μ l IP buffer and twice with 1×PBS/EDTA. The nucleosomes immobilized on the beads were labeled with rabbit polyclonal anti-H2A.X (Abcam, Cambridge, UK; 1 mg/ml), rabbit polyclonal anti-H3K4me3 (Abcam, Cambridge, UK; 1 mg/ml) or rabbit polyclonal anti-H3K27ac (Abcam, Cambridge, UK; 1 mg/ml) primary antibody at a titer of 1:800, diluted in 200 μ l 1×PBS/EDTA/1% BSA. Labeling was allowed to proceed for 1 hour on ice, followed by washing three times with 500 μ l 1×PBS/EDTA. Labeling with fluorophore-conjugated secondary antibody was performed in 200 μ l 1×PBS/EDTA supplemented with 12.5 μ g/ml propidium-iodide for 1 hour on ice, followed by washing three times with 500 μ l 1×PBS/EDTA.

Detection of nicks and nick proximal R-loops

Human peripheral blood lymphocyte (hPBL) cells were isolated by Ficol gradient centrifugation. The cells were washed three times with 5 ml 1×PBS and fixed with 1% formaldehyde as described above. An equal volume of cell suspension and 1% LMP agarose (low melting point agarose) diluted in 1×PBS, both kept at 37 °C, were mixed, resulting in a 0.5% final concentration of LMP agarose. The agarose blocks prepared contained 90 µl of agarose/cell suspension. The blocks were washed three times with 15 ml 1×PBS for 10 min on ice. 6 blocks/sample of agarose embedded cells were lysed in 4 ml lysis buffer (1% Sarcosyl, 10 mM Tris-HCl pH 8, 0.4 M EDTA, 0.5 mg/ml Proteinase K) twice, at 55°C for 24 hours. The lysed cells were washed three times with 15 ml ice cold TE (10mM Tris, 1 mM EDTA pH 8.0) for 20 min and treated with 1 mM PMSF diluted in 4 ml TE, for 10 min at room temperature on a rotator. PMSF was washed out 5 times with 15 ml ice cold TE at room temperature. The blocks were equilibrated with Pol I or with TdT buffer, three times for 50 min at room temperature on a rotator. After equilibration, the deproteinized chromatin was nick-translated by DNA Pol I (1×DNA Pol I buffer, 5 µM ddNTP mix, 1 µM dNTP mix, 22.5 U/block DNA Pol I enzyme) or by TdT (1×TdT buffer, 5 µM biotin-dUTP, 10 U/block TdT enzyme). The blocks were kept in the nick-translation solution for 30 min on ice, then transferred into 37°C for 20 min. During nick-translation, the blocks were continuously rotated. Reaction was stopped in a solution of 50 mM EDTA, 10 mM Tris, pH 8 for 15 min on ice. Blocks were washed with 15 ml ice cold TE 5 times for 10 min on ice. Blocks were transferred into „low binding” Eppendorf tubes, melted at 70°C for 10 min, then cooled down to 42°C for 10 min. After 10 min incubation at 42°C, the agarose was digested by adding β-agarase enzyme to the melted blocks at a concentration of 1U/block. Digested blocks were transferred to ice for 5 min and sonicated as above for 15 min at 4°C with maximum intensity. The DNA was cleaned by a DNA-midi Plasmid DNA Purification Kit (Intron Biotechnology, Seongnam-Si, South Korea) following the manufacturer’s instructions and immobilized on streptavidinated Dynabeads (60,000/sample) in 1 ml TE, rotated overnight at 4°C. After immobilization, the beads were washed 5 times in 1 ml TE and labeled with the S9.6 RNA/DNA-hybrid specific antibody in 200 µl 1×PBS/EDTA/1% BSA at a titer of 1:800, at room temperature, for 2 hours. Beads were washed three times with 1 ml 1×PBS/EDTA and labeled with fluorophore conjugated secondary antibody at a titer of 1:800 in 200 µl 1×PBS/EDTA supplemented with 12.5 µg/ml propidium-iodide. After antibody labeling, the beads were washed with 1 ml 1×PBS/EDTA and measured by a flow cytometer.

Flow cytometry

Melting point analyzes:

Measurements were performed using a Becton Dickinson FACSArray instrument (San Jose, California, USA). Fluorescence signals were detected in the PI/Yellow and Far Red channels through the 585/42 and 675 LP interference filters of the instrument, respectively.

Fluorescence signals were collected in the logarithmic mode and the data were analyzed using the ReFlex software (Szentesi et al. 2004).

Heteroduplex analyzes:

Measurements were performed using a Becton Dickinson FACScan instrument (San Jose, California, USA). Fluorescence signals were detected through the 530/30 and the 585/42 interference filter of the instrument, designated as FL1 and FL2 channels, respectively.

Fluorescence signals were collected in the logarithmic mode and the data were analyzed using the ReFlex software (Szentesi et al. 2004).

Detection of combinatorial histone PTMs and nick proximal R-loops:

Measurements were performed using a Becton Dickinson FACS Aria III instrument (San Jose, California, USA). Fluorescence signals were detected in the PI/Yellow and Far Red channels through the 585/42 and 675 LP interference filters of the instrument, respectively.

Fluorescence signals were collected in the logarithmic mode and the data were analyzed using the ReFlex software (Szentesi et al. 2004).

FACS Aria III measurements were performed by Szabolcs Tarapcsák.

Global „ChIP-on-beads” assay

Preparation of nuclei:

The pellet of 400 ml log phase culture of *S. cerevisiae* cells was resuspended and fixed in 10 ml freshly prepared 4% paraformaldehyde dissolved in 1×PBS, rotating the cells for 10 min at room temperature. After quenching in 2.5 M glycine and washing twice with 50 mM Tris-HCl (pH 7.5)/30 mM DTT, the cells were treated with 2 mg/ml lyticase dissolved in 0.9 M sorbitol/0.125 M EDTA/10 mM DTT at 37 °C for 30 min. The spheroplasts were washed twice with 10 ml ice cold 0.9 M sorbitol/0.125 M EDTA, lysed in 4 ml ice cold buffer N (30 mM HEPES pH 7.6, 3 mM DTT, 25 mM Na₂SO₄, 5 mM MgCl₂, 1 mM EDTA, 10% glycerol,

0.5% NP-40, 7.2 mM spermin, 1 mM PMSF) and disintegrated using a Dounce homogenizer on ice for 60 min.

Nickase treatment and nick-translation:

The nuclei were washed three times in ice cold 1×PBS/EDTA followed by washing in nickase buffer (10 mM Tris-HCl pH 8, 50 mM NaCl, 10 mM MgCl₂, 1 mg/ml BSA). Random nicks were introduced into the DNA of control samples using the frequent cutter Nt.CviPII nickase enzyme (recognition site: CCD; New England Biolabs Inc., Ipswich, Massachusetts, USA) at a final enzyme concentration of 0.5 U/ml. Limited nick-translation of the samples harboring only endogenous nicks and of the nickase treated control was performed as described above.

Fragmentation of chromatin, microbead capture:

The nick-translated samples of nuclei were resuspended in 700 µl IP lysis buffer (50 mM HEPES-KOH pH 7.5, 140 mM NaCl, 1 mM EDTA, 1% Triton X-100, 0.1% Na-deoxycholate) and disintegrated using a FastPrep-24™ 5G Instrument bead beater (MP Biomedicals, Santa Anna, California, USA) at default setting for *S. cerevisiae*, applying 200 µl glass beads/sample. Disintegration of the nuclei was checked under the microscope. After removal of the beads, the samples were sonicated with a Bioruptor Plus sonicator (Diagenode, Denville, New Jersey, USA) for 3 cycles (1 cycle: 30 sec ON, 30 sec OFF, for 5 min) and spun down in an Eppendorf centrifuge at 15 000 rpm at 4°C for 5 min. The supernatants were transferred into a clean Eppendorf tube and the fragment size was determined by gel electrophoresis in a proteinase K treated aliquot (~500 bp in the experiment shown in **Figure 38**). The streptavidinated Dynabeads (Thermo Fisher Scientific, Waltham, Massachusetts, USA) were blocked with 1% BSA dissolved in 1×PBS/EDTA and washed three times with 1×PBS/EDTA. 60 000 beads were added to the sonicated chromatin and rotated at 4°C overnight. The beads were washed with 1×PBS/EDTA and embedded into agarose in an 8-well chamber (Ibidi, Martinsried, Germany) see below.

Immunofluorescence labeling:

The agarose embedded Dynabeads were washed twice with lysis buffer, twice with lysis buffer supplemented with 360 mM NaCl, twice with washing buffer (10 mM Tris-HCl pH 8, 250 mM LiCl, 0.5% Na-deoxycholate, 1mM EDTA), finally twice with 1×PBS/EDTA. Indirect immunofluorescence labeling was performed using rabbit polyclonal anti-RNA Pol II

Ser2-P (Abcam, Cambridge, UK; 1 mg/ml) or rabbit polyclonal anti-RNA Pol II Ser5-P (Abcam, Cambridge, UK; 1 mg/ml) diluted in 200 μ l 1 \times PBS/EDTA/1% BSA at 4°C, overnight. The antibodies were applied to the wells at a titer of 1:400. After labeling with the primary antibodies, the beads were washed with 1 \times PBS/EDTA three times for 10 min. Labeling with the secondary antibody were performed in 200 μ l 1 \times PBS/EDTA on ice for two hours, using Alexa fluor 488 (A488) conjugated goat anti-rabbit IgG (Thermo Fisher Scientific, Waltham, Massachusetts, USA; 2 mg/ml). The secondary antibody was used at a titer of 1:800, diluted in 1 \times PBS/EDTA. After labeling, the agarose embedded beads were washed with 1 \times PBS/EDTA three times and stained with 200 μ l 12 μ g/ml propidium-iodide (in 1 \times PBS/EDTA) on ice for 30 min. All the washing steps were performed with ice-cold buffers. After washing, the fluorescence intensity distributions were recorded using a laser scanning cytometer (LSC; see below).

Determination of background fluorescence:

Following the first LSC measurement, the agarose embedded Dynabead samples were equilibrated with DNase I buffer (10 mM Tris-HCl pH 8, 0.1 mM CaCl₂, 2.5 mM MgCl₂) and digested with DNase I at a final concentration of 5 μ g/ml in 300 μ l DNase I buffer at 37 °C for 60 min. After enzymatic treatment, the agarose-embedded beads were washed with 500 μ l ice-cold 1 \times PBS/EDTA and measured again by LSC in a second run, performed on the same beads. The mean fluorescence intensity remaining after DNase digestion was subtracted from the mean of the first LSC run, to correct for the background fluorescence.

Embedding live cells into low melting point agarose

Prior to embedding the wells of 8-well chambers (Ibidi, Martinsried, Germany) were coated with 1% (m/v) LMP agarose. 150 μ l liquid agarose, diluted in distilled water was dispensed into each well and was immediately removed so that a thin agarose layer remained on the surfaces and was left to polymerize on ice for 2 minutes, then kept at 37°C until the surface of the wells dried out. This coating procedure was repeated once more on the same chambers. Embedding was performed keeping cells and agarose at 37°C. The cell suspension containing 6 \times 10⁶ cells/ml was mixed with 1% LMP agarose diluted in 1 \times PBS at a v/v ratio of 1:3. 22 μ l of the cell-agarose suspension was dispensed in the middle of the wells and the chambers were covered with home-made rectangular plastic coverslips (**Figure 42**) cut out from a 200 μ m thick medium weight polyvinyl chloride binding cover (Fellowes, Inc., Itasca,

Illinois, USA). Cells were left to sediment on the surface of the coated wells for 4 minutes at 37°C, then kept on ice for 2 minutes. After polymerization of the agarose 300 µl ice cold complete culture medium was added to each well, a step aiding removal of the coverslips.

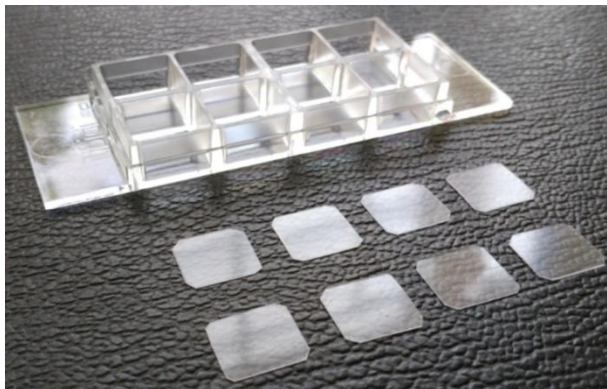


Figure 42. Plastic coverslips used to prevent meniscus formation and drying out of the agarose-embedded cells in the wells of the 8-well Ibidi cell culture chambers.

Preparation of nuclei/permeabilization and histone eviction by salt or intercalators

The agarose embedded cells at the bottom of the wells were washed with 500 µl ice cold 1×PBS, three times for three minutes each, then permeabilized with 500 µl ice cold 1% (v/v) Triton X-100 dissolved in 1×PBS/EDTA (5 mM EDTA in PBS), for 10 minutes. This step was repeated once more. After permeabilization, nuclei were washed with 500 µl ice cold 1×PBS/EDTA three times for three minutes and were treated with different concentrations of NaCl or intercalator solutions on ice. Ethidium bromide (EBr) and SYBR Gold (Thermo Fisher Scientific, Waltham, Massachusetts, USA) were diluted in 1×PBS/EDTA supplemented with 600 mM NaCl, to the final concentrations indicated in the Figures. EBr was used at 100 µg/ml when the salt concentration was titrated (**Figure 10**). Doxorubicin (TEVA, Debrecen, Hungary) was diluted and added to live cells in complete DMEM medium, or diluted in 1×PBS/EDTA when added to the permeabilized cells. Nuclei were washed with 400 µl of ice cold salt or intercalator solution six times, for 10 minutes. After this treatment, nuclei were washed with 500 µl ice cold 1×PBS/EDTA three times for 3 minutes. Since NaCl was diluted in 1×PBS/EDTA, the salt concentrations indicated on the X axes of the graphs in all the Figures show the total NaCl concentrations together with NaCl present in the PBS buffer. Analysis of the curves was made by SigmaPlot 12.0, using either ‘Sigmoid 3 parameter’ (in the case of linear plots) or ‘Standard curves: Four Parameter Logistic Curve’ (in the case of logarithmic plots) curve-fitting subroutines. Elution curves were normalized to '0' subtracting

the smallest value from all the others, and to '1' dividing the mean fluorescence intensities represented by the data points by that of the non-treated sample. At the experiments where eviction was partial, normalization was performed only for '1'. The number of analyzed G1 nuclei were between 200-1000/well, out of the about 500-2000 cells scanned. All the SEM values indicated in the Figures were calculated from the datapoints of the cell population analyzed in the given experiment. Standard deviations (SD) on **Figure 33B-E** were calculated from the means of distributions of three independent experiments.

Immunofluorescence labeling

After salt or intercalator treatment the samples were incubated with 500 μ l 5% (m/v) Blotto Non-Fat Dry Milk (Santa Cruz Biotechnology Inc., Santa Cruz, California, USA) in 1 \times PBS/EDTA for 30 minutes on ice, to decrease nonspecific binding of the antibodies. The blocking solution was washed out with 500 μ l ice cold 1 \times PBS/EDTA three times for three minutes and indirect immunofluorescence labeling was performed using rabbit polyclonal anti-H2A (Abcam, Cambridge, UK; 0.4 mg/ml), rabbit polyclonal anti-H2A.X (Abcam, Cambridge, UK; 1 mg/ml), mouse monoclonal anti- γ H2A.X (Merck-Millipore, Darmstadt, Germany; 1 mg/ml), mouse monoclonal anti-H3K4me3 ((Kimura et al. 2008); 0,5 mg/ml) or mouse monoclonal anti-H3K27me3 ((Hayashi-Takanaka et al. 2011); 0,5 mg/ml) primary antibodies, all diluted in 150 μ l of 1 \times PBS/EDTA/1% BSA (1 \times PBS/EDTA supplemented with 1% w/v bovine serum albumin), at 4°C, overnight. All the above antibodies were applied to the wells at a titer of 1:800. After labeling with the primary antibodies, the nuclei were washed with 500 μ l ice cold 1 \times PBS/EDTA three times for 10 minutes. Labeling with the secondary antibodies was performed in 150 μ l 1 \times PBS/EDTA for two hours on ice, using Alex fluor 488 (A488) or Alexa fluor 647 (A647) conjugated goat anti-mouse IgG or goat anti-rabbit IgG antibodies (Thermo Fisher Scientific, Waltham, Massachusetts, USA). The secondary antibodies were also used at a titer of 1:800, diluted in 1 \times PBS/EDTA from 2 mg/ml stock solutions. After labeling with the secondary antibodies the agarose embedded nuclei were washed with 500 μ l ice cold 1 \times PBS/EDTA three times, for 10 minutes. Then the samples were fixed in 1% formaldehyde (dissolved in 1 \times PBS/EDTA) at 4°C, overnight. After fixation the wells containing the embedded nuclei were washed with 500 μ l ice cold 1 \times PBS/EDTA three times, for 3 minutes and were stained with 200 μ l 25 μ g/ml propidium-iodide (PI, dissolved in 1 \times PBS/EDTA) for 30 minutes, on ice. The stained nuclei were washed three times with 500 μ l ice cold

1×PBS/EDTA for 3 minutes. Fluorescence intensity distributions were recorded using an iCys laser scanning cytometer (LSC), as described below.

Etoposide treatment

Agarose embedded live cells were treated with etoposide (TEVA, Debrecen, Hungary) used at a final concentration of 25 μ M. The drug was diluted in 300 μ l complete DMEM medium and the cells were incubated together with the drug at 37°C in 5% CO₂ atmosphere, for 1, 3 or 6 hrs.

Nickase and DNase I treatment

Live cells were embedded into agarose as described above and treated with 500 μ l ice cold lysis buffer (0.4% (v/v) Triton X-100, 300 mM NaCl, 1 mM EDTA, 10 mM Tris-HCl, pH8) for 10 minutes, followed by treatment with 500 μ l ice cold 1% (v/v) Triton X-100 dissolved in 1×PBS/EDTA, for 10 minutes, then washed three times with 500 μ l ice cold 1×PBS/EDTA. The frequent cutter Nt.CviPII nickase (recognition site: CCD; New England Biolabs Inc., Ipswich, Massachusetts, USA) and DNase I were applied after the washing steps following permeabilization (see above). Before digestion, the samples were equilibrated with nickase buffer (10 mM Tris-HCl pH 8, 50 mM NaCl, 10 mM MgCl₂, 1 mg/ml BSA) or with DNase I buffer (10 mM Tris-HCl pH 8, 0.1 mM CaCl₂, 2.5 mM MgCl₂) by washing three times with 500 μ l of the buffer solutions. Nickase treatment was performed in 300 μ l nickase buffer for 30 min at 37 °C, using the enzyme at a final concentration of 0.5 U/ml, titrated so as to maximize nuclear halo radii without losing DNA. DNase I digestion was performed in 300 μ l DNase I buffer for 10 min at 37 °C, at a final concentration of 0.1 μ g/ml DNase I; in these conditions both single and double strand breaks can be expected, but no significant loss of nuclear DNA content was seen. After enzymatic treatments, the samples were washed with 500 μ l ice cold 1×PBS/EDTA three times for three minutes.

Immuno- cross-linking experiments

Agarose embedded and permeabilized HeLa cells expressing H2B-GFP were incubated with 500 μ l 5% (m/v) Blotto Non-Fat Dry Milk dissolved in 1×PBS/EDTA, for 30 minutes, on ice, to decrease nonspecific binding. The blocking solution was washed out with 500 μ l ice cold 1×PBS/EDTA three times and indirect immunofluorescence labeling was

performed using rabbit polyclonal anti-H2A antibody at a titer of 1:800, diluted in 150 μ l of 1 \times PBS/EDTA/1% BSA, at 4°C, overnight. After labeling with the anti-H2A antibody, the nuclei were washed with 500 μ l ice cold 1 \times PBS/EDTA three times. Anti-H2A labeled histones were cross-linked with the secondary antibody in 150 μ l 1 \times PBS/EDTA for two hours on ice, using A647-conjugated goat anti-rabbit IgG. The secondary antibody was used at a titer of 1:800, diluted in 1 \times PBS/EDTA from its 2 mg/ml stock solution. After labeling with the secondary antibody, nuclei were washed with 500 μ l ice cold 1 \times PBS/EDTA three times and the samples were treated with NaCl or doxorubicin solutions as described above. Then the samples were fixed with formaldehyde, stained with propidium iodide and the fluorescence intensity distributions were recorded by LSC, as described above.

Gel electrophoretic analyzes

The permeabilized, agarose-embedded H2B-GFP expressing samples were deproteinized as described earlier (Szekvolgyi et al. 2007). Standard, nondenaturing agarose gel electrophoresis was performed with or without posttreatment of the nickase digested samples with S1 nuclease (1000 U/ml) used in its own buffer (1h at 37°C) to convert nicks into double-strand breaks. For pulsed-field gelectrophoresis of the S1-treated samples, either a CHEF mapper XA Pulse Field Electrophoresis System (Bio-Rad Laboratories Inc., Hercules, California, USA) was used following the manufacturer's instructions to resolve 3-300 kb fragments, or an MJ Research PPI-200 power inverter (Field Inversion Gelectrophoresis; FIGE) running 'program 5' to resolve the same size range. For markers, O'GeneRuler 1kb DNA ladder (Thermo Fisher Scientific, Waltham, Massachusetts, USA), lambda DNA (Thermo Fisher Scientific, Waltham, Massachusetts, USA) and Pulse Marker 2200-225 kb were used. Urea/agarose gel electrophoresis was performed as described in ref. (Hegedus et al. 2009).

Automated microscopy

Automated microscopic imaging was performed using an iCys instrument (iCys® Research Imaging Cytometer; CompuCyte, Westwood, Massachusetts, USA). Green fluorescent protein (GFP), SYBR Gold, A488, doxorubicin and PI were excited using a 488 nm Argon ion laser, A647 with a 633 nm HeNe laser. In the case of elution assays fluorescence signals were collected via an UPlan FI 20 \times (NA 0.5) objective, scanning each field with a step size of 1.5 μ m. For the measurement of agarose embedded microbeads,

fluorescence signals were collected via an UPlan FI 40× (NA 0.65) objective, scanning each field with a step size of 0.5 μm. GFP and A488 were detected through 510/21 nm and 530/30 nm filters, respectively, while doxorubicin, A647 and PI were detected through a 650/LP nm filter.

Data evaluation and hardware control were performed with the iCys 7.0 software for Windows XP. Gating of G1 phase cells was according to the fluorescence intensity distribution of the DNA labeled with PI or SYBR Gold. (The iCys laser scanning cytometer can be replaced with other automated imaging platforms and software applications (e.g. Olympus ScanR, Molecular Device ImageXpress, Perkin Elmer Opera Phenix, ThermoFisher CellInsight, GE IN Cell Analyzer). When appropriate image series are generated, software applications (like CellProfiler, Fiji, ImageJ, Micropilot) are readily available for their high content analyzes.)

Confocal Laser Scanning Microscopy (CLSM)

Confocal images were taken using an FLUOVIEW FV 1000 confocal microscope (Olympus, Center Valley, Pennsylvania, USA) based on an inverted IX-81 stand with an UPLS APO 60× (NA 1.35) oil immersion objective. GFP or A488 were excited by a 488 nm Argon ion laser. A647 and PI were excited by a 633 nm and 543 nm HeNe laser. Image analysis was performed using the Image J software (<http://imagej.nih.gov/ij/>).

STED microscopy

Superresolution images were taken by a Nikon NiE (Upright) microscope using a 100x NA=1.45 objective. For immunofluorescence labeling, antibodies conjugated with fluorophores (Abberior star 580, Abberior star red) appropriate for STED imaging were used as secondary antibodies. Co-localization was calculated by Image J software. STED microscopy was done by Péter Nánási.

Chromatin immunoprecipitation and sequencing

Chromatin immunoprecipitation and sequencing (ChIP-Seq) and ChIP-qPCR experiments were carried out as in (Barish et al. 2012), with minor modifications. Briefly, nuclei were crosslinked in 4% methanol-free ultrapure formaldehyde (Thermo Fisher Scientific, Waltham, Massachusetts, USA) for 10 minutes at room temperature. Glycine was

added for 5 min at a final concentration of 125 mM. After fixation chromatin was sonicated with a Diagenode Bioruptor to generate 200-1000 bp fragments. Chromatin was immunoprecipitated with rabbit polyclonal anti-H3K4me3 (Abcam, Cambridge, UK; 1 mg/ml) antibody using pre-blocked magnetic beads (Dynabeads Protein A, Thermo Fischer). Eluted DNA was purified (MinElute PCR Purification Kit; Qiagen Inc., Valencia, California, USA) and quantified with Qubit fluorometer (Thermo Fisher Scientific, Waltham, Massachusetts, USA). ChIP-Seq libraries were prepared from two biological replicates by Illumina according to manufacturer's instructions. ChIP-Seq experiments were performed by Zoltán Simándi.

Bioinformatics analyzes

Primary analyzes of the ChIP-Seq raw reads was carried out using a ChIP-Seq analyze command line pipeline (Nagy et al. 2011). Briefly, Burrows-Wheeler Alignment Tool (BWA, (Li and Durbin 2009)) was used to align the reads to the hg19 genome assembly (GRCh37), with default parameters. Histone regions were detected by findPeaks.pl (with options '-region', '-style histone', '-size 1000' and '-minDist 2500'). Intersections, subtractions and merging of the predicted peaks were made using BedTools. The center of the ChIP-Seq distributions of the TSS-negative H3K4me3 regions was found using getPeaks from Homer with option '-nfr'. Control and doxorubicin-treated H3K4me3 samples were analyzed by DiffBind v1.0.9 (with parameters 'minOverlap = 2' and 'full library size'; (Ross-Innes et al. 2012)), using duplicates. Genome coverage files (bedgraph files) for visualization were generated by makeUCSCfile.pl and then converted into tdf files using igvtools with 'toTDF' option. Integrative Genomics Viewer (IGV 2.3, Broad Institute) was used for data browsing (Thorvaldsdottir et al. 2013). Normalized tag counts for Meta histogram and Read Distribution (RD) plots were generated by annotatePeaks.pl with options '-ghist' and '-hist 25' from HOMER and then visualized by R using or Java TreeViewer. Bioinformatic analyzes were performed by Attila Horváth.

Sample preparation for MS measurement

80×10^6 H3-GFP expressing HeLa cells in 2.5 ml cell culture medium were mixed with an equal amount of 1% LMP agarose diluted in 1×PBS. Agarose blocks were prepared where each blocks contained 90 µl of agarose/cell suspension. Blocks were washed three times in 15 ml 1×PBS for 10 min. Permeabilization of cells was performed in ice cold 15 ml 1% Triton-X 100 diluted in 1×PBS/EDTA, twice for 10 min. Blocks were washed 5 times in 15 ml 1×PBS/EDTA. Blocks were treated with 15 ml EBr diluted in 1×PBS/EDTA/600 mM NaCl

in a concentration of 100 µg/ml, 6-times for 10 min. The proteins that remained in the nuclei after EBr treatment were eluted with 15 ml of 2 M NaCl diluted in 1×PBS/EDTA for 60 min. All the washing steps were performed with ice cold solutions. Eluted proteins were concentrated in a 10K Amicon tube (Merck-Millipore, Darmstadt, Germany) and the buffer was changed to 1×PBS. Proteins were eluted from the filter with 250 µl 1×PBS and stored at -20°C for MS analysis.

SDS-PAGE and LC-MS/MS analyzes

The protein concentration of each sample was measured using the Bradford method (Bradford 1976). 20µg protein was analyzed on a 10% SDS polyacrylamide gel. Electrophoresis was carried out in a Bio-Rad mini tetra cell (Bio-Rad) at 100 A constant current for one hour. The proteins were stained in the gel using Coomassie PageBlue (Fermentas) and scanned with a Pharos FX Plus laser scanner (Bio-Rad).

SDS-PAGE analyzes were done by Gergő Kalló at the Proteomics Core Facility of the Department of Biochemistry and Molecular Biology, University of Debrecen.

The bands of SDS-PAGE were excised, followed by in-gel digestion with trypsin. Reduction was performed using 20 mM dithiothreitol for one hour at 56°C, followed by alkylation with 55mM iodoacetamide for 45 min. Overnight trypsin digestion was carried out using stabilized MS grade TPCK-treated bovine trypsin (ABSciex) at 37 °C; thereafter, the digested peptides were extracted and lyophilized. The peptides were re-dissolved in 10 µl 1% formic acid before mass spectrometric analysis. The acquired LC-MS/MS data were used for protein identification with the help of Protein-Pilot 4.0 (ABSciex) search engine and the SwissProt database, using the biological modification table included in the ProteinPilot 4.0 software. A minimum of two peptide sequences with 95% confidence were used for protein identification.

MS analyzes were done by Gergő Kalló at the Proteomics Core Facility of the Department of Biochemistry and Molecular Biology, University of Debrecen

SUMMARY

Novel cytometric methods were developed for genetic and epigenetic analyzes: (A) for the detection of certain genetic alterations of the length or in the sequence of short genomic regions, (B) for the *in situ* evaluation of nucleosome stability and (C) for the “ChIP-on-beads” analyzes of nucleosome-associated epigenetic modifications.

(A) The flow cytometry assay I developed to address genetic diseases is based on the melting point analysis of PCR products carrying biotin and a fluorescent moiety on their two ends, and are immobilized on streptavidin-coated microbeads. The efficacy and sensitivity of the method is demonstrated in the case of CAG triplet expansion in Huntington’s disease and a BRCA1 point mutation.

(B) The laser scanning cytometric assay I developed for the purposes of *in situ* evaluation of nucleosome stability is based on the elution of histones using intercalators or salt, so as to assess stability features dependent on DNA superhelicity or electrostatic interactions, respectively. The assays can be performed on a PTM or histone variant dependent manner. The utility of the method is demonstrated via the comparative analyzes of different histone PTMs and histone variants, including H2A.Z, H2A.X and its phosphorylated form, γ H2A.X. It was also demonstrated that DNA relaxation (by nicking) destabilizes nucleosomes, what underscores the powerful potential of topological relaxation in the epigenetic regulation of DNA accessibility. Notably, nicking at ≥ 10 kb intervals is sufficient to induce global nucleosome destabilization, demonstrating that relaxation is propagated along most of the nucleosomes of the relaxed chromatin loops. The novel observations of biological significance I made employing this method include the demonstration of the nucleosome destabilizing effect of a reader protein in the case of H2A.Z.

(C) The cytometric assays developed for the “ChIP-on-beads” analyzes of nucleosome-associated epigenetic modifications are based on the measurement of PTM combinations on isolated mononucleosomes immobilized on microbeads. This experimental system proved useful also for the differential detection of initiating and elongating RNA Pol II molecules and R-loops juxtaposed with nicks.

As a general, methodical conclusion, suitable combinations of cytometric approaches with molecular biological methodology can offer a novel outlook on a wide variety of genetic and epigenetic questions of both practical and fundamental biological importance, with many potentialities yet to be exploited.

ÖSSZEFOGLALÁS

Új citometriai módszereket dolgoztam ki genetikai és epigenetikai kérdések megválaszolására: (A) rövid DNS régiókban bekövetkező hossz-változások, illetve DNS szekvenciabeli eltérések detektálására, (B) nukleoszóma stabilitás *in situ* mérésére, valamint (C) nukleoszómákkal asszociált epigenetikai módosítások analízisére.

(A) Az áramlási citometriás platformra épülő genetikai teszt sztreptavidint hordozó mikrogöngyök felszínén immobilizált és fluoreszcensen jelölt PCR termékek T_m analízisén alapul. A módszer felhasználhatóságát, érzékenységét a Huntington chorea hátterében álló triplet expanzió, illetve a BRCA1 gén egyik pontmutációjának kimutatásával demonstráltam.

(B) A pásztázó lézermikroszkópos (citometriás) platformra épülő nukleoszóma stabilitást vizsgáló *in situ* módszer a hisztonok sókezelés vagy interkalátorral történő kezelés hatására bekövetkező, kromatinról történő disszociációjának mérésén alapul. A sókezelés a nukleoszómák ionerősség-függő, az interkalátor kezelés a nukleoszómák DNS szuperhelicitás-függő stabilitásának mérését teszi lehetővé, hiszton PTM ill. hiszton variáns specifikus módon. A módszert különböző hiszton PTM-ek, illetve a H2A.Z, H2A.X és γ H2A.X hiszton variánsok összehasonlító vizsgálatára használtam fel. Kimutattam, hogy a kromatin relaxációja (nick-ek létrehozásával) nukleoszóma destabilizációt okoz, amelynek jelentős szerepe lehet a DNS hozzáférhetőségének epigenetikai szabályozásában. A ≥ 10 kb távolságban létrehozott nick-ek általi relaxáció már elégségesnek bizonyult a nukleoszómák többségének destabilizációjához, ami azt mutatja, hogy a bevitt nick-ek hatása nem lokális, a relaxáció tovaterjed kromatin hurok méretű távolságokra. A módszerrel végezhető megfigyelések potenciális biológiai jelentőségét mutatja a H2A.Z reader protein nukleoszóma stabilitást befolyásoló funkciójának kimutatása is.

(C) Az áramlási citometriás és pásztázó lézermikroszkópos citometriás platformra épülő epigenetikai teszt izolált, mikrogöngyökon immobilizált mononukleoszómák epigenetikai módosítás kombinációinak analízisén alapul. Ez a mérési elv alkalmasnak bizonyult nick-ekhez közeli, iniciáló ill. elongáló RNS-polimeráz II molekulák ill. R-loop-ok differenciális detektálására.

Általános konklúzióként megállapítható, hogy a citometriás analízisre épülő és a molekuláris biológiai metodikák előnyös kombinációi alapvető genetikai és epigenetikai kérdések megválaszolására, gyakorlati problémák megoldására kínálnak új, még kevésbé kiaknázott lehetőségeket.

REFERENCES

- Anderson JD, Lowary PT, Widom J. 2001. Effects of histone acetylation on the equilibrium accessibility of nucleosomal DNA target sites. *Journal of molecular biology* 307(4): 977-985.
- Andrews AJ, Luger K. 2011. Nucleosome structure(s) and stability: variations on a theme. *Annual review of biophysics* 40: 99-117.
- Angelov D, Vitolo JM, Mutskov V, Dimitrov S, Hayes JJ. 2001. Preferential interaction of the core histone tail domains with linker DNA. *Proceedings of the National Academy of Sciences of the United States of America* 98(12): 6599-6604.
- Antoniou AC, Pharoah PD, Narod S, Risch HA, Eyfjord JE, Hopper JL, Olsson H, Johannsson O, Borg A, Pasini B et al. 2005. Breast and ovarian cancer risks to carriers of the BRCA1 5382insC and 185delAG and BRCA2 6174delT mutations: a combined analysis of 22 population based studies. *J Med Genet* 42(7): 602-603.
- Ausio J, Seger D, Eisenberg H. 1984. Nucleosome core particle stability and conformational change. Effect of temperature, particle and NaCl concentrations, and crosslinking of histone H3 sulfhydryl groups. *Journal of molecular biology* 176(1): 77-104.
- Bahlo M, Bennett MF, Degorski P, Tankard RM, Delatycki MB, Lockhart PJ. 2018. Recent advances in the detection of repeat expansions with short-read next-generation sequencing. *F1000Research* 7.
- Barish GD, Yu RT, Karunasiri MS, Becerra D, Kim J, Tseng TW, Tai LJ, Leblanc M, Diehl C, Cerchietti L et al. 2012. The Bcl6-SMRT/NCoR cistrome represses inflammation to attenuate atherosclerosis. *Cell metabolism* 15(4): 554-562.
- Bjorndal MT, Fygenson DK. 2002. DNA melting in the presence of fluorescent intercalating oxazole yellow dyes measured with a gel-based assay. *Biopolymers* 65(1): 40-44.
- Blake RD, Delcourt SG. 1996. Thermodynamic effects of formamide on DNA stability. *Nucleic Acids Res* 24(11): 2095-2103.
- Bohm V, Hieb AR, Andrews AJ, Gansen A, Rocker A, Toth K, Luger K, Langowski J. 2011. Nucleosome accessibility governed by the dimer/tetramer interface. *Nucleic acids research* 39(8): 3093-3102.
- Bonisch C, Hake SB. 2012. Histone H2A variants in nucleosomes and chromatin: more or less stable? *Nucleic acids research* 40(21): 10719-10741.
- Bonner WM, Redon CE, Dickey JS, Nakamura AJ, Sedelnikova OA, Solier S, Pommier Y. 2008. GammaH2AX and cancer. *Nat Rev Cancer* 8(12): 957-967.
- Bowman GD, Poirier MG. 2015. Post-translational modifications of histones that influence nucleosome dynamics. *Chemical reviews* 115(6): 2274-2295.
- Bradford MM. 1976. A rapid and sensitive method for the quantitation of microgram quantities of protein utilizing the principle of protein-dye binding. *Analytical biochemistry* 72: 248-254.
- Brind'Amour J, Lansdorp PM. 2011. Analysis of repetitive DNA in chromosomes by flow cytometry. *Nature methods* 8(6): 484-486.
- Brodsky AS, Johnston AP, Trau M, Silver PA. 2003. Analysis of RNA-protein interactions by flow cytometry. *Curr Opin Mol Ther* 5(3): 235-240.
- Brower-Toland B, Wacker DA, Fulbright RM, Lis JT, Kraus WL, Wang MD. 2005. Specific contributions of histone tails and their acetylation to the mechanical stability of nucleosomes. *Journal of molecular biology* 346(1): 135-146.

- Chan PC, Wong BY, Ozcelik H, Cole DE. 1999. Simple and rapid detection of BRCA1 and BRCA2 mutations by multiplex mutagenically separated PCR. *Clin Chem* 45(8 Pt 1): 1285-1287.
- Cheema MS, Ausio J. 2015. The Structural Determinants behind the Epigenetic Role of Histone Variants. *Genes* 6(3): 685-713.
- Chen WT, Alpert A, Leiter C, Gong F, Jackson SP, Miller KM. 2013. Systematic identification of functional residues in mammalian histone H2AX. *Molecular and cellular biology* 33(1): 111-126.
- Chien FT, van der Heijden T. 2014. Characterization of nucleosome unwrapping within chromatin fibers using magnetic tweezers. *Biophysical journal* 107(2): 373-383.
- Darzynkiewicz Z, Halicka HD, Zhao H. 2010. Analysis of cellular DNA content by flow and laser scanning cytometry. *Advances in experimental medicine and biology* 676: 137-147.
- Davey CA, Sargent DF, Luger K, Maeder AW, Richmond TJ. 2002. Solvent mediated interactions in the structure of the nucleosome core particle at 1.9 Å resolution. *Journal of molecular biology* 319(5): 1097-1113.
- Deng CX, Wang RH. 2003. Roles of BRCA1 in DNA damage repair: a link between development and cancer. *Hum Mol Genet* 12 Spec No 1: R113-123.
- Deshpande A, Valdez Y, Nolan JP. 2005. Multiplexed SNP genotyping using primer single-base extension (SBE) and microsphere arrays. *Curr Protoc Cytom* Chapter 13: Unit13 14.
- Dimitrov RA, Zuker M. 2004. Prediction of hybridization and melting for double-stranded nucleic acids. *Biophys J* 87(1): 215-226.
- Dong L, Wu N, Wang S, Cheng Y, Han L, Zhao J, Long X, Mu K, Li M, Wei L et al. 2018. Detection of novel germline mutations in six breast cancer predisposition genes by targeted next-generation sequencing. *Human mutation* 39(10): 1442-1455.
- Dryhurst D, Ishibashi T, Rose KL, Eirin-Lopez JM, McDonald D, Silva-Moreno B, Veldhoen N, Helbing CC, Hendzel MJ, Shabanowitz J et al. 2009. Characterization of the histone H2A.Z-1 and H2A.Z-2 isoforms in vertebrates. *BMC biology* 7: 86.
- Elbel T, Langowski J. 2015. The effect of DNA supercoiling on nucleosome structure and stability. *Journal of physics Condensed matter : an Institute of Physics journal* 27(6): 064105.
- Fackenthal JD, Olopade OI. 2007. Breast cancer risk associated with BRCA1 and BRCA2 in diverse populations. *Nature reviews Cancer* 7(12): 937-948.
- Falk M, Vojtiskova M, Lukas Z, Kroupova I, Froster U. 2006. Simple procedure for automatic detection of unstable alleles in the myotonic dystrophy and Huntington's disease loci. *Genet Test* 10(2): 85-97.
- Fan JY, Gordon F, Luger K, Hansen JC, Tremethick DJ. 2002. The essential histone variant H2A.Z regulates the equilibrium between different chromatin conformational states. *Nature structural biology* 9(3): 172-176.
- Farrelly LA, Dill BD, Molina H, Birtwistle MR, Maze I. 2016. Current Proteomic Methods to Investigate the Dynamics of Histone Turnover in the Central Nervous System. *Methods in enzymology* 574: 331-354.
- Fink M, Imholz D, Thoma F. 2007. Contribution of the serine 129 of histone H2A to chromatin structure. *Molecular and cellular biology* 27(10): 3589-3600.
- Forment JV, Jackson SP. 2015. A flow cytometry-based method to simplify the analysis and quantification of protein association to chromatin in mammalian cells. *Nature protocols* 10(9): 1297-1307.

- Foulkes WD. 2004. BRCA1 functions as a breast stem cell regulator. *J Med Genet* 41(1): 1-5.
- Gansen A, Toth K, Schwarz N, Langowski J. 2009. Structural variability of nucleosomes detected by single-pair Forster resonance energy transfer: histone acetylation, sequence variation, and salt effects. *The journal of physical chemistry B* 113(9): 2604-2613.
- Gloss LM, Placek BJ. 2002. The effect of salts on the stability of the H2A-H2B histone dimer. *Biochemistry* 41(50): 14951-14959.
- Godet I, Gilkes DM. 2017. BRCA1 and BRCA2 mutations and treatment strategies for breast cancer. *Integrative cancer science and therapeutics* 4(1).
- Greene RF, Collins JM, Jenkins JF, Speyer JL, Myers CE. 1983. Plasma pharmacokinetics of adriamycin and adriamycinol: implications for the design of in vitro experiments and treatment protocols. *Cancer research* 43(7): 3417-3421.
- Gunther K, Mertig M, Seidel R. 2010. Mechanical and structural properties of YOYO-1 complexed DNA. *Nucleic acids research* 38(19): 6526-6532.
- Harada BT, Hwang WL, Deindl S, Chatterjee N, Bartholomew B, Zhuang X. 2016. Stepwise nucleosome translocation by RSC remodeling complexes. *eLife* 5.
- Hayashi-Takanaka Y, Maehara K, Harada A, Umehara T, Yokoyama S, Obuse C, Ohkawa Y, Nozaki N, Kimura H. 2015. Distribution of histone H4 modifications as revealed by a panel of specific monoclonal antibodies. *Chromosome research : an international journal on the molecular, supramolecular and evolutionary aspects of chromosome biology* 23(4): 753-766.
- Hayashi-Takanaka Y, Yamagata K, Wakayama T, Stasevich TJ, Kainuma T, Tsurimoto T, Tachibana M, Shinkai Y, Kurumizaka H, Nozaki N et al. 2011. Tracking epigenetic histone modifications in single cells using Fab-based live endogenous modification labeling. *Nucleic acids research* 39(15): 6475-6488.
- Hegedus E, Kokai E, Kotlyar A, Dombradi V, Szabo G. 2009. Separation of 1-23-kb complementary DNA strands by urea-agarose gel electrophoresis. *Nucleic acids research* 37(17): e112.
- Hegedüs É, Kókai E, Nánási P, Imre L, Halász L, Jossé R, Antunovics Z, Webb MR, El Hage A, Pommier Y et al. 2018. Endogenous single-strand DNA breaks at RNA polymerase II promoters in *Saccharomyces cerevisiae*. *Nucleic acids research: gky743-gky743*.
- Henikoff S, Henikoff JG, Sakai A, Loeb GB, Ahmad K. 2009. Genome-wide profiling of salt fractions maps physical properties of chromatin. *Genome research* 19(3): 460-469.
- Heo K, Kim H, Choi SH, Choi J, Kim K, Gu J, Lieber MR, Yang AS, An W. 2008. FACT-mediated exchange of histone variant H2AX regulated by phosphorylation of H2AX and ADP-ribosylation of Spt16. *Molecular cell* 30(1): 86-97.
- Heyse KS, Weber SE, Lipps HJ. 2009. Histone modifications are specifically relocated during gene activation and nuclear differentiation. *BMC genomics* 10: 554.
- Horikoshi N, Arimura Y, Taguchi H, Kurumizaka H. 2016. Crystal structures of heterotypic nucleosomes containing histones H2A.Z and H2A. *Open biology* 6(6).
- Horikoshi N, Sato K, Shimada K, Arimura Y, Osakabe A, Tachiwana H, Hayashi-Takanaka Y, Iwasaki W, Kagawa W, Harata M et al. 2013. Structural polymorphism in the L1 loop regions of human H2A.Z.1 and H2A.Z.2. *Acta crystallographica Section D, Biological crystallography* 69(Pt 12): 2431-2439.
- Hsu HY, Joos TO, Koga H. 2009. Multiplex microsphere-based flow cytometric platforms for protein analysis and their application in clinical proteomics - from assays to results. *Electrophoresis* 30(23): 4008-4019.

- Ikura T, Tashiro S, Kakino A, Shima H, Jacob N, Amunugama R, Yoder K, Izumi S, Kuraoka I, Tanaka K et al. 2007. DNA damage-dependent acetylation and ubiquitination of H2AX enhances chromatin dynamics. *Molecular and cellular biology* 27(20): 7028-7040.
- Imre L, Simandi Z, Horvath A, Fenyofalvi G, Nanasi P, Niaki EF, Hegedus E, Bacso Z, Weyemi U, Mauser R et al. 2017. Nucleosome stability measured in situ by automated quantitative imaging. *Scientific reports* 7(1): 12734.
- Jin C, Felsenfeld G. 2007. Nucleosome stability mediated by histone variants H3.3 and H2A.Z. *Genes & development* 21(12): 1519-1529.
- Jin C, Zang C, Wei G, Cui K, Peng W, Zhao K, Felsenfeld G. 2009. H3.3/H2A.Z double variant-containing nucleosomes mark 'nucleosome-free regions' of active promoters and other regulatory regions. *Nature genetics* 41(8): 941-945.
- Kass EM, Jasin M. 2010. Collaboration and competition between DNA double-strand break repair pathways. *FEBS Lett* 584(17): 3703-3708.
- Khandelwal G, Bhyravabhotla J. 2010. A phenomenological model for predicting melting temperatures of DNA sequences. *PLoS one* 5(8): e12433.
- Kimura H, Cook PR. 2001. Kinetics of Core Histones in Living Human Cells: Little Exchange of H3 and H4 and Some Rapid Exchange of H2B. *The Journal of Cell Biology* 153(7): 1341-1353.
- Kimura H, Hayashi-Takanaka Y, Goto Y, Takizawa N, Nozaki N. 2008. The organization of histone H3 modifications as revealed by a panel of specific monoclonal antibodies. *Cell structure and function* 33(1): 61-73.
- Kinkley S, Helmuth J, Polansky JK, Dunkel I, Gasparoni G, Frohler S, Chen W, Walter J, Hamann A, Chung HR. 2016. reChIP-seq reveals widespread bivalency of H3K4me3 and H3K27me3 in CD4(+) memory T cells. *Nat Commun* 7: 12514.
- Kornberg RD, Lorch Y. 1991. Irresistible force meets immovable object: transcription and the nucleosome. *Cell* 67(5): 833-836.
- Kouzine F, Gupta A, Baranello L, Wojtowicz D, Ben-Aissa K, Liu J, Przytycka TM, Levens D. 2013. Transcription-dependent dynamic supercoiling is a short-range genomic force. *Nature structural & molecular biology* 20(3): 396-403.
- Krietenstein N, Wal M, Watanabe S, Park B, Peterson CL, Pugh BF, Korber P. 2016. Genomic Nucleosome Organization Reconstituted with Pure Proteins. *Cell* 167(3): 709-721 e712.
- Kungulovski G, Kycia I, Tamas R, Jurkowska RZ, Kudithipudi S, Henry C, Reinhardt R, Labhart P, Jeltsch A. 2014. Application of histone modification-specific interaction domains as an alternative to antibodies. *Genome research* 24(11): 1842-1853.
- Kusakabe M, Oku H, Matsuda R, Hori T, Muto A, Igarashi K, Fukagawa T, Harata M. 2016. Genetic complementation analysis showed distinct contributions of the N-terminal tail of H2A.Z to epigenetic regulations. *Genes to cells : devoted to molecular & cellular mechanisms* 21(2): 122-135.
- Kwok PY. 2001. Methods for genotyping single nucleotide polymorphisms. *Annu Rev Genomics Hum Genet* 2: 235-258.
- Lauberth SM, Nakayama T, Wu X, Ferris AL, Tang Z, Hughes SH, Roeder RG. 2013. H3K4me3 interactions with TAF3 regulate preinitiation complex assembly and selective gene activation. *Cell* 152(5): 1021-1036.
- Lee JY, Wei S, Lee TH. 2011. Effects of histone acetylation by Piccolo NuA4 on the structure of a nucleosome and the interactions between two nucleosomes. *The Journal of biological chemistry* 286(13): 11099-11109.

- Levens D, Benham CJ. 2011. DNA stress and strain, in silico, in vitro and in vivo. *Physical biology* 8(3): 035011.
- Li A, Yu Y, Lee SC, Ishibashi T, Lees-Miller SP, Ausio J. 2010. Phosphorylation of histone H2A.X by DNA-dependent protein kinase is not affected by core histone acetylation, but it alters nucleosome stability and histone H1 binding. *The Journal of biological chemistry* 285(23): 17778-17788.
- Li H, Durbin R. 2009. Fast and accurate short read alignment with Burrows-Wheeler transform. *Bioinformatics* 25(14): 1754-1760.
- Li J, Makrigiorgos GM. 2009. COLD-PCR: a new platform for highly improved mutation detection in cancer and genetic testing. *Biochemical Society transactions* 37(Pt 2): 427-432.
- Linger RJ, Kruk PA. 2010. BRCA1 16 years later: risk-associated BRCA1 mutations and their functional implications. *FEBS J* 277(15): 3086-3096.
- Link S, Spitzer RMM, Sana M, Torrado M, Volker-Albert MC, Keilhauer EC, Burgold T, Punzeler S, Low JKK, Lindstrom I et al. 2018. PWWP2A binds distinct chromatin moieties and interacts with an MTA1-specific core NuRD complex. *Nat Commun* 9(1): 4300.
- Liu J, Vidi PA, Lelievre SA, Irudayaraj JM. 2015. Nanoscale histone localization in live cells reveals reduced chromatin mobility in response to DNA damage. *Journal of cell science* 128(3): 599-604.
- Liu LF, Wang JC. 1987. Supercoiling of the DNA template during transcription. *Proceedings of the National Academy of Sciences of the United States of America* 84(20): 7024-7027.
- Liu Q, Zhang P, Wang D, Gu W, Wang K. 2017. Interrogating the "unsequenceable" genomic trinucleotide repeat disorders by long-read sequencing. *Genome medicine* 9(1): 65.
- Loomis EW, Eid JS, Peluso P, Yin J, Hickey L, Rank D, McCalmon S, Hagerman RJ, Tassone F, Hagerman PJ. 2013. Sequencing the unsequenceable: expanded CGG-repeat alleles of the fragile X gene. *Genome research* 23(1): 121-128.
- Madabhushi R, Gao F, Pfenning AR, Pan L, Yamakawa S, Seo J, Rueda R, Phan TX, Yamakawa H, Pao PC et al. 2015. Activity-Induced DNA Breaks Govern the Expression of Neuronal Early-Response Genes. *Cell* 161(7): 1592-1605.
- Margolis RL, Ross CA. 2003. Diagnosis of Huntington disease. *Clin Chem* 49(10): 1726-1732.
- Martin M, Terradas M, Hernandez L, Genesca A. 2014. gammaH2AX foci on apparently intact mitotic chromosomes: not signatures of misrejoining events but signals of unresolved DNA damage. *Cell cycle* 13(19): 3026-3036.
- Matsuda R, Hori T, Kitamura H, Takeuchi K, Fukagawa T, Harata M. 2010. Identification and characterization of the two isoforms of the vertebrate H2A.Z histone variant. *Nucleic acids research* 38(13): 4263-4273.
- McMurray CT, Small EW, van Holde KE. 1991. Binding of ethidium to the nucleosome core particle. 2. Internal and external binding modes. *Biochemistry* 30(23): 5644-5652.
- McMurray CT, van Holde KE. 1986. Binding of ethidium bromide causes dissociation of the nucleosome core particle. *Proceedings of the National Academy of Sciences of the United States of America* 83(22): 8472-8476.
- Milunsky JM, Maher TA, Loose BA, Darras BT, Ito M. 2003. XL PCR for the detection of large trinucleotide expansions in juvenile Huntington's disease. *Clin Genet* 64(1): 70-73.

- Morgan E, Varro R, Sepulveda H, Ember JA, Apgar J, Wilson J, Lowe L, Chen R, Shivraj L, Agadir A et al. 2004. Cytometric bead array: a multiplexed assay platform with applications in various areas of biology. *Clin Immunol* 110(3): 252-266.
- Muglia M, Leone O, Annesi G, Gabriele AL, Imbrogno E, Grandinetti C, Conforti FL, Naso F, Brancati C. 1996. Nonisotopic method for accurate detection of (CAG)_n repeats causing Huntington disease. *Clin Chem* 42(10): 1601-1603.
- Mutskov V, Gerber D, Angelov D, Ausio J, Workman J, Dimitrov S. 1998. Persistent interactions of core histone tails with nucleosomal DNA following acetylation and transcription factor binding. *Molecular and cellular biology* 18(11): 6293-6304.
- Myers RH. 2004. Huntington's disease genetics. *NeuroRx* 1(2): 255-262.
- Nagy A, Kenesi E, Rentsendorj O, Molnar A, Szenasi T, Sinko I, Zvara A, Oommen ST, Barta E, Puskas LG et al. 2011. Evolutionarily conserved, growth plate zone-specific regulation of the matrilin-1 promoter: L-Sox5/Sox6 and Nfi factors bound near TATA finely tune activation by Sox9. *Molecular and cellular biology* 31(4): 686-699.
- Naughton C, Avlonitis N, Corless S, Prendergast JG, Mati IK, Eijk PP, Cockroft SL, Bradley M, Ylstra B, Gilbert N. 2013. Transcription forms and remodels supercoiling domains unfolding large-scale chromatin structures. *Nature structural & molecular biology* 20(3): 387-395.
- Nikitina T, Norouzi D, Grigoryev SA, Zhurkin VB. 2017. DNA topology in chromatin is defined by nucleosome spacing. *Science advances* 3(10): e1700957.
- Nolan JP, Yang L, van der Heyde HC. 2006. Reagents and instruments for multiplexed analysis using microparticles. *Curr Protoc Cytom* Chapter 13: Unit13 18.
- Nollau P, Wagener C. 1997. Methods for detection of point mutations: performance and quality assessment. IFCC Scientific Division, Committee on Molecular Biology Techniques. *Clin Chem* 43(7): 1114-1128.
- Ordu O, Lusser A, Dekker NH. 2016. Recent insights from in vitro single-molecule studies into nucleosome structure and dynamics. *Biophysical reviews* 8(Suppl 1): 33-49.
- Ornatsky O, Bandura D, Baranov V, Nitz M, Winnik MA, Tanner S. Highly multiparametric analysis by mass cytometry. *J Immunol Methods* 361(1-2): 1-20.
- Ostendorf BN, Hansmann L, Ludwig WD, Dorken B, Ratei R, Westermann J. 2016. [Flow-cytometric immunophenotyping in clinical diagnostics]. *Deutsche medizinische Wochenschrift* 141(21): 1569-1574.
- Pang B, de Jong J, Qiao X, Wessels LF, Neefjes J. 2015. Chemical profiling of the genome with anti-cancer drugs defines target specificities. *Nature chemical biology* 11(7): 472-480.
- Pang B, Qiao X, Janssen L, Velds A, Groothuis T, Kerkhoven R, Nieuwland M, Ovaas H, Rottenberg S, van Tellingen O et al. 2013. Drug-induced histone eviction from open chromatin contributes to the chemotherapeutic effects of doxorubicin. *Nature communications* 4: 1908.
- Panjkevich A, Melo F. 2005. Comparison of different melting temperature calculation methods for short DNA sequences. *Bioinformatics* 21(6): 711-722.
- Park YJ, Dyer PN, Tremethick DJ, Luger K. 2004. A new fluorescence resonance energy transfer approach demonstrates that the histone variant H2AZ stabilizes the histone octamer within the nucleosome. *The Journal of biological chemistry* 279(23): 24274-24282.
- Pataki J, Szabo M, Lantos E, Szekvolgyi L, Molnar M, Hegedus E, Bacso Z, Kappelmayer J, Lustyik G, Szabo G. 2005. Biological microbeads for flow-

- cytometric immunoassays, enzyme titrations, and quantitative PCR. *Cytometry Part A : the journal of the International Society for Analytical Cytology* 68(1): 45-52.
- Petrucelli N, Daly MB, Feldman GL. 2010. Hereditary breast and ovarian cancer due to mutations in BRCA1 and BRCA2. *Genetics in medicine : official journal of the American College of Medical Genetics* 12(5): 245-259.
- Pichler G, Jack A, Wolf P, Hake SB. 2012. Versatile toolbox for high throughput biochemical and functional studies with fluorescent fusion proteins. *PloS one* 7(5): e36967.
- Pozarowski P, Darzynkiewicz Z. 2004. Analysis of cell cycle by flow cytometry. *Methods in molecular biology* 281: 301-311.
- Price BD, D'Andrea AD. 2013. Chromatin remodeling at DNA double-strand breaks. *Cell* 152(6): 1344-1354.
- Puc J, Aggarwal AK, Rosenfeld MG. 2017. Physiological functions of programmed DNA breaks in signal-induced transcription. *Nature reviews Molecular cell biology* 18(8): 471-476.
- Punzeler S, Link S, Wagner G, Keilhauer EC, Kronbeck N, Spitzer RM, Leidescher S, Markaki Y, Mentele E, Regnard C et al. 2017. Multivalent binding of PWWP2A to H2A.Z regulates mitosis and neural crest differentiation. *The EMBO journal* 36(15): 2263-2279.
- Rabbani A, Finn RM, Ausio J. 2005. The anthracycline antibiotics: antitumor drugs that alter chromatin structure. *BioEssays : news and reviews in molecular, cellular and developmental biology* 27(1): 50-56.
- Rabbani A, Iskandar M, Ausio J. 1999. Daunomycin-induced unfolding and aggregation of chromatin. *The Journal of biological chemistry* 274(26): 18401-18406.
- Ramachandran S, Henikoff S. 2016. Nucleosome dynamics during chromatin remodeling in vivo. *Nucleus* 7(1): 20-26.
- Ramus SJ, Gayther SA. 2009. The contribution of BRCA1 and BRCA2 to ovarian cancer. *Mol Oncol* 3(2): 138-150.
- Redon CE, Weyemi U, Parekh PR, Huang D, Burrell AS, Bonner WM. 2012. gamma-H2AX and other histone post-translational modifications in the clinic. *Biochimica et biophysica acta* 1819(7): 743-756.
- Reguart N, Cardona AF, Carrasco E, Gomez P, Taron M, Rosell R. 2008. BRCA1: a new genomic marker for non-small-cell lung cancer. *Clin Lung Cancer* 9(6): 331-339.
- Rogakou EP, Boon C, Redon C, Bonner WM. 1999. Megabase chromatin domains involved in DNA double-strand breaks in vivo. *J Cell Biol* 146(5): 905-916.
- Ross-Innes CS, Stark R, Teschendorff AE, Holmes KA, Ali HR, Dunning MJ, Brown GD, Gojis O, Ellis IO, Green AR et al. 2012. Differential oestrogen receptor binding is associated with clinical outcome in breast cancer. *Nature* 481(7381): 389-393.
- Rothbart SB, Strahl BD. 2014. Interpreting the language of histone and DNA modifications. *Biochimica et biophysica acta* 1839(8): 627-643.
- Roy D, Zhang Z, Lu Z, Hsieh CL, Lieber MR. 2010. Competition between the RNA transcript and the nontemplate DNA strand during R-loop formation in vitro: a nick can serve as a strong R-loop initiation site. *Molecular and cellular biology* 30(1): 146-159.
- Rudnizky S, Malik O, Bavly A, Pnueli L, Melamed P, Kaplan A. 2017. Nucleosome mobility and the regulation of gene expression: Insights from single-molecule studies. *Protein science : a publication of the Protein Society* 26(7): 1266-1277.

- Saksouk N, Simboeck E, Dejardin J. 2015. Constitutive heterochromatin formation and transcription in mammals. *Epigenetics & chromatin* 8: 3.
- Sambrook J, Russell DW. 2001. *Molecular Cloning: a laboratory manual*. Cold Spring Harbor Laboratory Press, New York.
- Sanders MM. 1978. Fractionation of nucleosomes by salt elution from micrococcal nuclease-digested nuclei. *J Cell Biol* 79(1): 97-109.
- Santos-Pereira JM, Aguilera A. 2015. R loops: new modulators of genome dynamics and function. *Nature reviews Genetics* 16(10): 583-597.
- Sarcinella E, Zuzarte PC, Lau PN, Draker R, Cheung P. 2007. Monoubiquitylation of H2A.Z distinguishes its association with euchromatin or facultative heterochromatin. *Molecular and cellular biology* 27(18): 6457-6468.
- Scherzinger E, Sittler A, Schweiger K, Heiser V, Lurz R, Hasenbank R, Bates GP, Lehrach H, Wanker EE. 1999. Self-assembly of polyglutamine-containing huntingtin fragments into amyloid-like fibrils: implications for Huntington's disease pathology. *Proceedings of the National Academy of Sciences of the United States of America* 96(8): 4604-4609.
- Schroter H, Maier G, Ponstingl H, Nordheim A. 1985. DNA intercalators induce specific release of HMG 14, HMG 17 and other DNA-binding proteins from chicken erythrocyte chromatin. *The EMBO journal* 4(13B): 3867-3872.
- Semaka A, Creighton S, Warby S, Hayden MR. 2006. Predictive testing for Huntington disease: interpretation and significance of intermediate alleles. *Clin Genet* 70(4): 283-294.
- Seo J, Kim SC, Lee HS, Kim JK, Shon HJ, Salleh NL, Desai KV, Lee JH, Kang ES, Kim JS et al. 2012. Genome-wide profiles of H2AX and gamma-H2AX differentiate endogenous and exogenous DNA damage hotspots in human cells. *Nucleic acids research* 40(13): 5965-5974.
- Shapiro HM. 1981. Flow cytometric estimation of DNA and RNA content in intact cells stained with Hoechst 33342 and pyronin Y. *Cytometry* 2(3): 143-150.
- Shema E, Jones D, Shores N, Donohue L, Ram O, Bernstein BE. 2016. Single-molecule decoding of combinatorially modified nucleosomes. *Science* 352(6286): 717-721.
- Siddiqui MS, Francois M, Fenech MF, Leifert WR. 2015. Persistent gammaH2AX: A promising molecular marker of DNA damage and aging. *Mutation research Reviews in mutation research* 766: 1-19.
- Simandi Z, Czipa E, Horvath A, Koszeghy A, Bordas C, Poliska S, Juhasz I, Imre L, Szabo G, Dezso B et al. 2015. PRMT1 and PRMT8 regulate retinoic acid-dependent neuronal differentiation with implications to neuropathology. *Stem cells* 33(3): 726-741.
- Singh I, Ozturk N, Cordero J, Mehta A, Hasan D, Cosentino C, Sebastian C, Kruger M, Looso M, Carraro G et al. 2015. High mobility group protein-mediated transcription requires DNA damage marker gamma-H2AX. *Cell Res* 25(7): 837-850.
- Squitieri F, Gellera C, Cannella M, Mariotti C, Cislighi G, Rubinsztein DC, Almqvist EW, Turner D, Bachoud-Levi AC, Simpson SA et al. 2003. Homozygosity for CAG mutation in Huntington disease is associated with a more severe clinical course. *Brain : a journal of neurology* 126(Pt 4): 946-955.
- Szekvolgyi L, Balint BL, Imre L, Goda K, Szabo M, Nagy L, Szabo G. 2006. Chip-on-beads: flow-cytometric evaluation of chromatin immunoprecipitation. *Cytometry Part A : the journal of the International Society for Analytical Cytology* 69(10): 1086-1091.

- Szekvolgyi L, Imre L, Minh DX, Hegedus E, Bacso Z, Szabo G. 2009. Flow cytometric and laser scanning microscopic approaches in epigenetics research. *Methods in molecular biology* 567: 99-111.
- Szekvolgyi L, Rakosy Z, Balint BL, Kokai E, Imre L, Vereb G, Bacso Z, Goda K, Varga S, Balazs M et al. 2007. Ribonucleoprotein-masked nicks at 50-kbp intervals in the eukaryotic genomic DNA. *Proceedings of the National Academy of Sciences of the United States of America* 104(38): 14964-14969.
- Szentesi G, Horvath G, Bori I, Vamosi G, Szollosi J, Gaspar R, Damjanovich S, Jenei A, Matyus L. 2004. Computer program for determining fluorescence resonance energy transfer efficiency from flow cytometric data on a cell-by-cell basis. *Computer methods and programs in biomedicine* 75(3): 201-211.
- Szollosi J, Vereb G, Nagy P. 2016. The flow of events: How the sequence of molecular interactions is seen by the latest, user-friendly high throughput flow cytometric FRET. *Cytometry Part A : the journal of the International Society for Analytical Cytology* 89(10): 881-885.
- Taguchi H, Horikoshi N, Arimura Y, Kurumizaka H. 2014. A method for evaluating nucleosome stability with a protein-binding fluorescent dye. *Methods* 70(2-3): 119-126.
- Teves SS, Deal RB, Henikoff S. 2012. Measuring genome-wide nucleosome turnover using CATCH-IT. *Methods in enzymology* 513: 169-184.
- Teves SS, Henikoff S. 2014. Transcription-generated torsional stress destabilizes nucleosomes. *Nature structural & molecular biology* 21(1): 88-94.
- Thambirajah AA, Dryhurst D, Ishibashi T, Li A, Maffey AH, Ausio J. 2006. H2A.Z stabilizes chromatin in a way that is dependent on core histone acetylation. *The Journal of biological chemistry* 281(29): 20036-20044.
- Thorvaldsdottir H, Robinson JT, Mesirov JP. 2013. Integrative Genomics Viewer (IGV): high-performance genomics data visualization and exploration. *Briefings in bioinformatics* 14(2): 178-192.
- Toth T, Findlay I, Nagy B, Papp Z. 1997. Accurate sizing of (CAG)_n repeats causing Huntington disease by fluorescent PCR. *Clin Chem* 43(12): 2422-2423.
- Tubbs A, Nussenzweig A. 2017. Endogenous DNA Damage as a Source of Genomic Instability in Cancer. *Cell* 168(4): 644-656.
- Varga T, Szilagyi I, Szabo G, Jr. 1999. Single-strand breaks in agarose-embedded chromatin of nonapoptotic cells. *Biochemical and biophysical research communications* 264(2): 388-394.
- Venkatesh S, Workman JL. 2015. Histone exchange, chromatin structure and the regulation of transcription. *Nature reviews Molecular cell biology* 16(3): 178-189.
- Vlijm R, Lee M, Lipfert J, Lusser A, Dekker C, Dekker NH. 2015. Nucleosome assembly dynamics involve spontaneous fluctuations in the handedness of tetrasomes. *Cell reports* 10(2): 216-225.
- Voigt P, LeRoy G, Drury WJ, 3rd, Zee BM, Son J, Beck DB, Young NL, Garcia BA, Reinberg D. 2012. Asymmetrically modified nucleosomes. *Cell* 151(1): 181-193.
- Vos P, Hogers R, Bleeker M, Reijans M, van de Lee T, Hornes M, Frijters A, Pot J, Peleman J, Kuiper M et al. 1995. AFLP: a new technique for DNA fingerprinting. *Nucleic Acids Res* 23(21): 4407-4414.
- Wallace AJ. 2016. New challenges for BRCA testing: a view from the diagnostic laboratory. *European journal of human genetics : EJHG* 24 Suppl 1: S10-18.
- Wand T, Fang M, Chen C, Hardy N, McCoy JP, Jr., Dumitriu B, Young NS, Biancotto A. 2016. Telomere content measurement in human hematopoietic cells:

- Comparative analysis of qPCR and Flow-FISH techniques. *Cytometry Part A : the journal of the International Society for Analytical Cytology* 89(10): 914-921.
- Wang J, Chuang K, Ahluwalia M, Patel S, Umblas N, Mirel D, Higuchi R, Germer S. 2005. High-throughput SNP genotyping by single-tube PCR with Tm-shift primers. *Biotechniques* 39(6): 885-893.
- Weber CM, Henikoff JG, Henikoff S. 2010. H2A.Z nucleosomes enriched over active genes are homotypic. *Nature structural & molecular biology* 17(12): 1500-1507.
- Wei S, Falk SJ, Black BE, Lee TH. 2015. A novel hybrid single molecule approach reveals spontaneous DNA motion in the nucleosome. *Nucleic Acids Res* 43(17): e111.
- Weiner A, Lara-Astiaso D, Krupalnik V, Gafni O, David E, Winter DR, Hanna JH, Amit I. 2016. Co-ChIP enables genome-wide mapping of histone mark co-occurrence at single-molecule resolution. *Nature biotechnology* 34(9): 953-961.
- Wexler A, Wild EJ, Tabrizi SJ. 2016. George Huntington: a legacy of inquiry, empathy and hope. *Brain : a journal of neurology* 139(Pt 8): 2326-2333.
- Wierer M, Mann M. 2016. Proteomics to study DNA-bound and chromatin-associated gene regulatory complexes. *Hum Mol Genet* 25(R2): R106-R114.
- Wlodkowic D, Telford W, Skommer J, Darzynkiewicz Z. 2011. Apoptosis and beyond: cytometry in studies of programmed cell death. *Methods in cell biology* 103: 55-98.
- Wojcik K, Zarebski M, Cossarizza A, Dobrucki JW. 2013. Daunomycin, an antitumor DNA intercalator, influences histone-DNA interactions. *Cancer biology & therapy* 14(9): 823-832.
- Wong MM, Belew MD, Kwieraga A, Nhan JD, Michael WM. 2018. Programmed DNA Breaks Activate the Germline Genome in *Caenorhabditis elegans*. *Developmental cell* 46(3): 302-315 e305.
- Wrattling D, Thistlethwaite A, Harris M, Zeef LA, Millar CB. 2012. A conserved function for the H2A.Z C terminus. *The Journal of biological chemistry* 287(23): 19148-19157.
- Wu M, Singh AK. 2012. Single-cell protein analysis. *Current opinion in biotechnology* 23(1): 83-88.
- Yager TD, McMurray CT, van Holde KE. 1989. Salt-induced release of DNA from nucleosome core particles. *Biochemistry* 28(5): 2271-2281.
- Yang F, Kemp CJ, Henikoff S. 2013. Doxorubicin enhances nucleosome turnover around promoters. *Current biology : CB* 23(9): 782-787.
- Zentner GE, Henikoff S. 2013. Regulation of nucleosome dynamics by histone modifications. *Nature structural & molecular biology* 20(3): 259-266.
- Zhang T, Wei G, Millard CJ, Fischer R, Konietzny R, Kessler BM, Schwabe JWR, Brockdorff N. 2018. A variant NuRD complex containing PWWP2A/B excludes MBD2/3 to regulate transcription at active genes. *Nat Commun* 9(1): 3798.
- Zhao M, Cheah FSH, Chen M, Lee CG, Law HY, Chong SS. 2017. Improved high sensitivity screen for Huntington disease using a one-step triplet-primed PCR and melting curve assay. *PLoS one* 12(7): e0180984.
- Zheng Y, Tipton JD, Thomas PM, Kelleher NL, Sweet SM. 2014. Site-specific human histone H3 methylation stability: fast K4me3 turnover. *Proteomics* 14(19): 2190-2199.
- Zhu Y, Wu J, Zhang C, Sun S, Zhang J, Liu W, Huang J, Zhang Z. 2016. BRCA mutations and survival in breast cancer: an updated systematic review and meta-analysis. *Oncotarget* 7(43): 70113-70127.

KEYWORDS

Flow cytometry, MMA, melting temperature, Huntington, BRCA, nick, R-loop, ChIP, histone PTM, histone variant, laser scanning cytometry, nucleosome stability, histone eviction, superhelicity.

ACKNOWLEDGEMENTS

I am grateful to the recent and former head of the Department of Biophysics and Cell Biology, Professor György Panyi, Professor János Szöllősi and Professor Rezső Gáspár who made it possible to work on my Ph.D project in the department. I would like to thank for the support of my supervisor, Professor Gábor Szabó who was never out of ideas if any difficulties emerged during my work and who was always open to my own ideas and let me realize my own concepts as well. I would like to also thank to Miklós Szabó who made it possible to start my work within the confines of the Institute of Isotope Co., Ltd. I would like to also thank Adél Nagy Vezendiné and Gyöngyi Dajka for conscientious technical assistance and the contributions of the recent and former members of our research group: Dr. Katalin Goda, Szabolcs Tarapcsák, Dr. Péter Nánási, Dr. Erfaneh Firouzi Niaki, Zsuzsanna Gyöngy, Rosevalentine Bosire, Dr. György Fenyőfalvi, Dr. Zsolt Bacsó, Dr. Lóránt Székvölgyi, Dr. Éva Hegedüs and Dr. Quang-Minh Doan-Xuan. I would like to thank for the collaboration of Professor Erich E. Wanker who kindly provided plasmid constructs containing different length of CAG triplet repeats. I would like to also thank Professor Béla Melegh who provided the Huntington patient samples. I would like to thank the employees of the Department of Biophysics and Cell Biology who were involved in the study of Huntington's disease as healthy control patients. I am also grateful to Professor János Kappelmayer and Dr. István Balogh for the BRCA PCR protocol and for the patent sample. I would like to thank Dr. Hiroshi Kimura who kindly provided monoclonal antibodies specific for histone PTMs. I am grateful to Dr. Zoltán Simándi for the H3K4me3 ChIP-seq experiments and Attila Horváth for the bioinformatics analyzes. I would like to also thank Dr. Juan Ausio who kindly provided plasmid constructs containing different isoforms of the histone variant H2A.Z. I would like to thank Dr. Masahiko Harata who kindly suggested as well as provided knock-out cell lines for the H2A.Z-related work.

Finally but not lastly I wish to thank my wife, my daughters and all my family for their infinite love and patience.

This work was supported by TÁMOP 4.2.4. A/2-11-1-2012-0001 and GINOP-2.3.2-15-2016-00044, National Excellence Program.


 Registry number: DEENK/358/2018.PL
 Subject: PhD Publikációs Lista

 Candidate: László Imre
 Neptun ID: LQVY78
 Doctoral School: Doctoral School of Molecular Cellular and Immune Biology
 MTMT ID: 10038939

List of publications related to the dissertation

1. Hegedűs, É., Kókai, E., Nánási, P. P., **Imre, L.**, Halász, L., Jossé, R., Antunovics, Z., Webb, M. R., El Hage, A., Pommier, Y., Székvölgyi, L., Dombrádi, V., Szabó, G.: Endogenous single-strand DNA breaks at RNA polymerase II promoters in *Saccharomyces cerevisiae*. *Nucleic Acids Res.* 2018, 1-20, 2018.
DOI: <http://dx.doi.org/10.1093/nar/gky743>
IF: 11.561 (2017)
2. **Imre, L.**, Simándi, Z., Horváth, A., Fenyőfalvi, G., Ifj., N. P. P., Niaki, E. F., Hegedűs, É., Bacsó, Z., Weyemi, U., Mauser, R., Ausio, J., Jeltsch, A., Bonner, W., Nagy, L., Kimura, H., Szabó, G.: Nucleosome stability measured in situ by automated quantitative imaging. *Sci Rep.* 7 (1), 1-15, 2017.
DOI: <http://dx.doi.org/10.1038/s41598-017-12608-9>
IF: 4.122
3. **Imre, L.**, Balogh, I., Kappelmayer, J., Szabó, M., Melegh, B., Wanker, E., Szabó, G.: Detection of mutations by flow cytometric melting point analysis of PCR products. *Cytometry A.* 79 (9), 720-726, 2011.
DOI: <http://dx.doi.org/10.1002/cyto.a.21104> [doi]
IF: 3.729
4. Hegedűs, É., **Imre, L.**, Pataki, J., Lizanecz, E., Székvölgyi, L., Fazakas, F., Bacsó, Z., Tóth, A., Szabó, M., Seres, Z., Szabó, G.: Heteroduplex analysis using flow cytometric microbead assays to detect deletions, insertions, and single-strand lesions. *Cytometry A.* 73 (3), 238-245, 2008.
DOI: <http://dx.doi.org/10.1002/cyto.a.20492>
IF: 3.259





List of other publications

5. Hrubí, E., **Imre, L.**, Robaszkievicz, A., Virág, L., Kerényi, F., Nagy, K., Varga, G., Jenei, A., Hegedűs, C.: Diverse effect of BMP-2 homodimer on mesenchymal progenitors of different origin.
Hum. Cell. 31 (2), 139-148, 2018.
DOI: <http://dx.doi.org/10.1007/s13577-018-0202-5>
IF: 2.109 (2017)
6. Hrubí, E., **Imre, L.**, Bacsó, Z., Biró, S., Jenei, A., Hegedűs, C.: BMP-2 hatása a humán embrionális szájpadról származó mesenchymalis preosteoblast sejtek morfológiájára és proliferációjára.
Fogorv. Szle. 108 (3), 99-105, 2015.
7. Simándi, Z., Czipa, E., Horváth, A., Kőszeghy, Á., Bordás, C., Póliska, S., Juhász, I., **Imre, L.**, Szabó, G., Dezső, B., Barta, E., Sauer, S., Károlyi, K., Kovács, I., Hutóczki, G., Bognár, L., Klekner, Á., Szűcs, P., Bálint, B. L., Nagy, L.: PRMT1 and PRMT8 regulate retinoic acid-dependent neuronal differentiation with implications to neuropathology.
Stem Cells. 33 (3), 726-741, 2015.
DOI: <http://dx.doi.org/10.1002/stem.1894>
IF: 5.902
8. Székvölgyi, L., **Imre, L.**, Doan-Xuan, Q. M., Hegedűs, É., Bacsó, Z., Szabó, G.: Flow Cytometric and Laser Scanning Microscopic Approaches in Epigenetics Research.
Methods Mol. Biol. 567, 99-111, 2009.
DOI: http://dx.doi.org/10.1007/978-1-60327-414-2_7
9. Székvölgyi, L., Rákossy, Z., Bálint, B. L., Kókai, E., **Imre, L.**, Vereb, G., Bacsó, Z., Goda, K., Varga, S., Balázs, M., Dombrádi, V., Nagy, L., Szabó, G.: Ribonucleoprotein-masked nicks at 50-kbp intervals in the eukaryotic genomic DNA.
Proc. Natl. Acad. Sci. U.S.A. 104 (38), 14964-14969, 2007.
DOI: <http://dx.doi.org/10.1073/pnas.0702269104>
IF: 9.598





10. Székvölgyi, L., Bálint, B. L., **Imre, L.**, Goda, K., Szabó, M., Nagy, L., Szabó, G.: Chip-on-beads: flow-cytometric evaluation of chromatin immunoprecipitation.
Cytometry A. 69A (10), 1086-1091, 2006.
DOI: <http://dx.doi.org/10.1002/cyto.a.20325>
IF: 3.293

Total IF of journals (all publications): 43,573

Total IF of journals (publications related to the dissertation): 22,671

The Candidate's publication data submitted to the iDEa Tudóstér have been validated by DEENK on the basis of Web of Science, Scopus and Journal Citation Report (Impact Factor) databases.

15 November, 2018

